TECHNICAL REPORT STANDARD TITLE PAGE

1. Report No.	2. Government Accession No.	3. Recipient's Catalog No.
FHWA/TX-93-1268-1F		

4. Title and Subtitle	5. Report Date
NDE TECHNIQUES FOR DETECTING GROUT DEFECTS IN CABLE STAYS	August 1993
	6. Performing Organization Code

7. Author(s)	8. Performing Organization Report No.
Roger P. Bligh, Ray W. James, Don E. Bray, and Sreenivas Nakirekanti	1268-1F

9. Performing Organization Name and Address	10. Work Unit No.
Texas Transportation Institute The Texas A&M University System College Station, Texas 77843-3135	11. Contract or Grant No. 0-1268

12. Sponsoring Agency Name and Address	13. Type of Report and Period Covered
Texas Department of Transportation Transportation Planning Division P. O. Box 5051 Austin, Texas 78763	Final - September 1990 August 1992
	14. Sponsoring Agency Code

15. Supplementary Notes

Research performed in cooperation with the Texas Department of Transportation and the Federal Highway Administration
Research Study Title: NDE Techniques for Detecting Grout Defects in Cable Stays

16. Abstract

Problems with corrosion of steel strands in grouted bridge cable stays have raised concern about the integrity of the grout layer protecting the strands. Bleed water that may accumulate in the grout layer if voids or bubbles are trapped during the grouting process can lead to corrosion of the cables. This research study was undertaken to evaluate various nondestructive evaluation (NDE) methods for inspection of this grout layer. Methods which were studied include ultrasonics, film radiography, computed tomography (CT), and neutron radiography.

The feasibility of using computed tomography for inspection of the grout layer has been demonstrated. Voids as small as 0.04 in. (1 mm) in diameter were identified in both the annular region of grout and inside the steel cable bundle. Although some of these voids were manufactured, many of those found were a result of the grouting operation during fabrication of the specimens, an observation which lends urgency to the need for an inspection system.

Laboratory experiments were conducted with a prototype ultrasonic inspection unit which utilizes two rolling contact probes with 500 kHz transducers. A digital signal subtraction technique was found to be particularly useful in analyzing the received signals. The ultrasonic system was successful in identifying the location of defects, but information regarding the size and content of the defects was inconclusive.

Three distinct regions exist along the cable which will most likely require different inspection schemes. It is envisioned that the main section of cable will be inspected by one technique, possibly ultrasonics, while the lower regions of cable, where extra layers are added for fire and crash protection, will require a radiographic technique. The third region, which includes the saddles and anchorages, will likely require a third inspection technique, such as a portable linear accelerator.

17. Key Words	18. Distribution Statement
NDE, Nondestructive, Inspection, Cable Stay, Bridge, Defect, Grout, Ultrasonics, Radiography, Tomography	No restrictions. This document is available to the public through the National Technical Information Service 5285 Port Royal Road Springfield, Virginia 22161

19. Security Classif. (of this report)	20. Security Classif. (of this page)	21. No. of Pages	22. Price
Unclassified	Unclassified	101	

Form DOT F 1700.7 (8-69)

NDE TECHNIQUES FOR DETECTING GROUT DEFECTS IN CABLE STAYS

by

Roger P. Bligh
Ray W. James
Don E. Bray
and
Sreenivas Nakirekanti

Research Report 1268-1F
Research Study 0-1268
NDE Techniques for Detecting Grout Defects in Cable Stays

Sponsored by the

Texas Department of Transportation

in cooperation with the

U.S. Department of Transportation
Federal Highway Administration

Texas Transportation Institute
The Texas A&M University System
College Station, Texas 77843-3135

August 1993

IMPLEMENTATION STATEMENT

Results of the study indicated that nondestructive inspection of the grout layer surrounding the steel strands in cable stays is feasible. Specifications for a portable computed tomography inspection unit are presented. A first generation prototype of an ultrasonic inspection unit was constructed and tested in the laboratory. Recommendations are offered regarding the development of an operational field unit.

KEY WORDS

NDE, Nondestructive, Inspection, Cable Stay, Bridge, Defect, Grout, Ultrasonics, Radiography, X-ray, Gamma Ray, Neutrons, Tomography

ACKNOWLEDGMENTS

This research study was conducted under a cooperative program between the Texas Transportation Institute (TTI), the Texas Department of Transportation (TxDOT), and the Federal Highway Administration (FHWA). Valuable guidance and input were provided throughout the course of the study by Mr. Jeff Cotham, Technical Coordinator, TxDOT, and Mr. Charles McGogney, FHWA. The authors are also indebted to Ms. Charlotte Warner, District 20, and Mr. Dennis Warren, District 12, for providing information and assistance at the bridge sites. The contributions of International Digital Modeling (IDM) Corp. and Scientific Measurement Systems (SMS) in conducting the computed tomography is also acknowledged and appreciated.

TABLE OF CONTENTS

LIST OF FIGURES

LIST OF TABLES

SUMMARY

Problems with corrosion of steel strands in grouted bridge cable stays have raised concern about the integrity of the grout layer protecting the strands. Bleed water that may accumulate in the grout layer if voids or bubbles are trapped during the grouting process can lead to corrosion of the cables. This research study was undertaken to evaluate various nondestructive evaluation (NDE) methods for inspection of this grout layer. Methods which were studied include ultrasonics, film radiography, computed tomography (CT), and neutron radiography.

The feasibility of using computed tomography for inspection of the grout layer has been demonstrated. Voids as small as 0.04 in. (1 mm) in diameter were identified in both the annular region of grout and inside the steel cable bundle. Although some of these voids were manufactured, many of those found were a result of the grouting operation during fabrication of the specimens, an observation which lends urgency to the need for an inspection system.

Laboratory experiments were conducted with a prototype ultrasonic inspection unit which utilizes two rolling contact probes with 500 kHz transducers. A digital signal subtraction technique was found to be particularly useful in analyzing the received signals. The ultrasonic system was successful in identifying the location of defects, but information regarding the size and content of the defects was inconclusive.

Three distinct regions exist along the cable which will most likely require different inspection schemes. It is envisioned that the main section of cable will be inspected by one technique, possibly ultrasonics, while the lower regions of cable, where extra layers are added for fire and crash protection, will require a radiographic technique. The third region, which includes the saddles and anchorages, will likely require a third inspection technique, such as a portable linear accelerator.

INTRODUCTION

Background

The cable-stayed bridge consists of a superstructure of steel or reinforced concrete members supported by a system of inclined cables or stays passing over or attached to towers located at the main abutments or piers. The history of cable-stayed bridges dates back to the 18th century when C.J. Löscher, a German carpenter, built a timber bridge of this type (1). However, some of these early bridges failed prematurely due to the lack of advanced technical knowledge and unavailability of suitable materials for construction.

The renewal of the cable-stayed bridge is a relatively recent development, dating from the 1955 Stromsund bridge in Sweden and the 1958 North Bridge at Dusseldorf (2). This development originated in West Germany during the post-war years when rebuilding provided the opportunity to apply new concepts of design and construction. During this period great emphasis was placed on obtaining optimum structural performance using minimum weight of materials.

Since this time, cable-stayed bridges have continued to evolve and have become an increasingly popular choice of bridge engineers for medium to long span structures due to their economy in material, weight, and cost. The concept is very versatile and lends itself to a wide variety of geometrical configurations. The arrangement of the cables and spans, type of superstructure, and style of towers can be easily adapted to suit various purposes, site requirements, and aesthetics. For these reasons, cable-stayed bridge design has seen widespread and successful application in Europe and, more recently, in the United States where numerous bridges have been built since the late 1970's (3).

A typical elevation of a multispan cable-stayed bridge is shown in Figure 1 with the standard bridge terminology. The girders of these bridges act as beams on an elastic foundation, with discrete elastic supports provided by the cables at their respective attachment points. In a typical arrangement, the towers and the superstructure will be in compression, whereas the cables will be in tension.

The first cable-stayed bridge in Texas, which crosses the Neches River near Port Neches, was recently opened to traffic, and a second bridge, over the Houston Ship Channel near

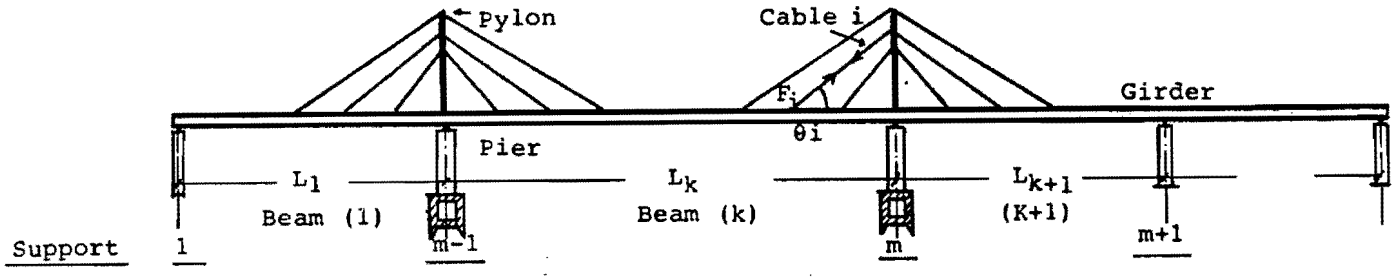

Figure 1. Typical multi-span cable-stayed bridge (4).

Baytown, is presently under construction. The Neches River Bridge employs precast box-girder construction and has a 640-ft (195-m) main span with a clearance of 143 ft (43.6 m). It utilizes two vertical planes of cables in a harp configuration located at each edge of the superstructure and supported by twin towers. In a harp configuration, the cables are parallel and equidistant from each other with uniform spacing along the tower and deck. Figure 2 is a photo of the bridge showing one of the two cable planes. This photo was taken during the grouting of the cable stays.

The Baytown Bridge, which incorporates a composite deck design, will have a center span of 1250 ft (381 m), making it the longest cable-stayed span in the U.S. The twin 72-ft (22-m) wide, 4-lane decks will make it the largest cable-stayed bridge in the world in terms of deck area. Two diamond-shaped towers with double-plane cable systems deployed in a fan arrangement support the twin decks.

Problem Statement

As worldwide experience with these bridges has accumulated, new bridge engineering problems have been encountered and addressed. Noteworthy among these problems is the development of corrosion protection systems for the cables themselves. The usual practice in the U.S. is to encase each cable stay in a steel or polyethylene (PE) pipe and fill the annular region

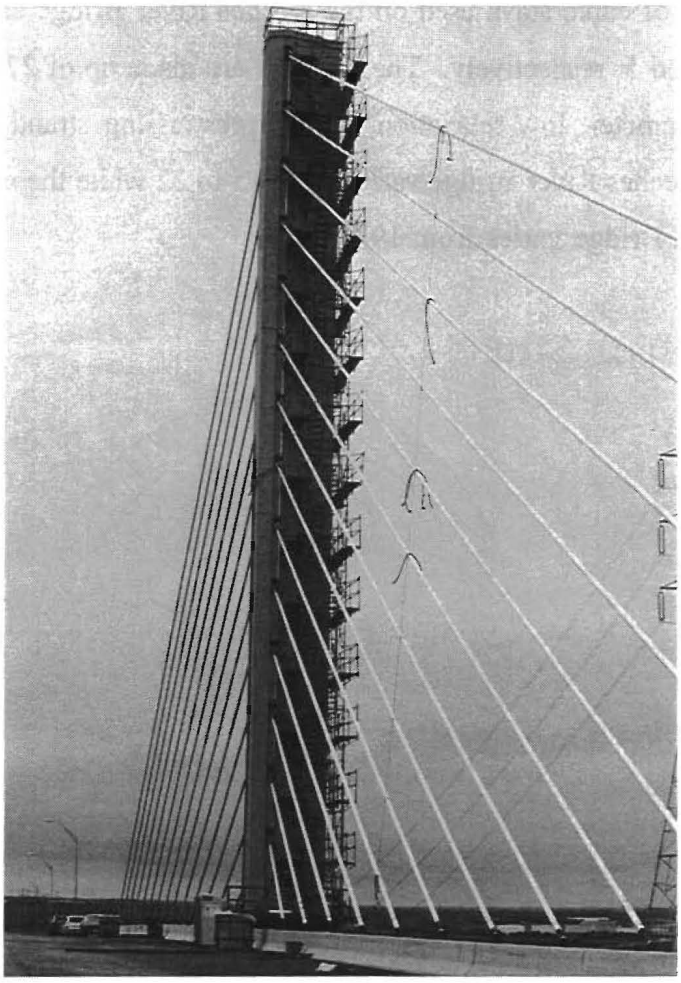

Figure 2. Neches River cable-stayed bridge.

between the cable and pipe with a portland cement or epoxy grout. A typical arrangement is shown in Figure 3. Special admixtures may be added to the grout for the purposes of: (a) increasing flowability; (b) minimizing bleed water; (c) minimizing shrinkage; (d) preventing separation of water and grout as it flows inside the pipe; and (e) increasing, as necessary, the time before initial set. Additional corrosion protection may be obtained by use of greased, plastic-sheathed, or epoxy-coated strand.

The cable itself consists of multiple steel strands which in turn may consist of one or more parallel or twisted individual wires. A tedlar tape is wrapped around the outer surface of the PE pipe to protect the pipe from environmental attack, mainly from solar heating. Representative

cross-sectional views of cable stays used on the Neches River Bridge and Baytown Bridge are shown in Figures 4 and 5, respectively. These cables are made up of 270,000 psi (1,860 MPa), 0.6 in. (15.2 mm) diameter, low relaxation, 7-wire prestressing strand. The number of steel strands used on the Neches River Bridge varies from 15 to 22 while the number of strands in the stays on the Baytown Bridge varies from 19 to 61.

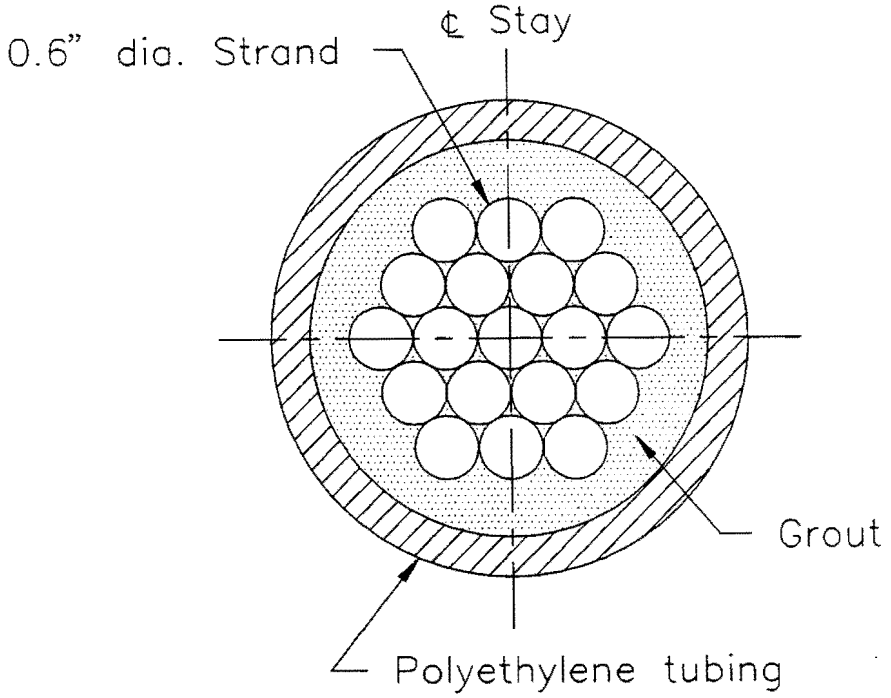

Figure 3. Cross-sectional view of a typical cable stay.

Grouting takes place after all permanent loads are applied to the cables. The grouting procedure involves pressure-filling the PE pipe in several lifts in order to limit the hydrostatic head and prevent damage to the pipe. For the Neches River Bridge, the maximum lift height was limited to 65 ft (20 m) with a maximum head pressure of 114 psi (786 kPa). Specifications to be used on the Baytown Bridge limit the injected grout to a maximum vertical height of 125 ft (38 m), a maximum grout pressure of 120 psi (827 kPa), or 2 percent radial expansion of the PE pipe, whichever is lowest (5).

The grouting operation begins at a fill port near the bottom of the stay and continues until the grout mixture reaches a vent hole further up the pipe. The fill port is closed and a secondary outlet, located just below the initial vent port, is opened to drain off any bleed water which might

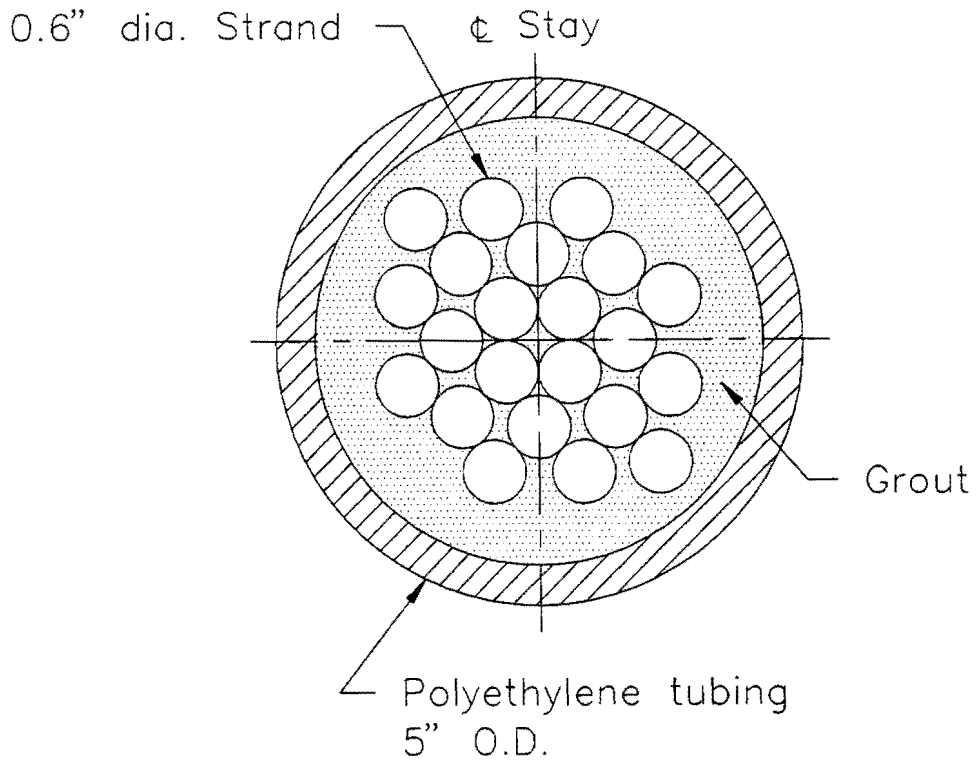

Figure 4. 22-strand cable stay used on Neches River Bridge.

accumulate at the top of the lift. After the grout has hardened, this secondary vent port is used as the filling port for the next lift, and the grouting process is repeated until the entire stay cable is completely filled with grout. This operation is illustrated in Figure 6.

In principle, this procedure should result in complete filling of the pipe, but in practice, voids or bubbles may be trapped in the grout. These voids can then act as storage points for the accumulation of bleed water and, if adjacent to the steel strands, may result in localized corrosive attack.

Although cable stays carry mostly dead load (7), the problem of stay fatigue is still present due to superimposed live loading. While it is possible to design cables and anchorages for acceptable fatigue lives under controlled environmental conditions, it is extremely difficult to assure that the cable will not be subjected to environmental attack, particularly corrosion, for the expected life of the structure. If permitted to occur, corrosion may result in premature degradation of the cables and a significantly reduced fatigue life of the structure.

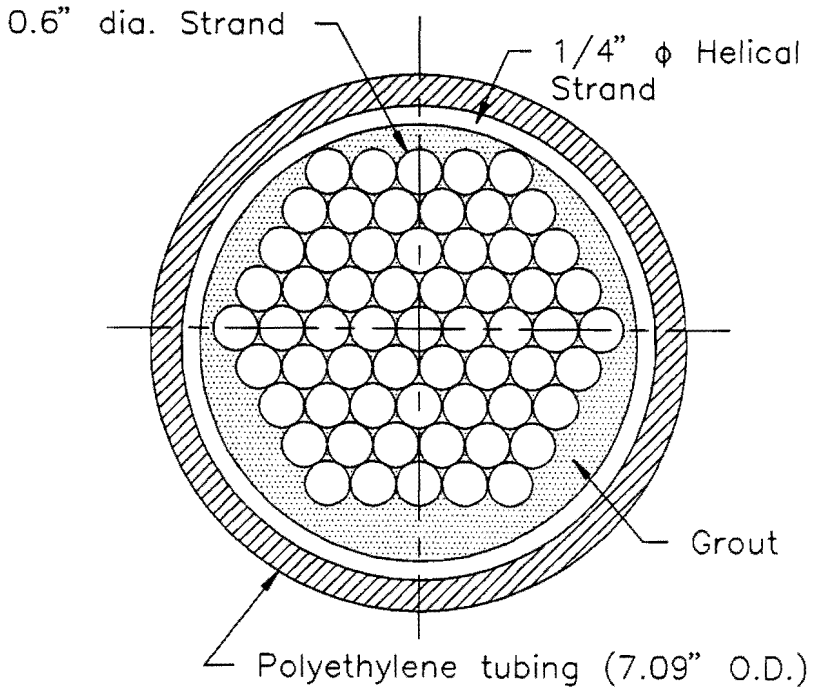

Figure 5. 61-strand cable stay used on Baytown Bridge.

In fact, corrosion is known to be the chief cause of cable deterioration in cable-stayed bridges (4). When exposed to a conducive environment, high strength steel under sustained tensile stress and vibratory loads are susceptible to general corrosion, stress corrosion cracking, fretting corrosion, and/or hydrogen embrittlement. Inspections have indicated that many of the nearly 200 cable-stayed bridges built around the world within the past few decades are in danger because of corrosion attacking their cables (8,9). Many different cable protection systems have been implemented on these bridges and nearly all of these methods have suffered problems to one extent or another. In Venezuela, the Maracaibo Bridge was designed with concrete covered stay tendons which had to be replaced in the past ten years and must soon have its cables replaced for a second time (8). Only three years after completion, the Kohlbrand Estuary Bridge in Hamburg, Germany required complete replacement of all cable tendons because of severe corrosion (9). Prompted by this premature corrosion, inspections of other cable-stayed bridges in Germany yielded other significant damage-related findings including:

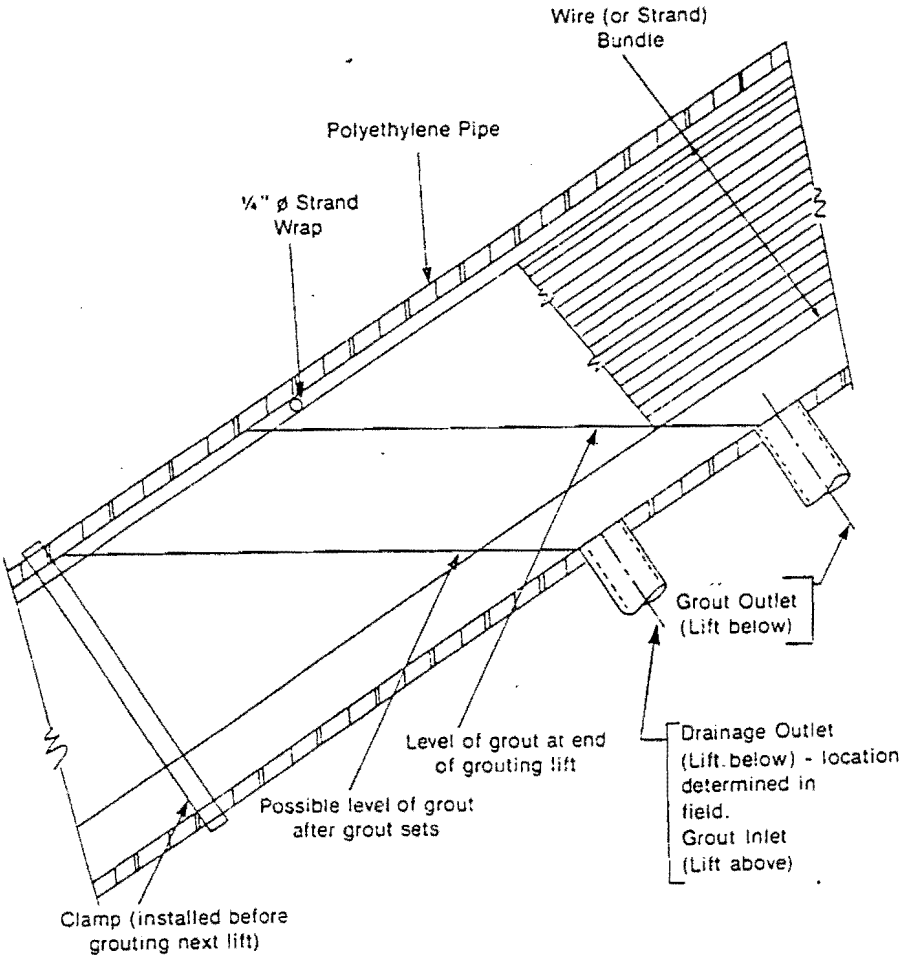

Figure 6. Grouting operation (6).

- Damage to the corrosion protection,
- Evidence of external and internal corrosion,
- Broken or cracked wires, and
- Material damage caused by fatigue.

Perhaps equally distressing is the fact that three of four cable-stay specimens constructed from new cable for purposes of acceptance testing for the Baytown Bridge were found to have significant corrosion when disassembled after testing (10,11,12). During testing of a 43-strand cable stay, all seven wires of one of the exterior strands in the cable bundle experienced fatigue fractures in the free length of the stay (10). Significant rusting of the center and outer wires was found at the point of fracture with the center wire fracture surface being completely corroded. This corrosion was not detected in an inspection performed prior to assembly of the stay.

After sustaining $2x10^6$ load cycles during a fatigue test, a 55-strand cable stay specimen failed to achieve the required ultimate load during a subsequent static tensile test (11). During disassembly, corrosion was observed in three areas of the stay, including: (1) on the strand along the entire length of the specimen, (2) on the face of the lower anchorhead, and (3) on the inner face of the upper tension ring which, it was reported, was exposed to bleed water during the grouting process. In addition, a layer of grout latents was present at the interface of the primary and secondary grout lifts, and two small voids were observed in the secondary grout. A subsequent 55-strand specimen was also observed to have severe corrosion on the strands, anchorheads, and the fixtures connecting the anchorheads to the polyethylene (PE) pipe (12). The corrosion present in these newly fabricated cable-stay specimens is attributed by some to bleed water exposure during the grouting process (13).

As these examples indicate, current methods of corrosion protection, in and of themselves, are not sufficient to ensure that cable stays will be adequately safeguarded from corrosion and/or a corrosive environment. Since the removal and replacement of deteriorated cables is so costly, it is important to develop efficient and accurate means of inspecting these cables for defects in the protective grout layer so that corrective measures may be taken to help prevent the onset of corrosion.

Objective

The objective of this study was to evaluate promising nondestructive evaluation (NDE) technologies and develop inspection techniques for detecting voids and other defects in the protective grout layer surrounding the steel strands in a cable stay.

OVERVIEW OF NDE TECHNIQUES

Applicability of NDE

The complete inspection of cable stays poses numerous problems. When encased in grout, the load carrying steel strands cannot be visually inspected, making an assessment of their condition difficult. Nondestructive inspection techniques can offer an efficient and convenient means of inspecting these cable stays without destructive excavation. However, all of these methodologies have limitations and their application is not necessarily straightforward. The presence of different materials and multiple interfaces alone can cause difficulties. In addition, variations in the dimensions of the stays and the number and arrangement of the strands inside the PE pipe further complicate inspection.

The thickness of the grout layer can also vary significantly around the circumference of the cable bundle. In the field, the PE pipe will sag and lay on top of the tensioned steel strands, as depicted in Figure 7, creating contact at several locations along the length of the strands. Therefore, the thickness of the protective grout layer can vary from no grout at the points of contact, to a relatively large area of grout between the bottom of the PE pipe and the strands. Some designs use a helically wound spacer wire to provide a minimum amount of grout coverage equal to the diameter of the spacer wire (see Figure 5).

Inspection of the lower portion of the cable stays is further complicated by the addition of anchorage details and fire and crash protection measures. For example, on the Houston Ship Channel bridge, an oversize 0.25 in. (6.4 mm) thick steel guide pipe extends from the anchorage box to the elevation of the traffic barrier. Fire protection for the cables then extends from the top of the steel pipe to a point 50 ft (15.2 m) above the roadway surface. This treatment consists of placing an outer, oversized PE pipe over the stay assembly and grouting the region between the two polyethylene pipes. A wire reinforcing cage is placed between the pipes, and a minimum 1.5 in. (38 mm) of fire protection grout is required. Figure 8 shows a typical section through the cable stay in this region.

Considering the amount of capital invested in our cable-stayed bridges and the extent of the corrosion problem facing them, relatively little effort has been devoted to their inspection. Much of the research on corrosion protection systems has focused on the development of new,

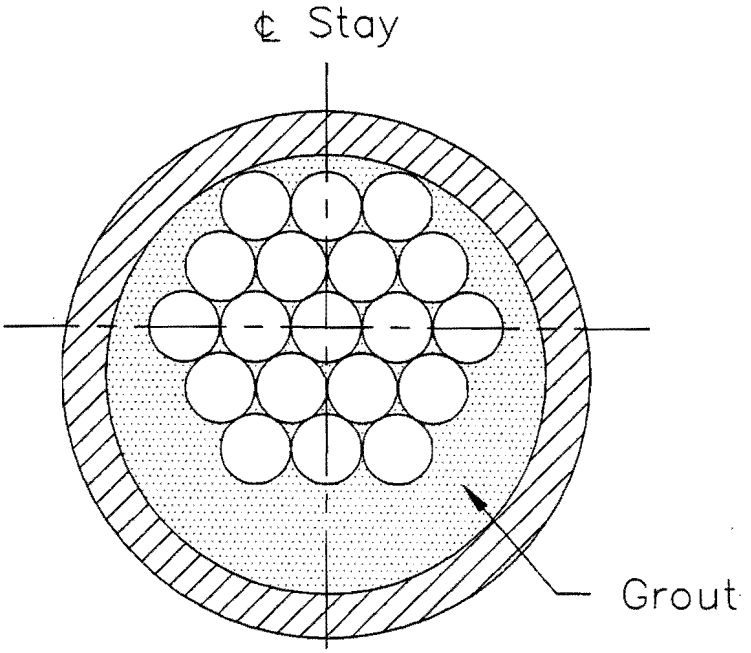

Figure 7. PE pipe/cable contact.

innovative solutions rather than the evaluation of existing systems. While this research is certainly needed, there is also a parallel need for developing nondestructive evaluation techniques which can assess the condition of grout layer surrounding the cables on the many structures which have already been built, planned, or are under construction, and which utilize current methods of corrosion protection. A review of various NDE techniques and their applicability to the this problem is presented below.

Magnetic Flux Leakage

Previous work regarding the inspection of cable stays has been limited to the development of systems designed to detect damage in the steel strands in the form of significant section loss, fracture of individual wires, and fatigue cracks using magnetic field disturbance (MFD) principles. The electromagnetic test instrumentation magnetizes the cable close to saturation. Any distortion of the cable structure disrupts the magnetic field, resulting in a leakage flux which can be detected by sensor coils or hall sensors. Limited testing of one device (14) indicates a potential

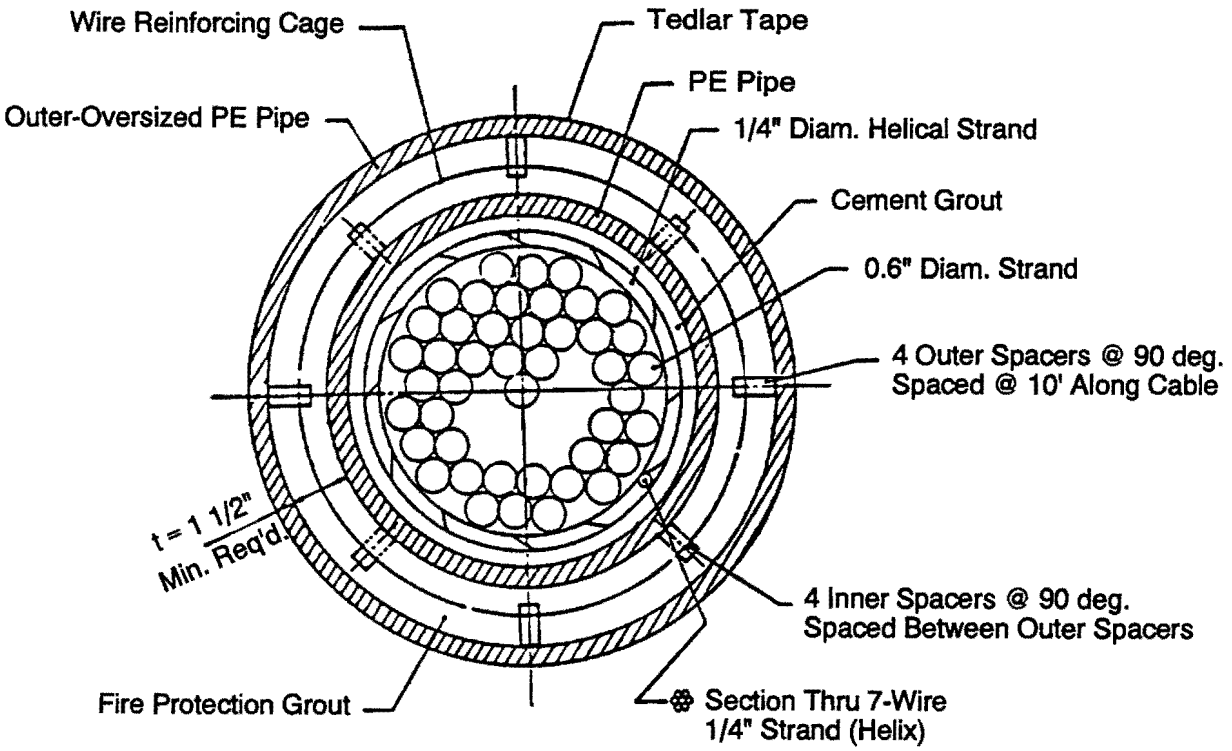

Figure 8. Typical section through cable stay with fire protection.

for locating significant section-loss flaws in bars and strands in precast concrete beams. However, the effectiveness of the device was affected by other interfering signals.

Other research (15) resulted in the development of a magnetic perturbation cable (MPC) inspection system which consists of a remote control module with mechanisms for self-propulsion and precise positioning and scanning. The operation of this system, which is 16 ft (4.9 m) long and weighs 2,800 lb (2,700 kg), was demonstrated on the cable stays of the Pasco-Kennewick Bridge in Washington. Although no defects were found in the trials, indications of spiral wrap and other characteristics of the cable indicated that an adequate inspection was performed. Recent laboratory tests of the MPC system have shown that the device is capable of detecting a single broken wire in a 7-wire strand at the center of a polyethylene covered, grouted cable stay similar to those used on the Baytown Bridge (16). Similar devices have been in use in Germany for many years (9).

However, although MFD techniques offer considerable promise for the detection of defects in the cable bundle, they are not useful for detecting voids or bleed water accumulations in the grout, as they are only sensitive to significant changes in the presence of ferromagnetic materials.

Both radiography and ultrasonics, however, have shown some ability to detect anomalies in grout and/or concrete as discussed in more detail below.

Radiographic Techniques

Radiographic techniques, employing both X-ray and gamma ray sources, have demonstrated an ability to inspect concrete (17). In a study to evaluate film performance in concrete inspection, a 300 curie (Ci), ^{60}Co source was used to image reinforcing bars in concrete samples up to 18 in. (460 mm) thick (18). Exposure times ranged from 20 sec to 4 hr. ^{137}Cs and ^{192}Ir are reported to have been used for monitoring the density and movement of grout during the installation of piling for offshore platforms (19). The density measurements are based on a decrease in intensity of a beam of γ-radiation passing through grout between a radiographic source and a radiation detector. Computed tomography studies of concrete using both x-rays and gamma rays have also been reported (20,21).

A portable miniature linear accelerator (MINAC), developed by Schonberg Radiation Labs, has been used effectively in the inspection of suspension bridge sockets and cable-stay anchorages (22). The system is capable of producing exposures through approximately 14 in. (356 mm) of steel. More recently, radiographs were made through 60 in. (1.5 m) of concrete (22). The MINAC uses accelerating voltages as high as 6 MeV and operates at a higher frequency than conventional accelerators. The 1.5 MeV unit has a total system weight of 250 lb (113 kg) with the accelerator unit weighing only 35 lb (16 kg). This system can be interfaced with real-time imaging systems for filmless radiography.

Although the studies cited above demonstrate the feasibility of using radiographic techniques for the inspection of the grout layer, geometry of the stay, shielding requirements, and relatively long exposure times may cause operational restrictions.

Ultrasonic Techniques

Considerable ultrasonic NDE work has been directed toward determining of properties and soundness of concrete. The basic operating principle of ultrasonics consists of emitting pulses of energy from a transducer which are transmitted through the concrete or grout and then received either by the same transducer (pulse-echo), or by a second transducer positioned

elsewhere on the specimen (through-transmission). Using variations of these methods, a number of factors can be investigated including compressive strength, degree and uniformity of consolidation, location and orientation of cracks or cold joints, the thickness of slabs on grade, and the presence and size of voids (23). A laboratory study evaluated the capabilities of ultrasonics through-transmission methods to detect cracks in concrete (24). Using frequencies of 54 and 150 kHz, pulse velocity and amplitude measurements were used to study crack diffraction patterns in 6 in. (152 mm) unreinforced cubes with fabricated internal cracks. Cracked samples showed significantly lower wave speeds, since the diffraction around the crack delays the travel of the pulse.

Other researchers have noted similar reductions in pulse velocity and amplitude through fully cured, unreinforced concrete containing voids (25). In this same study, a method for assessing the uniformity of concrete and detecting the presence of "sizable" voids was developed. The volume of concrete is scanned in an orthogonal grid and the resulting pulse-velocity contours are plotted. A rapid change in pulse velocity over a short distance indicates the presence of a defect.

An evaluation of ultrasonic techniques for detecting voids in grouted tendon ducts yielded mixed results (26). Seven metal ducts were cast into a concrete wall for use in the laboratory investigation. Five of the ducts were grouted and steel strand was included in two ducts. Voids were from plexiglass tubes which were sealed with air or water and placed in the ducts before grouting. An ultrasonic pulse-velocity technique proposed by Chung and Law (25) indicated some correlation for areas in which approximately 47 percent of the section thickness was void. In areas where only a single voided duct was present (approximately 23 percent of the section thickness) the results were inconclusive and the various void configurations (air-filled, water-filled, with strand) could not be differentiated. An impact-echo procedure developed by the National Bureau of Standards (27), was found to have the best potential for successful application in the field. The procedure uses the mechanical impact of a steel ball to create a stress wave which is received by a point-contact transducer. Although numerous "false calls" were indicated where voids did not exist, the technique was demonstrated to be capable of identifying deep voids in a heavily reinforced concrete wall.

Burdekin et al. investigated the ability of ultrasonic techniques to detect serious deterioration of high-strength tendons or rods embedded in concrete such as those used in segmentally constructed or prestressed concrete bridges (28). Extensive experimental trials were carried out on concrete samples containing voids, corrosion, and broken wires using probes of different frequencies in the range of 50 to 500 kHz. Due to the inherent problems of scatter and attenuation, analyses using conventional ultrasonic testing methods were not successful in either the time or frequency domains. Using advanced signal-processing techniques combined with the use of rolling transducers, a prototype system for scanning concrete beams was developed. The unit used two wheels traveling parallel to each other and spaced 70 mm apart, with one probe acting as transmitter and the other as a receiver. The system was shown to be capable of locating major faults in embedded steel components under shallow concrete cover. However, the development did not reach the stage of a robust field prototype system, and field trials were not conducted.

Other Techniques

Several researchers have used acoustic emission techniques to study concrete structures (29,30,31). An acoustic emission system requires the installation of permanently attached sensors and is essentially a passive monitoring technique rather than an inspection tool (28). Noise can be generated by cracking concrete due to expansive forces resulting from a build up of corrosion products, breaking of wires, or movement at the concrete/wire interfaces. While this technique has potential for studying problems such as crack initiation and propagation, bond degradation, and corrosion of reinforcing steel, it has no application in the detection of voids formed during the grouting of cable stays such as this study addresses.

Radar systems have been used recently to examine the condition of concrete bridge decks, measure pavement thickness, and locate interfaces or layers within pavements (32,33,34). The technique uses high frequency electromagnetic waves, reflections from which change as discontinuities are encountered (28). Although promising, the current technology did not appear to be readily adaptable to the inspection of cable stays and this technique was not pursued further.

The potential for using fiber optic technology for nondestructive testing of concrete structures is only beginning to be explored. To date, only a handfull of studies report moderate

amounts of research in this area (35,36,37). These techniques essentially measure phase, intensity, or wavelength of lightwaves propagating through embedded fibers. A change in one or more of these properties, such as a loss in intensity, indicate the presence of a crack or void. Since the fibers must be embedded during construction and prior to grouting, this technology is not applicable for inspecting existing cable-stay structures. However, with further research, fiber optics may hold promise for incorporation into future designs for initial quality control and long term monitoring of the protective grout layer.

As indicated by the discussion of the state-of-the-art techniques described above, progress toward a solution of the problem posed herein has been slow and difficult. Many of these techniques which were developed for the inspection of concrete do not directly apply to the testing of grout due to differences in aggregate content, reinforcement, etc. The techniques which appeared to offer the most promise for being adapted to the problem of grout inspection in cable stays were radiography and ultrasonics. These methods were therefore selected for further laboratory evaluation as described in the following sections of this report.

RESEARCH APPROACH

After conducting a literature review and identifying the most promising methods, an experimental laboratory analysis was performed to study the feasibility of the selected nondestructive evaluation (NDE) techniques for inspecting the protective grout layer which surrounds the steel strands of cable stays. Various radiographic and ultrasonic techniques were evaluated in essentially parallel efforts. The first task involved establishing relevant material properties and determining optimum values for the parameters required for each technique. The applicability of each technique was then further evaluated using representative samples of actual cable stays. From the results of these investigations, performance specifications were developed. Prototype hardware was then constructed and tested in a laboratory environment. Details of these analyses are described in the sections which follow.

Sample Preparation

For the purpose of conducting laboratory investigations, several representative cable-stay samples conforming to specifications for the Neches River bridge were constructed. The first sample contained 19 steel cable strands placed in a 4.5 in. (114 mm) outer diameter (O.D.) PE pipe, 12 in. (305 mm) in length. The cables were made from standard 7-wire, 270 ksi (1,860 MPa), 0.6 in. (15 mm) diameter pre-stressing strand. The strands were centered inside the PE pipe using wooden templates. A cross section of this cable appears in Figure 9. Another sample, representing the largest cable cross section used on the Neches River bridge, contained 22 cable strands placed in a 5 in. (127 mm) O.D. pipe 18 in. (457 mm) long. A third sample was constructed without any internal strands and was simply comprised of a 4.5 in. (114 mm) outer diameter (O.D.) PE pipe, 18 in. (305 mm) in length. These samples were capped at both ends and fitted with a 1 in. (25.4 mm) diameter filling port at the lower end of the pipe. A 0.5 in. (12.7 mm) vent hole was provided through the top end cap. The samples were then grouted under field conditions at the Neches River bridge site. The grouting operation was halted after the grout began ejecting out of the vent hole as shown in Figure 10.

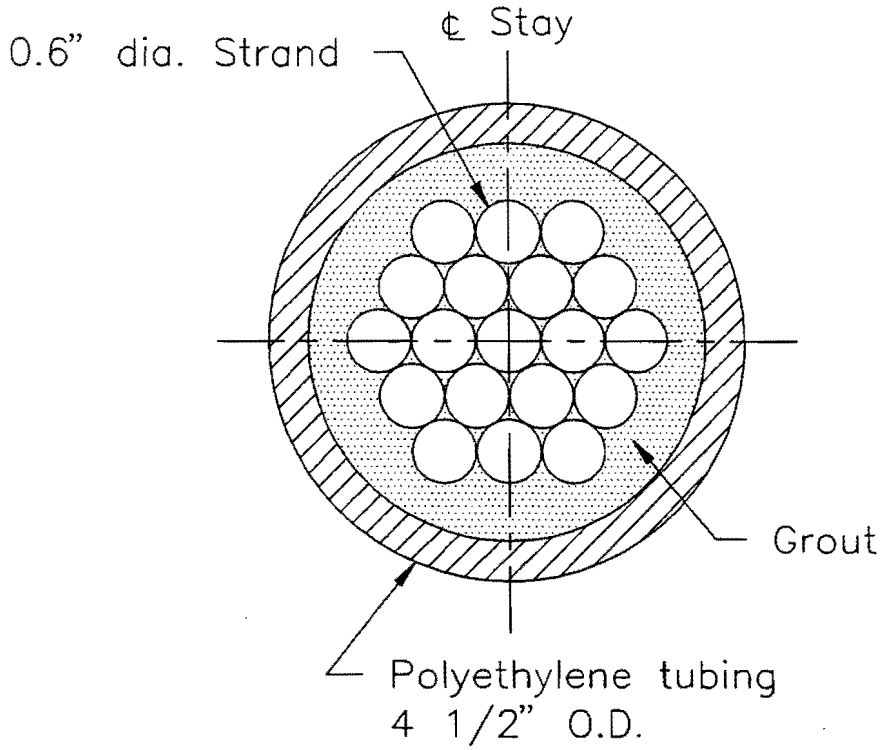

Figure 9. Cross section of cable stay specimen used in laboratory experiments.

The grout mixture used on the Neches River bridge contained type II portland cement, water, and various proprietary additives. The function of the special admixtures was to increase flowability, reduce bleed water, and minimize shrinkage.

Once the samples had cured sufficiently, manufactured defects were introduced to simulate idealized grout defects. These defects were in the form of drilled holes in the longitudinal and radial directions, ranging in diameter from 0.1875 in. (4.76 mm) to 0.5 in. (13 mm). Similar defects were introduced into standard cubes and cylinders made from portland cement grout with and without the special admixtures mentioned above. These samples were then used in a laboratory evaluation of the various NDE methods selected for investigation.

Figure 10. Field-grouted cable-stay specimens.

RADIOGRAPHY

Theory

The principles of radiography and radiographic techniques for nondestructive evaluation of welded products and castings have been well defined. However, applications on concrete structures have developed very slowly. The mechanism of radiographic inspection is the propagation of energy from a source through an object and the evaluation of the energy pattern received on the opposite side (38). The methods available use radiation produced by radioisotopes, X-ray generators, and nuclear reactors to bombard fresh or hardened concrete or grout samples. The object attenuates radiation according to its density, thickness, and the type and size of defects present. Hence, an intensity distribution of radiation that varies with the flaw distribution is created. This radiation pattern is collected and made visible by means of photographic film, fluoroscopic screens, or digitized computer-aided systems. A general description of these processes is provided below, followed by the findings and results obtained from the individual techniques.

Various sources generate two types of radiation: electromagnetic waves and particles. Neutrons are typically the only particles of interest in the testing of concrete or grout. There are three basic ways of producing free neutrons for use in radiography. These are nuclear reactors, particle accelerators, and isotopes. The highest quality of neutron radiographs are typically achieved using reactor neutron sources due to the high thermal neutron beam intensities available from nuclear reactors. Neutrons can also be produced by accelerator units which bombard suitable neutron emitting targets, such as beryllium or deuterium, with protons or high-energy X-rays or gamma rays. Another source of neutrons is Californium-252. This unique isotope undergoes fission spontaneously as part of its radioactive decay process and emits a large number of neutrons.

Both gamma rays and X-rays are forms of electromagnetic radiation, indistinguishable except by the nature of the source (38). Gamma radiation is generated by the radioactive decay of unstable isotopes. Each isotope emits one or more discrete wave lengths of radiation as opposed to the broad spectrum of radiation generated by X-ray tubes. This wave radiation is characterized by the energy it carries and is usually expressed in units of electron volts, eV.

These energy levels remain constant for a particular isotope, but the intensity decays with time. This decaying process is logarithmic and each radioactive isotope has a characteristic half-life which is the amount of time required for the intensity of emitted radiation to be reduced by half. The intensity is measured in roentgens per hour at one meter from the source (rhm) where a roentgen is defined to be the amount of energy absorbed from a beam of radiation passing through 1 cm^3 of air at standard conditions (38). Table 1 lists pertinent characteristics of the isotopes most commonly used in NDE.

Table 1. Characteristics of common radiographic isotopic sources (38).

Isotope	Half-Life	Energy (MeV)	Intensity (rhm)
^{60}Co	5.3 yr	1.33, 1.17	1.35
^{137}Cs	30.1 yr	0.66	0.34
^{192}Ir	74 days	0.31, 0.47, 0.60	0.55
^{170}Tm	129 days	0.084, 0.052	0.003

X-rays are generated when high-speed electrons strike a suitable target causing an unstable condition at the target area that results in the release of radiation (38). Two electrical circuits are involved in the operation of the X-ray tube. A low-voltage circuit heats a filament (cathode) to raise the energy level of the conduction electrons so that they physically leave the filament surface. A high voltage circuit then accelerates the free electrons from the filament to the target (anode). The target, along with the circuitry to generate and accelerate the electrons, is enclosed in a vacuum tube. The rapid deceleration of electrons at the target caused a continuous spectrum of emission of X-ray wavelengths. The penetrating characteristics or intensity of the excited X-rays are a function of the energy level which is determined by the tube voltage and the target material. The maximum intensity of the X-ray spectrum occurs at approximately 1/3 the tube voltage.

The interaction of gamma and X-rays with concrete or grout can be characterized as penetration with attenuation (39). That is, when a beam of radiation strikes a specimen, some of the radiation will pass through the sample, some of the beam will be absorbed, and some will be scattered out of the beam. The intensity of the beam falls off exponentially according to the relationship:

$$I_g = I_o \, e^{(-\mu_g \, \rho_g \, x)}$$

where:

I_g = final intensity of the beam

I_o = initial or reference intensity of the beam

μ_g = mass attenuation coefficient of the grout

ρ_g = density of the grout

x = length of the beam path through the grout.

While electromagnetic forms of radiation interact with orbiting electrons and their attenuation is proportional to material density and atomic number, neutrons interact with atomic nuclei and their attenuation is proportional to material density and neutron absorption (40). Figure 11 depicts the characteristic differences between X-ray and neutron radiography. Note that X-ray attenuation, depicted by the solid line, increases with atomic number, while neutron attenuation, indicated by the scattered dots, has a random relationship with atomic number. Thus, many materials that strongly absorb X-rays, such as most metals, permit easy passage of neutrons, while other materials that readily pass X-rays easily attenuate neutrons.

Having interacted with the specimen, the transmitted radiation carries information about the sample's properties or structure. Radiographic methods traditionally employ photographic film as detectors. In X- and gamma radiography, the rays strike the film emulsion and expose it in much the same manner as light exposes conventional film. Neutron radiography is slightly more complex. Since neutrons will not expose the film directly, the neutrons strike a screen of a material such as gadolinium which absorbs them and then emits secondary radiation which exposes the film.

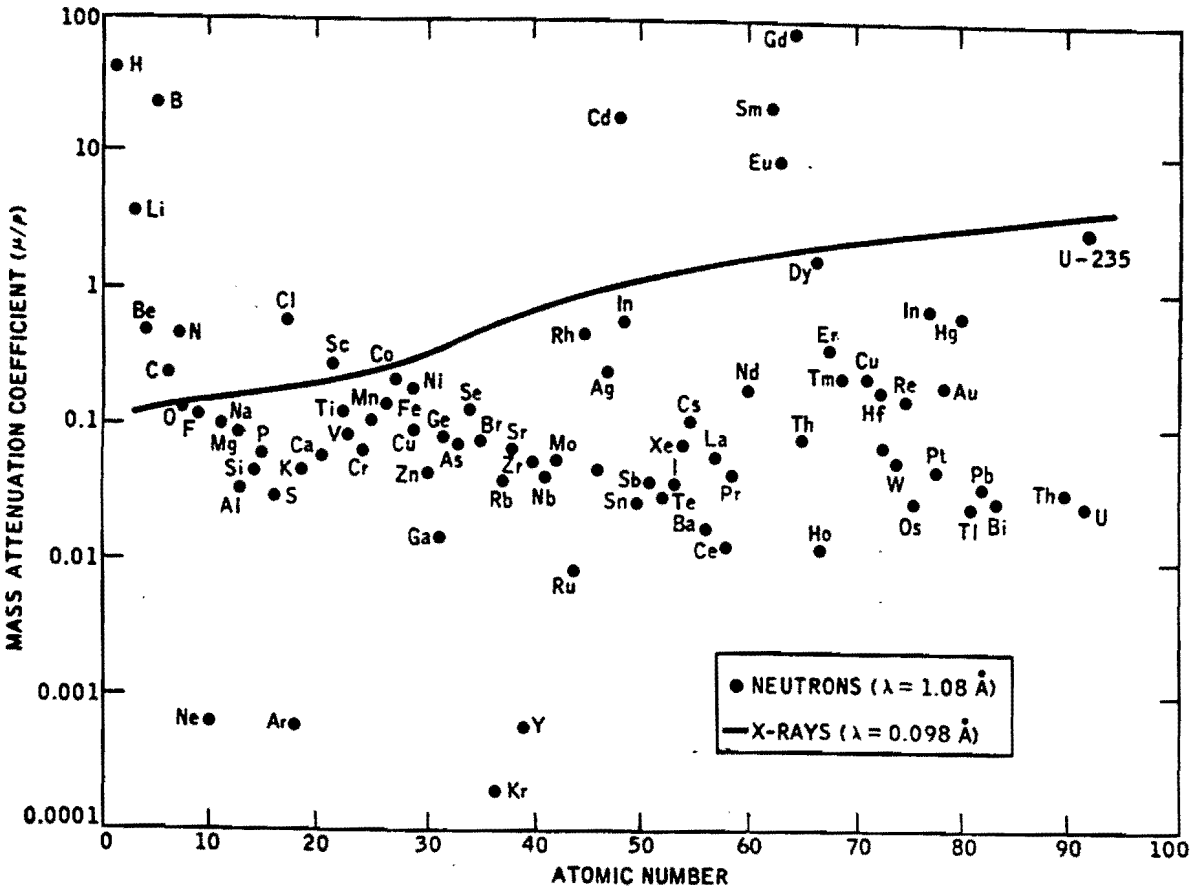

Figure 11. Mass Attenuation Coefficient Versus Atomic Number (40).

The advantage of film lies in the fact that a permanent, direct photograph type copy of the exposure is obtained. However, the time advantages and enhanced contrast provided by digital image software has promoted the use of real-time image display and analysis systems such as fluorescent screens with television-like monitors, and computer-aided tomographic systems.

Neutron Radiography

One of the initial techniques that was investigated was inspection by neutron radiography. As shown in Figure 11, steel is relatively transparent to neutrons. Therefore, it was theorized that the multiple steel strands inside the stay would not hinder the inspection of the protective grout layer. It was envisioned that neutron radiography might be particularly useful for inspection of the lower portions of the cable stays near the anchorages where, as discussed previously, an outer steel guide pipe is positioned over the cable stay. Since hydrogen is very absorptive of neutrons (see Figure 11), it was anticipated that a void containing bleed water would be readily detectable.

The main concern regarding this technique was whether or not the polyethylene pipe, which has a high hydrogen and carbon content, would permit passage of the neutrons and allow inspection of the grout. Just as the bleed water would be highly attenuating, the PE pipe had similar potential for attenuating a large percentage of the neutrons and rendering the inspection ineffective.

For this evaluation, real-time neutron radiography of the cable-stay sample was performed at the Nuclear Science Center located at Texas A&M University. The Nuclear Science Center contains a TRIGA reactor that operates at a steady state power of 1 MW with a peak neutron flux of 10^{13} neutrons/(cm^2-s). The cable-stay specimens were lowered into a shielded chamber (see Figure 12) and placed in the path of the neutron beam by turning off a water shutter within the beam port. The cable samples were remotely manipulated in the neutron beam to allow complete inspection and optimal assessment of the manufactured defects.

The real-time imaging system consists of a neutron image intensifier, closed circuit television monitor, video tape recorder and printer, and a computer with an image processing board and software. The image of the test object contained in the neutron beam is change to visible light by a neutron scintillator screen. This light image is converted to an electron image by a photoemissive layer of material. The electron image is processed by focusing electrodes and displayed on a phosphor screen as a visible image. Finally, a television camera was used to view the image in real time as shown in Figure 13.

Various digital image enhancement and subtraction techniques were performed in an attempt to visualize the grout inside the PE pipe. Results of these experiments verified that the

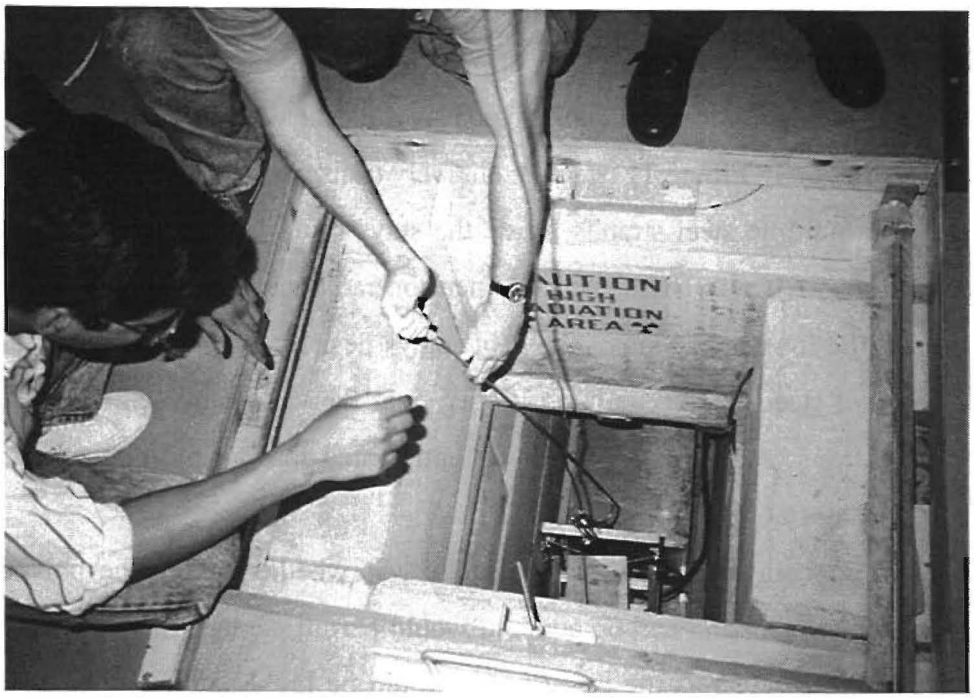

Figure 12. Positioning cable-stay specimen for neutron radiographic inspection.

PE pipe was too absorptive of neutrons to allow an effective inspection of the grout layer. It should be noted, however, that a few bridges in the U.S. have been built using steel-sleeved cables rather than polyethylene pipe. For these bridges, inspection of the stays with a portable neutron source such as ^{252}Cf may have merit. The steel sleeve and interior strands would be virtually transparent to the neutrons and an effective inspection of the grout could be performed. However, neutron radiography was found to be unproductive for polyethylene-sleeved cables and, therefore, was not pursued beyond the initial feasibility study.

Film Radiography

In an effort to evaluate the feasibility of using standard X-ray radiographic techniques for inspection of the grout, experimentation with conventional film radiography was conducted using a Philips 160 kV constant potential X-ray system. The system incorporates an MCN 165 directional beam X-ray tube of metal-ceramic construction. The tube has a voltage range of 8 to 160 kV, focal spots of 0.4 x 0.4 mm and 3.0 x 3.0 mm, and an emergent beam angle of 40 deg. Filtration is provided by a thin beryllium window and a removable 3 mm aluminum screen.

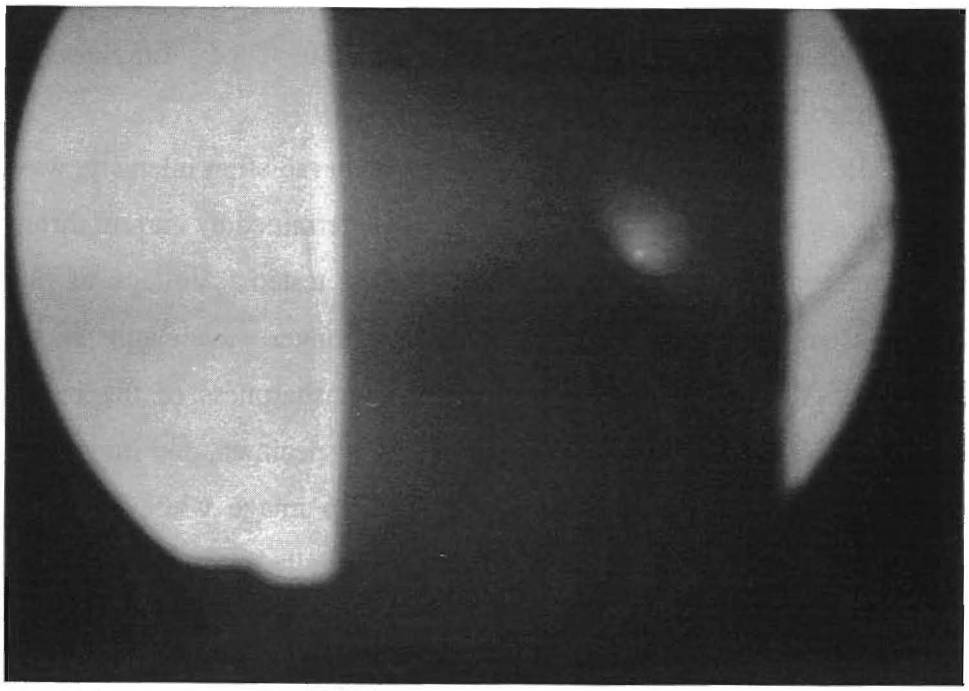

Figure 13. Real-time image of cable-stay specimen subjected to neutron radiography.

Initially, experiments were conducted using 6 in. (152 mm) diameter grout cylinders to determine appropriate energy levels and exposure times for imaging the annular region of grout surrounding the steel cables. Defects were created in two of these samples through the use of ice cubes and dry ice. As the grout set, ice cubes were introduced into the sample in anticipation that the ice would melt and create water filled voids. In a similar manner, dry ice was introduced into another sample with the intent of entrapping gas bubbles to form voids and porosity. Additionally, holes ranging in size from 0.25 in. (6.4 mm) to 0.5 in. (12.7 mm) were drilled into the sides of the cylinders using a masonry bit.

Radiographic film is classified according to speed, contrast, and graininess. The grain size, or graininess of the film, has a significant effect on the exposure rate and resolution of the film. Film speed is expressed in terms of the reciprocal of exposure time and is based on exposure times required to obtain a corresponding transmission density obtained for one selected film type. The speed of the selected film is arbitrarily assigned a value of 100, and the speeds of other film types are expressed as a percentage relative to this one. Two types of radiographic film were tested in this initial investigation: type 1 and type 2. Type 1 film has an extremely fine

grain, very high contrast, and has an intermediate speed of 50. Type 2 film has very fine grain, high contrast, and medium speed of 100.

Variables affecting a radiographic film are primarily radiation intensity, wavelength, and time of exposure. As mentioned previously, intensity is determined by current through the X-ray tube and the distance of the tube from the object being tested. Voltage of the X-ray tube determines the wavelength range. For a given intensity, longer wavelengths expose film more than shorter wavelengths. In addition, the geometric unsharpness of the image is directly proportional to the focal spot size and the thickness of the specimen, and inversely proportional to the source-to-film distance (SFD). Achieving a sharp image while maintaining realistic exposure times must therefore involve compromises. Generally, to obtain good image contrast, it is best to use the lowest tube voltage that gives good penetration and increase tube current as much as is practical. To the extent that physical constraints will allow, it is also helpful to maximize the SFD as long as exposure times remain reasonable.

Based on radiographs obtained from a parametric study of the grout cylinders, the experimental parameters which produced the best images were as follows:

- film type 2
- source-to-film distance = 36 in. (914 mm)
- focal spot size = 3.0 mm x 3.0 mm
- tube voltage = 120 kv
- tube current = 30 mA

The appropriate exposure time varied with the thickness of the specimen. For a thickness of 6 in. (152 mm), the optimal exposure time using the parameters listed above was found to be approximately 9 min.

Due to the circular geometry of the cable stays, the thickness of the specimen varies continuously through the cross section. For this reason, for a given exposure time, only a small portion of a given radiograph provides a sharp image. The other areas are either under or overexposed. To compensate for this effect and, thereby, expand the useful portion of the radiograph, equalizing blocks were fabricated from portland cement grout. As shown in Figure 14, these blocks were fitted around the circumference of the cable-stay specimens to provide uniform thickness across the cable and thus uniform exposure of the film. These blocks for the

4.5 in. (114 mm) and 5.0 in. (127 mm) diameter cable-stay samples varied in thickness in order to provide a constant depth of 6 in. (152 mm).

Since X-rays of sufficiently high energy to penetrate through the steel strands would lead to difficulty resolving small defects in the grout when using conventional film radiographs, a low-energy X-ray beam was directed along a chord through the outer grout layer. In this manner the location of a defect could be more readily identified.

Figure 14. Exposure equalization blocks for X-ray inspection.

Using the parameters determined previously, the cable-stay samples were radiographed as shown in Figure 15. It was concluded from the results of these experiments that the ability to detect defects in the grout was dependent on the position of the hole within the grout layer. While defects of sufficient size are detectable when centered in the grout layer, defects adjacent to the cables could be obscured by energy scattered by the steel cables. Since flaws adjacent to the steel strands are critical in terms of their corrosion-causing potential, it was essential that such defects be detected. For this same reason, it was also desirable to be able to inspect the grout within the cable bundle for similar types of defects. Therefore, in order to more accurately detect

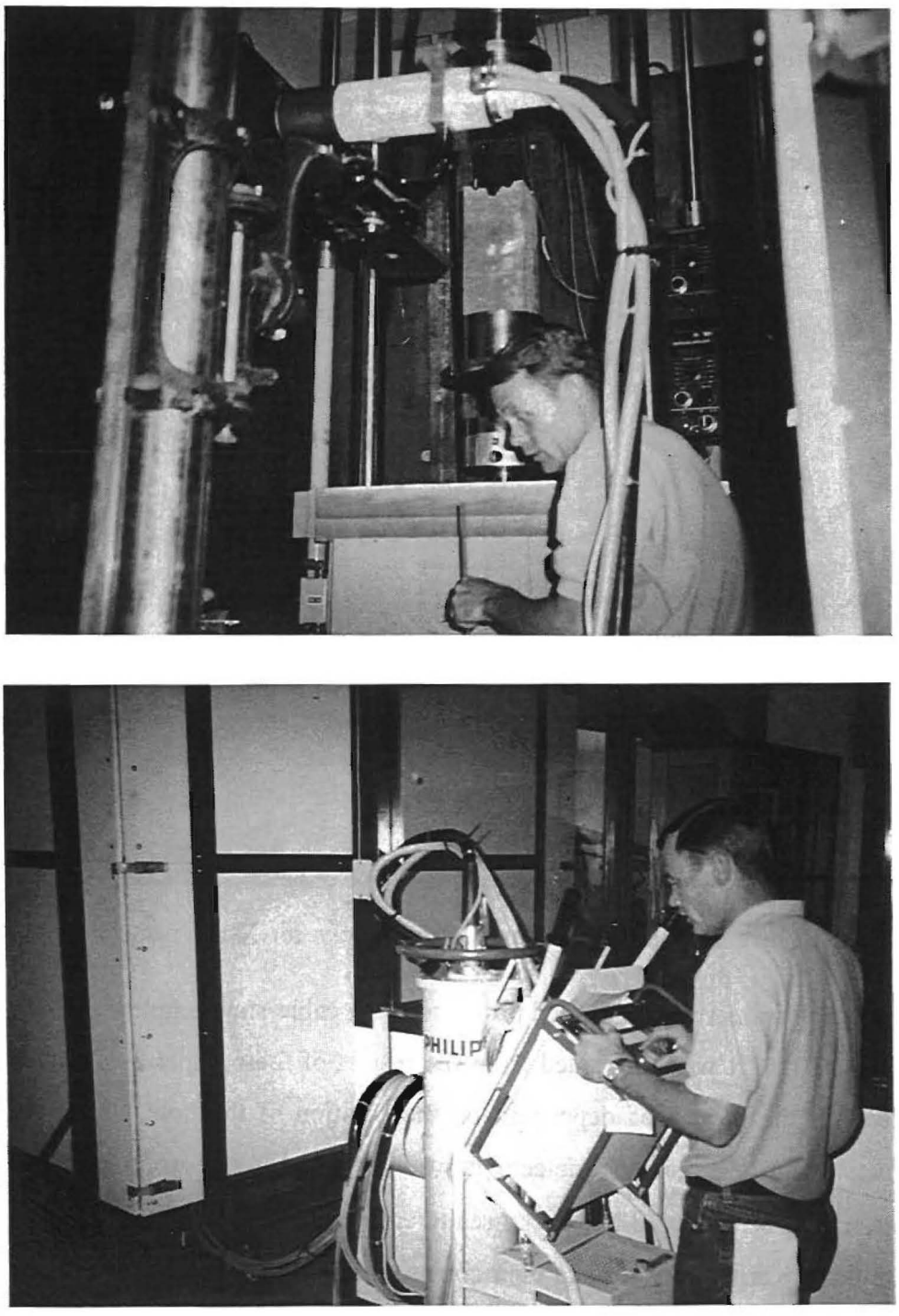

Figure 15. X-ray inspection of cable-stay specimens.

and characterize voids, both outside and inside the steel cable bundle, the emphasis of the radiographic laboratory investigations was redirected toward computed tomography.

Computed Tomography

Simply stated, a tomograph is a cross-sectional image or picture of a slice of an object. Computed tomography utilizes scatter data from radiographic scans obtained at a larger number of orientations of source, object, and receiver. The source and detector are moved in each scan plane as shown in Figure 16. The scatter data are digitized, stored, and analyzed, and the results appear as a reconstructed image of the cross section. In this procedure, a well collimated beam of X-rays or gamma rays is synchronized with a radiation detector. The image plane may be scanned with a fan-shaped beam, in which case the radiation detector is an array or bank of transducers. The projection data are stored in a computer and one of several image reconstruction methods is used to develop a picture of the cross section.

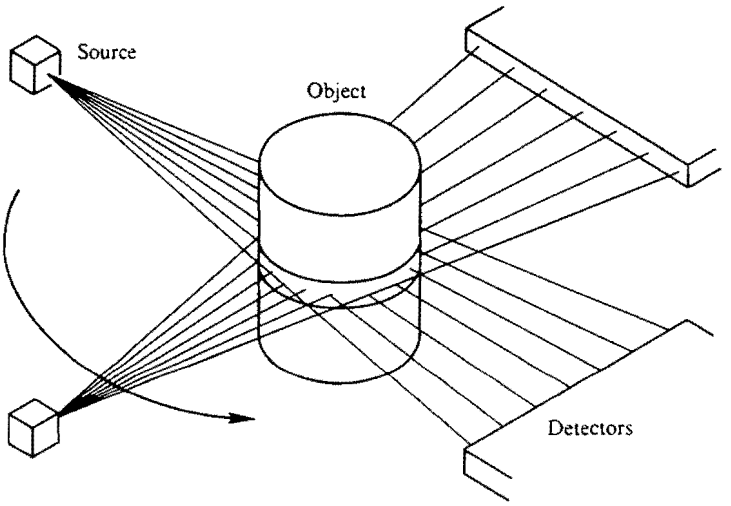

Figure 16. Scanning setup for computer-aided tomography (41).

The preliminary evaluation regarding the feasibility of inspecting the cable stays with computed tomography (CT) was conducted at the TEES Engineering Imaging Center located at

Texas A&M University. The initial experiment, utilizing a 120 keV X-ray machine shown in Figure 17, was performed on a polyethylene-sleeved grout sample without steel strands. As shown in Figure 18 (a), this technique was very effective not only in locating all of the manufactured defects, but in characterizing their shape and size as well. In addition, an unexpected water-filled void, which is believed to have originated during the pressure grouting operation, was also discovered during the CT procedure (see Figure 18 (b)). However, subsequent inspection of an actual cable-stay sample was ineffective. This was attributed to a beam-hardening phenomenon precipitated by the polychromatic nature of the X-ray source and/or scatter from the steel strands (see Figure 19).

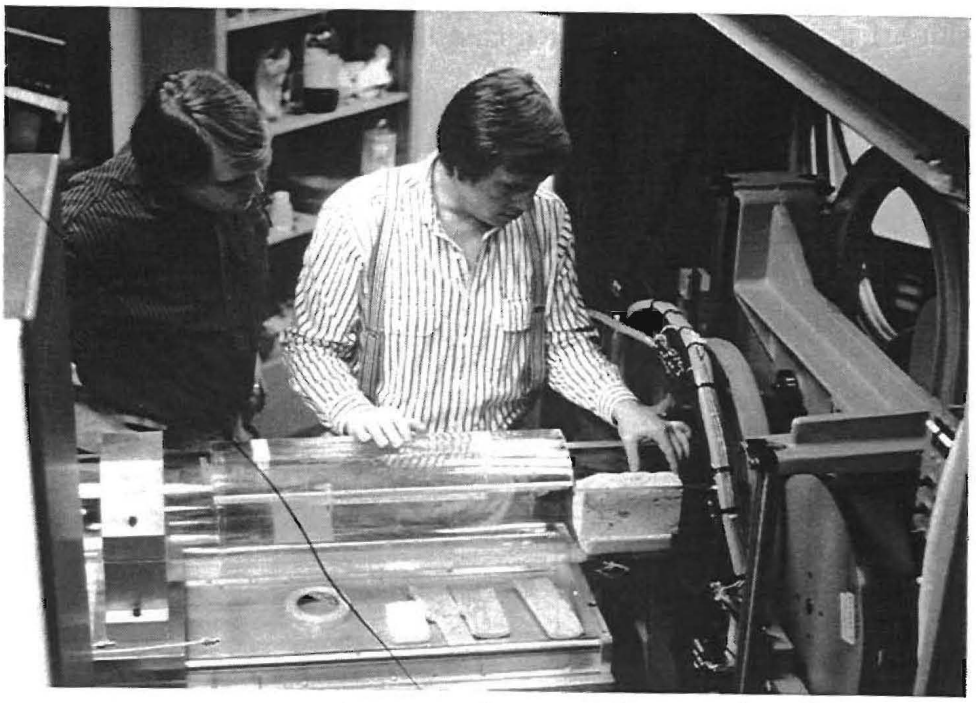

Figure 17. Initial computed tomography scanning setup.

It was theorized that these problems could be overcome by using either a monochromatic gamma-ray source or a higher energy X-ray source which would be more penetrating and thus produce less scatter. However, there was some concern that the energy levels required to penetrate several inches of steel cable would not provide the resolution necessary to assess the

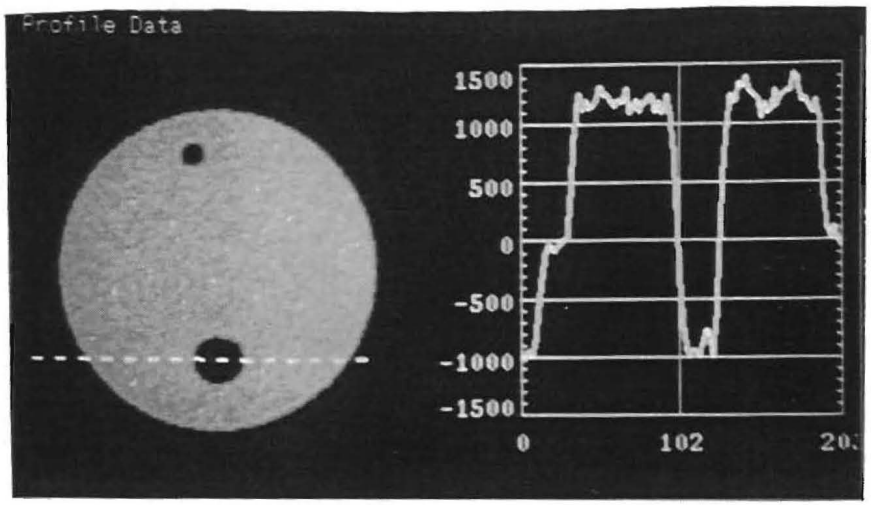

(a) manufactured defect

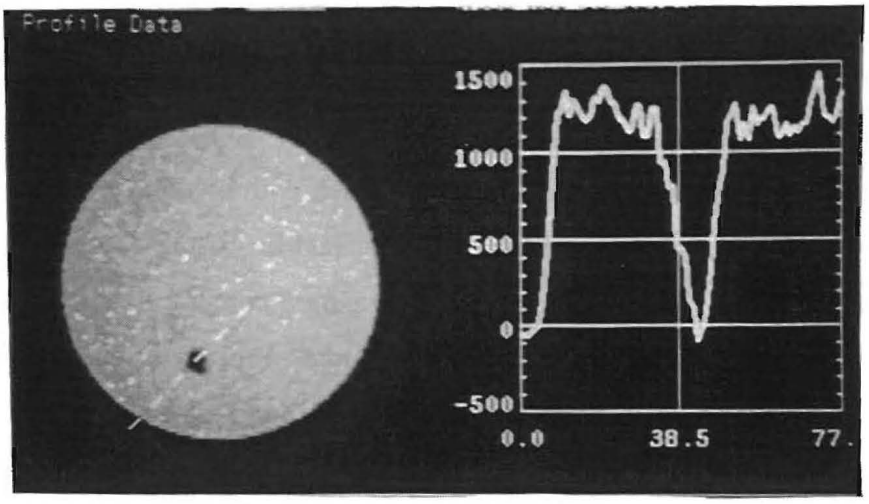

(b) water-filled void

Figure 18. Tomographs of grout-filled polyethylene pipe.

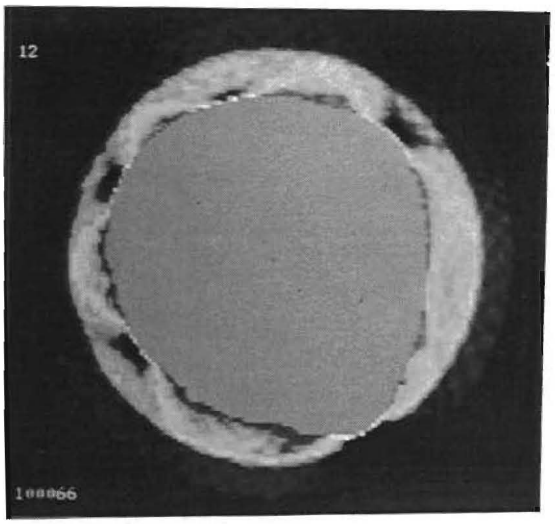

Figure 19. Tomographs of cable stay showing energy scatter off steel strands.

quality of the grout among the individual steel strands. These and other problems were further investigated as described below.

X-Ray Source

The 4.5 in. (114 mm) O.D. cable-stay specimen with manufactured defects was imaged by Scientific Measurement Systems (SMS), Inc., located in Austin, Texas. Several scans were obtained at various cross sections along the cable using a computerized industrial tomographic analyzer with a 420 kV constant potential X-ray source. Initially, a high resolution mode was used to investigate the feasibility of inspecting the cable and to assess the resolution requirements for detection of various flaw sizes. Figure 20 shows the results of one of these high-resolution scans taken at a cross-section just below the upper cap of the cable sample. The two manufactured defects present in this slice plane, namely, 0.25 in. (6.4 mm) and 0.375 in. (9.53 mm) diameter holes, are clearly visible, as are the individual wires of each cable strand. Several glass tubes, ranging in size from 0.04 in. (1 mm) to 0.16 in. (4 mm) in diameter, were placed

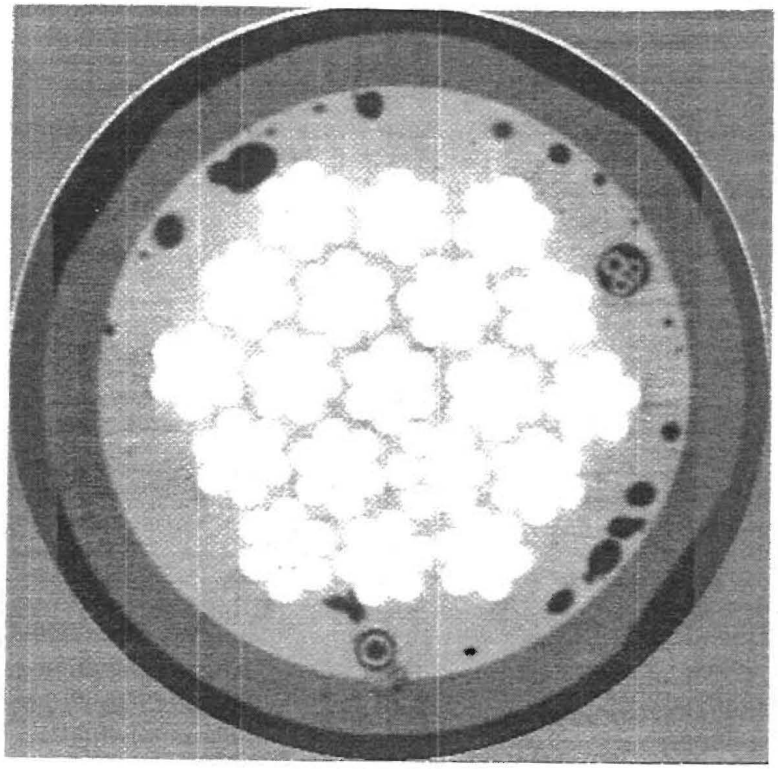

Figure 20. High-resolution scan of 4.5 in. (114 mm) cable stay below end cap using X-ray source.

within the longitudinally drilled holes in an effort to determine minimum flaw size resolution. It was determined that voids smaller than 0.04 in. (1 mm) in diameter were discernable at this level of resolution. Also obvious in Figure 20 are numerous air-filled voids that were trapped under the end cap during the grouting operation.

Based on the results of the high-resolution images, it was determined that a low-resolution scan would provide adequate resolution for this application. For verification of this hypothesis, several low-resolution scans, with imaging times from 1 to 4 min, were made at the same cross sections as the previous scans. The results of one of these low-resolution scans is shown in Figure 21. Although the level of noise was slightly increased, the level of resolution was more than satisfactory, and voids as small as 0.04 in. (1 mm) in diameter were still detectable.

Another problem addressed with this series of scans was the determination of content, i.e., whether a void or defect was air or water filled. Although voids of any type are undesirable, those containing bleed water would be particularly detrimental to the cable due to the high

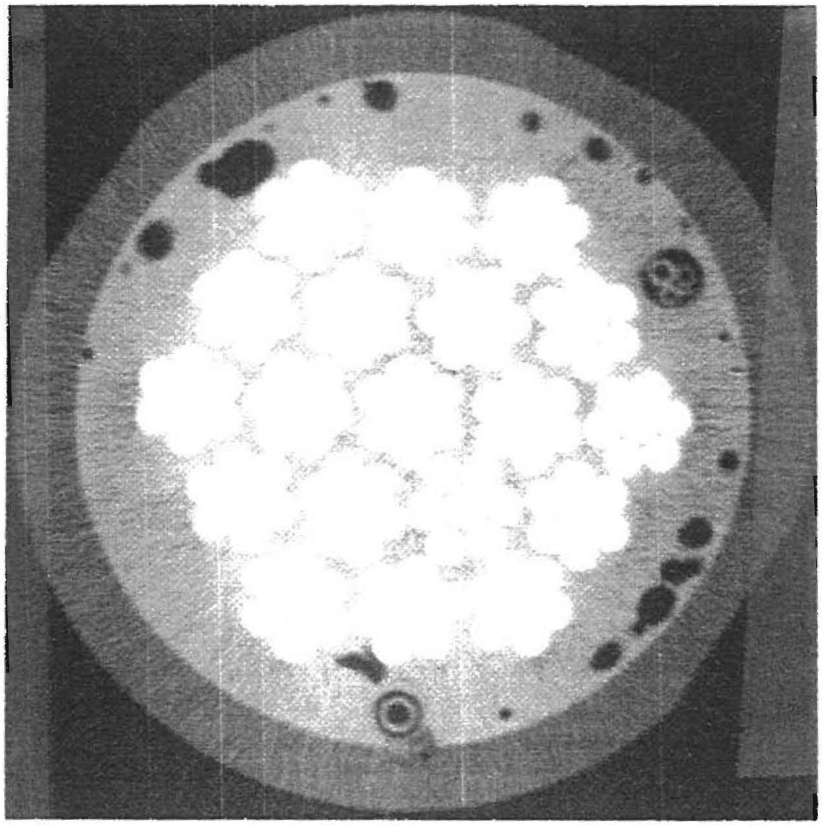

Figure 21. Low-resolution scan of 4.5 in. (114 mm) cable below cap using X-ray source.

probability of corrosion. In additional scans, both air-filled and water-filled glass tubes were inserted into the manufactured holes. Based on the results of a low-resolution scan shown in Figure 22 (a), the contents of the voids were differentiable down to a size of approximately 0.08 in. (2 mm) in diameter. Figure 22 (b) shows a closeup of a water and air-filled tube.

Gamma-Ray Source

The same 4.5 in. (114 mm) O.D., 19 strand cable-stay specimen was also analyzed by International Digital Modeling (IDM) Corporation located in Austin, Texas. Scans were taken with an in-house integrated real time inspection (IRIS) system, shown in Figure 23, using an 8 Ci, ^{60}Co isotope. The detector bank consisted of 71 individual detectors, collimated to a 2 mm by 5 mm size. A total of 39 cross-sectional slices were taken through the 12 in. (305 mm) sample, providing over 80% coverage. Two different scanning modes were used to produce the cross-sectional images, ultra-high resolution (UHR) and very-high resolution (VHR). The UHR mode, which has an imaging time of approximately 80 min, effectively increases the number of

a

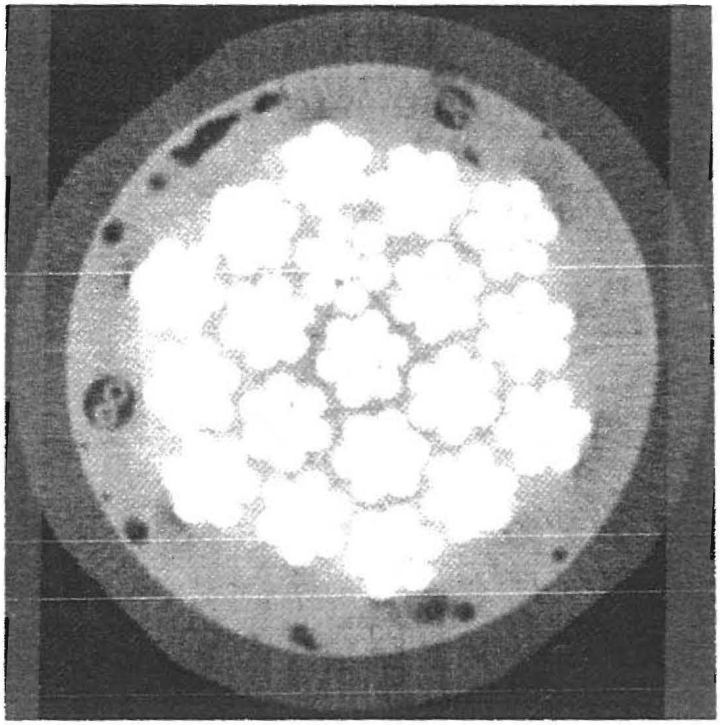

b

Figure 22. Low-resolution scan of cable stay with water and air-filled tubes.

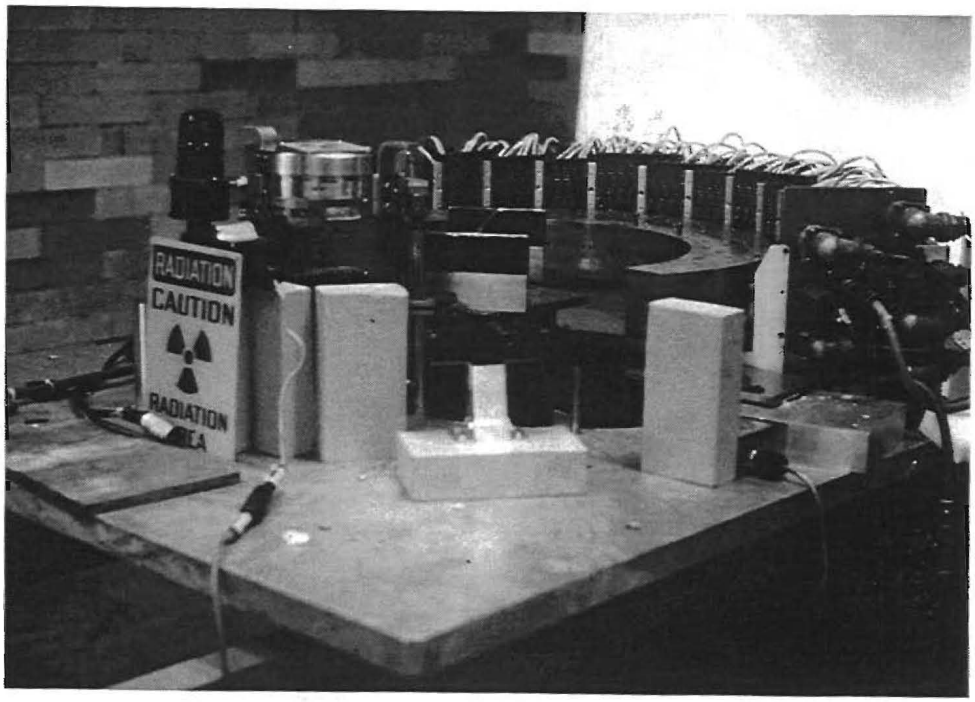

Figure 23. Integrated real time inspection system (IRIS) developed by IDM.

detectors by a factor of 7, whereas the VHR mode, with an imaging time of 40 min, increases the number of detectors by a factor of 5.

As was the case with the X-ray source, all of the manufactured defects, including the smaller glass tubes, were easily found in both scan modes. Numerous voids originating from the grouting operation were found in both the annular region of grout and among the individual steel strands throughout the length of the sample. The voids ranged in size from a minimum of 0.03 in. (0.8 mm) to a maximum of 0.375 in. (9.53 mm) just below the top end cap (see Figure 24). Figure 25 shows a slice taken at 2.6 in. (66 mm) from the top of the cable specimen. As shown in this figure, the manufactured defects are still visible at this cross-section. In addition, voids ranging in size from 0.04 in. (1 mm) to approximately 0.098 in. (2.5 mm) are visible inside the bundle of steel strands. A cross-sectional image through the fill port of the cable specimen is shown in Figure 26. A 0.25 in. (6.35 mm) diameter manufactured defect is visible, as are several small defects in both the annular region of grout and inside the cable bundle.

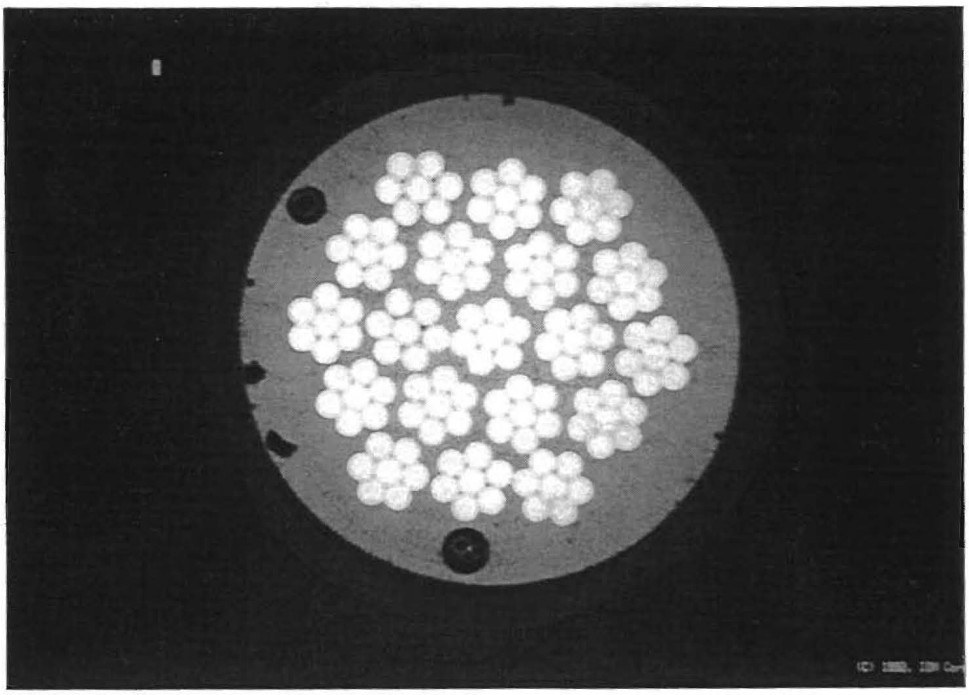

Figure 24. UHR scan of 4.5 in. (114 mm) cable below end cap using gamma-ray source. (C 1992, IDM Corp.)

Figure 27 (a) shows a scan taken in VHR mode, in which an 8.5 in. (216 mm) diameter steel pipe with a 1.1 in. (27.9 mm) wall thickness was placed over the cable-stay sample. The purpose of this experiment was to roughly approximate the effect of the steel guide pipe present in the lower regions of the cable stays. Although the wall thickness of the actual guide pipe is only 0.25 in. (6.4 mm), a larger wall thickness was used to account for the effects of greater thicknesses of steel that must be penetrated on larger cable stays, such as those used on the Baytown Bridge. As mentioned previously, up to 61 strands are used to form a single cable stay, with a maximum of nine cables in the path of the gamma-rays. This corresponds to a maximum thickness of 5.4 in. (137 mm) of steel through which the gamma-rays must penetrate. The steel pipe mentioned above, along with the steel strands present in the cable, had a combined steel thickness of about 5.2 in. (132 mm). Figure 27 (b) is a close of the cable-stay image taken through the steel pipe. As shown in this figure, there was no loss of resolution in the image, and small voids are visible in the annular region of grout.

It should be noted that, in addition to the UHR and VHR scan modes, the IRIS system also has a low-resolution mode with an imaging time of less than 90 sec. This mode is

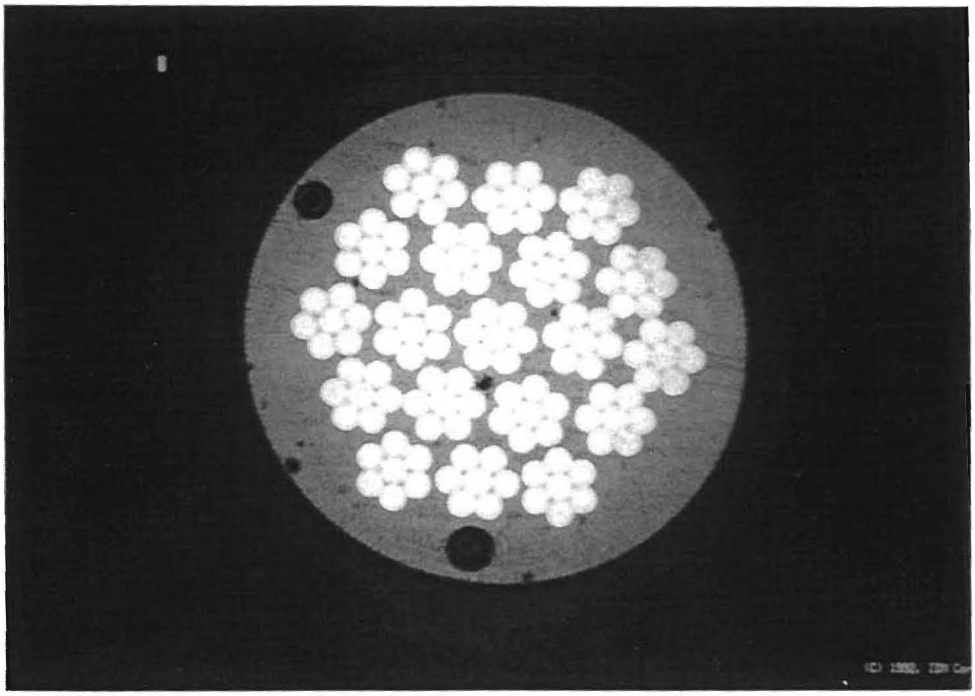

Figure 25. UHR scan of 4.5 in. (114 mm) cable 2.6 in. (66 mm) from top end using ^{60}Co source. (C 1992, IDM Corp.)

purportedly capable of resolving voids in the grout smaller than 0.125 in. (3.18 mm) in size and should provide sufficient resolution for the grout inspection.

Linear Accelerators

One problem that has yet to be addressed is the inspection of the anchorages and saddles through which the cables are attached to the structure. These locations present a unique problem due to limited access, complex geometry, and considerable material thicknesses. As discussed previously, one system that has been effective in inspecting sockets on suspension bridges and anchorages on cable-stay bridges is a portable linear accelerator system, known as the MINAC, which was developed by Schonberg Radiation Corporation (22).

This system has a demonstrated capability of producing exposures through approximately 14 in. (0.4 m) of steel. More recently, radiographs were made through 60 in. (1.5 m) of concrete (22). The MINAC uses accelerating voltages as high as 6 MeV. The 1.5 MeV unit has a total system weight of 250 lb (113 kg) with the accelerator itself weighing only 35 lb (16 kg). The system can be interfaced with real-time imaging systems for filmless radiography. A similar

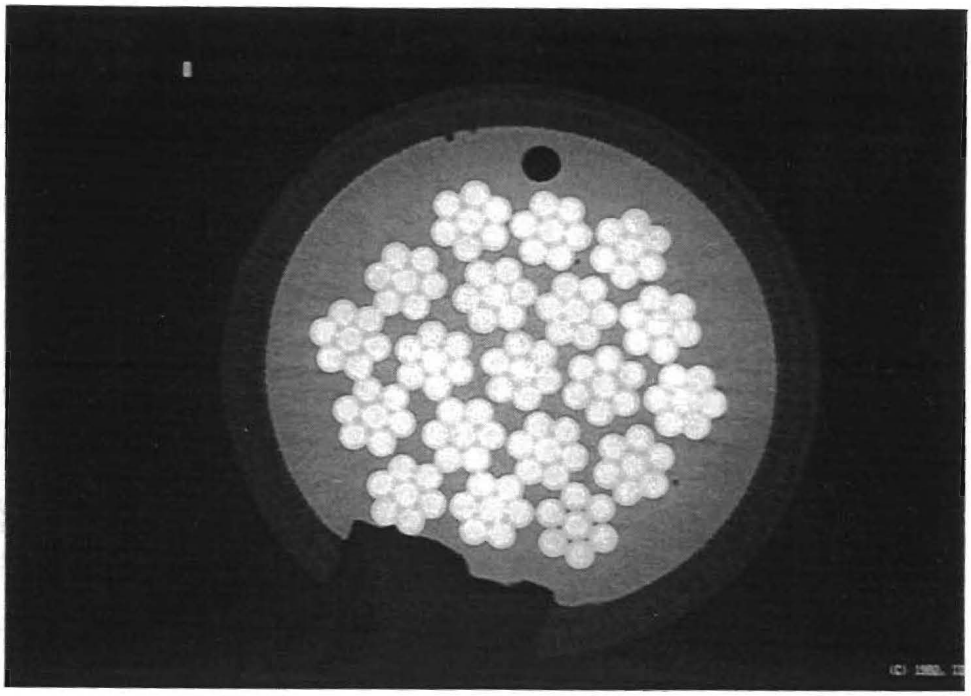

Figure 26. UHR scan of 4.5 in. (114 mm) cable through fill port. (C 1992, IDM Corp.)

device, the Scorpion II, has been developed and tested in France (44). This system incorporates a linear accelerator X-ray source which generates X-rays up to 4.5 MeV. It is mounted on a movable crane and was originally designed for evaluating prestressed concrete bridges. The Scorpion II has been used for examining the quality of grout and concrete and for establishing the location and condition of prestressing cables.

Although these systems were not evaluated in this study, their capabilities and applications have been clearly demonstrated. Such devices have been shown to be capable of inspecting the saddles and anchorages of the cable-stays, and further evaluation was not pursued.

Specifications

As evident from the discussions presented above, computed tomography holds great promise for the detection of grout defects, not only in the annular region, but inside the cable bundle as well. In fact, radiographic techniques appear to be the only feasible choice for inspecting the lower regions of the cable stays in which anchorage details and fire and crash protection measures significantly complicate the geometry.

a

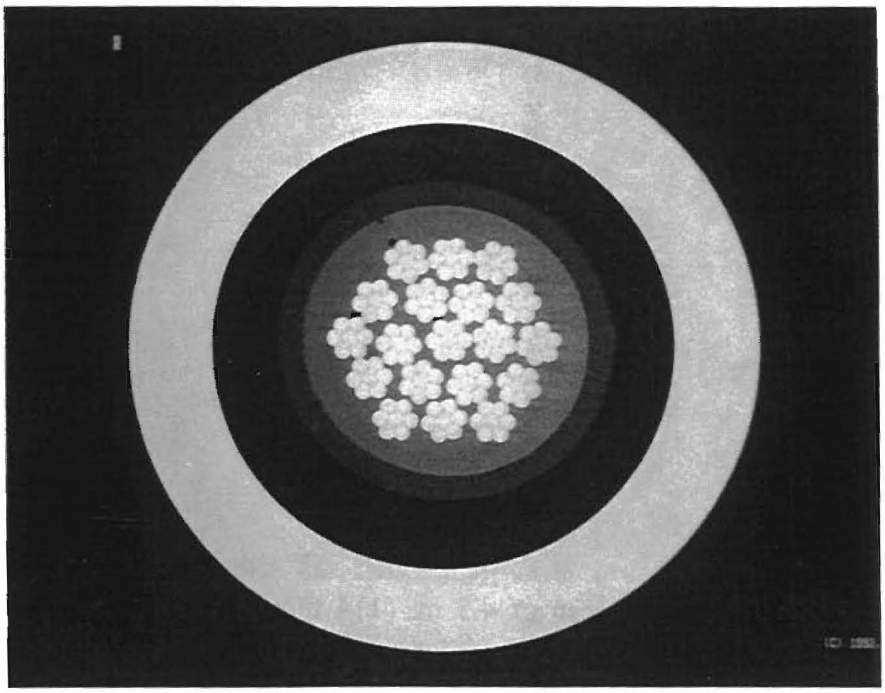

b

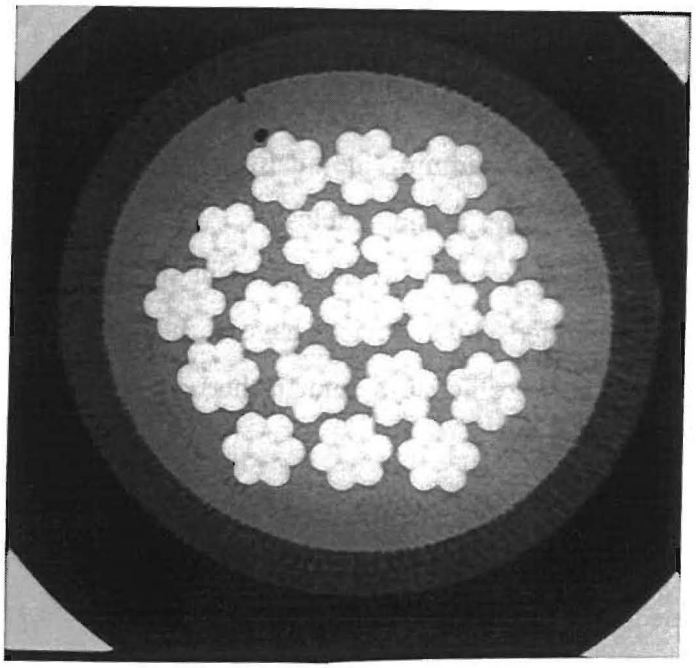

Figure 27. VHR scan of cable through 1.1 in. (27.9 mm) external steel pipe. (C 1992, IDM Corp.)

Although both of the CT inspections described above were performed on fixed in-house machines, the technology for portable field units does exist. IDM Corporation currently has a mobile unit which is transported in a tractor trailer and has been used in the field to scan high temperature and pressure steam lines at operating temperature and pressure. In addition, Miller (42) has developed a portable computerized axial tomography system for field use. The device uses a ^{241}Am source, weighs 53 lb (24 kg), is battery powered (providing eight hours of use without recharge), and fits into two small suitcases. The device has been used for in-field inspection of wooden utility poles with an image time of 8 min (43). Although the energy output of the unit is not suitable for inspection of cable stays, it demonstrates that the technology for such systems exists and can be adapted for such applications.

The limitations of using CT include initial cost, scan time, data storage, and shielding requirements. The estimated cost of adapting current technology and developing a portable device for use on cable stays is on the order of $1,000,000. Such a system would weigh about 600 lb (272 kg) and would require only about 4 to 6 in. (102 to 152 mm) of clearance around the stay. A isotope such as ^{60}Co or ^{192}Ir would be incorporated as the radiation source. Use of a gamma-ray source, as opposed to an X-ray tube, will reduce the overall cost of the prototype and will allow easier field application.

The amount of data storage required clearly depends on the resolution of the image. Very high resolution requires as much as 6-7 Mb of memory per slice. Optical disks, with capacities over 650 Mb, can store up to 100 slices at this resolution. These requirements can be reduced to a more practical limit with the use of low-resolution scans.

Based on the results presented above, and discussions with experts in the field, it appears that a scan time of 1 min/in. (39.4 min/m) of cable may be feasible since the resolution requirements for inspection of the grout are not very demanding. Although such scan times clearly make field inspection of cable stays feasible, complete inspection of all the stays on a bridge would still be impractical. For example, the Neches River Bridge has approximately 20,500 linear ft (6,250 m) of cable stays. At a scan time of 1 min/in. (39.4 min/m), complete inspection would take about 171 days working around the clock.

One solution to this problem would be to use the unit to inspect a predetermined number of cables to form a statistical basis from which the overall quality of the grout or condition of

the stays could be assessed. Another alternative is to use more than one technique to inspect the cables. For instance, an inspection of the main length of cable could be performed using a much faster technique such as ultrasonics. The CT unit could be used to inspect the more complicated lower regions of the stays and could be used as a follow-up technique to perform a more detailed inspection of problem locations identified by the faster system. An evaluation of ultrasonics for use in this regard is described in the following sections.

ULTRASONICS

Theory

The science of ultrasonics utilizes the phenomenon of a propagating mechanical disturbance in matter. Once a mechanical disturbance is generated, the elements of the matter or medium will be deformed and the disturbance is transmitted from one point to the next, thus progressing through the medium in the form of kinetic and potential energies. A typical ultrasonic signal used for NDE inspection is basically a superposition of many waves of various frequencies.

Stress waves in matter can be generated in many ways, such as a disturbance caused by a rifle bullet, a hammer, a laser pulse, or a piezoelectric transducer. Although techniques such as impact-echo methods use more unconventional sources to generate stress waves, the most common technique used in ultrasonic nondestructive testing is pulse excitation by means of a piezoelectric transducer.

The basic operating mechanism of piezoelectric transducers lies in their ability to convert electrical energy to mechanical or stress waves and vice versa. When a high voltage electrical spike strikes a piezoelectric ceramic, it undergoes a mechanical deformation. A thin disk is the most common shape of piezoelectric ceramic used for nondestructive testing applications. With the application of an electrical spike, the disk may either expand or contract in an extensional mode to produce a longitudinal wave. Shear motion for the transverse mode can also be obtained using a different polarization.

A typical ultrasonic transducer consists of a piezoelectric ceramic of specified thickness, which is a function of the designated frequency of excitation, backed by a suitable backing material to provide the necessary damping. The relative impedances of the piezoelectric ceramic and the backing material, together with the impedance of the test or load material, determine most of the probe-related parameters in the ultrasonic inspection process, such as the ring-down time, the net energy that can be transmitted into the load material, etc.

The specific acoustic impedance of a material is given by:

$$z = \rho\ C_1 \tag{2}$$

where:

ρ = density of the material, and

C_1 = dilatational wave velocity in that material.

Based on the relative impedances of the piezoelectric material and the load material, the pressure reflection coefficient (R) and the pressure transmission coefficient (T) at the face of the probe are defined as:

$$R = \frac{Z_2 - Z_1}{Z_2 + Z_1} \quad ; \quad T = \frac{2\ Z_2}{Z_2 + Z_1} \tag{3}$$

where:

Z_1 = impedance of the piezoelectric crystal material, and

Z_2 = impedance of the load material.

Examination of these equations indicates that maximum energy transfer takes place when the impedances of the piezoelectric material and the load material are equal, resulting in 100 percent transmission of the generate stress wave. However, in practice, this equality is seldom achieved, although suitable performance can be obtained by matching these impedances as closely as possible.

There are many types or classifications of waves defined by their specific characteristics. Longitudinal and shear waves are the most commonly used wave forms for ultrasonic NDE. A longitudinal or compressional wave is defined to exist when the direction of particle displacement in the load material is the same as that of the direction of motion of the wave front. Particle displacements for a plane shear wave are perpendicular to the direction of travel of the wave front.

These waves will propagate with a wave speed C and will have a frequency given by:

$$f = \frac{C}{\lambda} \tag{4}$$

where:

C = wave propagation velocity, and

λ = wavelength.

Dispersion of a pulse is said to occur when its shape changes as it travels through a material. One of the important factors that contributes to pulse distortion is attenuation, which is a loss in signal strength through a material. Attenuation is given by:

$$P = P_o e^{-aL}$$

where:

P_o = pressure level at an initial reference location,

P = pressure level at some reference location,

a = attenuation coefficient (Nepers/cm), and

L = distance of pulse travel.

Inspection Methods

The two basic methods of ultrasonic inspection are pulse-echo and through-transmission techniques. The pulse-echo method consists of sending the signal generated by an ultrasonic transducer through the load or test material and receiving any reflected signals with the same transducer. A typical laboratory ultrasonic set-up for a pulse-echo inspection method is shown in Figure 28. Here, the pulser starts the system by firing a high voltage spike, initiating the ringing in the piezoelectric ceramic. At the same time, a trigger pulse starts the display on the oscilloscope. The time base of the display unit corresponds to the distance travelled by the energy through the test material, and the repetition rate represents the firing rate of the pulser. Attenuation controls the overall vertical gain of the received signal. The filtering unit controls the frequency components of the signal. Some ultrasonic units have a built-in auxiliary pre-amplifier to enhance the vertical gain of the signal.

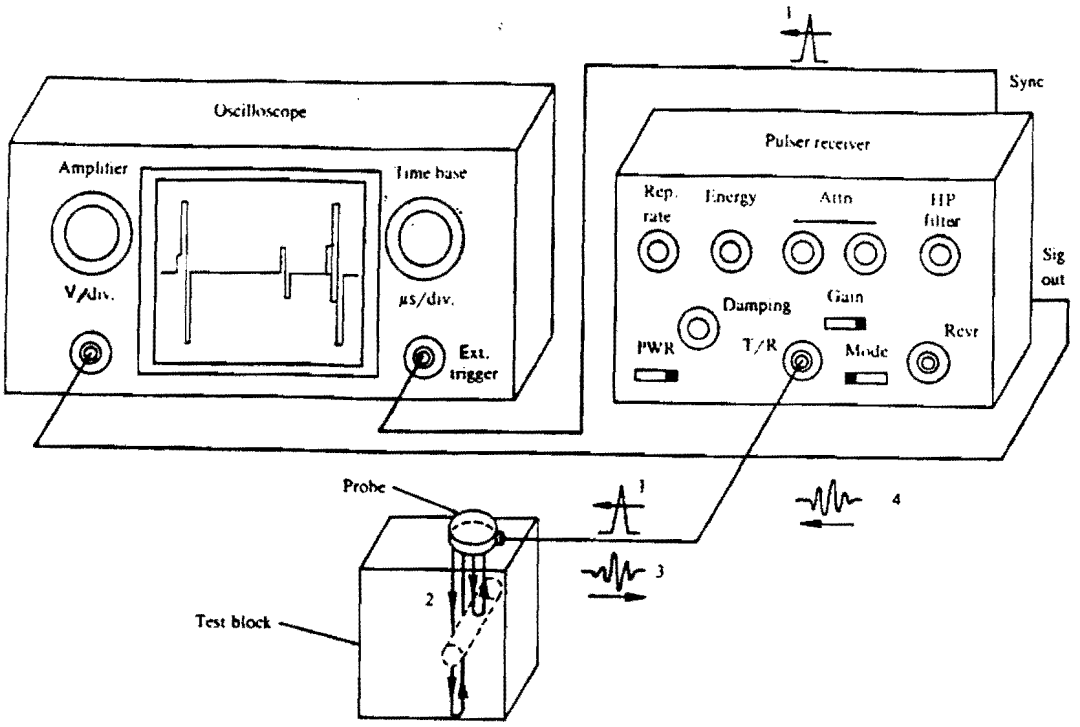

Figure 28. Typical laboratory setup for ultrasonic pulse-echo inspection (38).

The initial pulse at time zero created at the interface between the transducer and the load material is called the main bang. The main bang will appear on the oscilloscope display simultaneously with the voltage spike striking the probe. A back echo will be received as a result of a reflection of the incident signal off the opposite side of the test specimen. When a defect is present, the incident signal will be reflected off of the defect and, due to the shorter travel path, will arrive back at the transducer before the back echo arrives.

The operating principle of through-transmission inspection is very similar to that of the pulse-echo method, except that two ultrasonic transducers are employed at opposite ends of the test specimen. The ultrasonic signal is generated by the sending transducer, transmitted through the test piece, and received by the second transducer. Note that the through-pulse in through-

transmission inspection will arrive in half the time of the back echo in pulse-echo mode due to the direct travel path through the material.

A variation of these methods includes angle-beam inspection wherein the ultrasonic signal is transmitted into the test material at some incident angle rather than normal to the surface. By using angle-beam techniques it is possible to inspect unusual geometries and some areas which are inaccessible with normal beam inspection.

Experimental Analysis

Parallel to the evaluation of radiographic technologies described earlier, a laboratory investigation was conducted to evaluate the feasibility of applying ultrasonic technology to the inspection of the grout layer. The experimental procedure is described below.

It is well known that ultrasonic frequencies in the range of 20 to 300 kHz are best suited for the inspection of concrete due to its highly attenuating nature (24, 25, 27). However, the grout mixture used in the stay cables does not contain any fine or coarse aggregate. Hence, traditional frequencies recommended for inspection of concrete are not necessarily optimal for inspection of the grout within the stays. Using several sets of standard 2 in. (51 mm) grout cubes, and various probes with frequencies ranging from 0.1 MHz to 1 MHz, the optimal frequency was experimentally determined to be 0.5 MHz. This evaluation was based primarily on the level of attenuation and the resolution of the displayed signal.

In order to achieve a sufficiently strong signal, a Panametrics 5058 high voltage pulser-receiver, which offers excitation spikes up to 900 V, was employed. The pulser-receiver unit combines an impulse type pulser with a versatile receiving system. It has the capability of filtering the signal in the required band, and has a built-in preamplifier to enhance the received signal. Other pertinent specifications of the pulser-receiver unit are given in Appendix A.

This pulser-receiver unit was used with two 0.5 MHz, 1 in. (25.4 mm) diameter probes which were designed to be used with high voltage spikes for maximum energy input. Data collection was accomplished with a digitizing oscilloscope and a personal computer-based data acquisition system (PCDAS). This high-speed data acquisition system from General Research Corporation employs a PCTR A/D board and is used for collecting and analyzing transient wave forms.

Initially, there was some concern regarding the ability to transmit energy across the polyethylene/grout interface. Using the experimentally observed longitudinal wave speeds (c_l), material densities (ρ), and specific acoustic impedances (z) shown in Table 2, the power reflection and transmission coefficients at the interface were calculated using the previously defined equations. These calculations showed that approximately 72% of the incident energy would pass through the interface, while the remaining 28% would be reflected back. This demonstrated the potential for successful transmission of a signal through the grout layer, However, if an adequate physical bond does not exist between these two materials because of grout shrinkage, ultrasonic techniques might still be ineffective.

Table 2. Ultrasonic properties of P.E. pipe and grout.

Material	c_l (m/s)	ρ (kg/m^3)	z x 10^3 (kg/m^2-s)
Grout	3,560	1,831	6,517
Polyethylene Pipe	2,160	940	2,030

To initially inspect the integrity of this bond and the transmission of a signal across the interface, through-transmission experiments were conducted on a grouted-filled polyethylene pipe. Results of the experiments verified the integrity of the bond and confirmed that energy could be successfully transmitted through the grout.

Inspection Procedure

Figure 29 shows a typical probe arrangement used for investigating the effect of a defect or void on the ultrasonic energy travelling through the cable-stay sample. Both the transmitting and receiving probes were placed on normal beam polymethylmethacrylate (PMMA) wedges. A digital signal subtraction technique was employed to readily analyze the difference in waveforms obtained from a no-defect control signal and a signal obtained along a path in which a known defect was present. This was accomplished by subtracting the corresponding digitized amplitude data of these waveforms at the same locations in the time domain. This technique was desirable because multiple reflections off of the steel strands obscured the information pertaining

to the defect. The subtraction technique effectively filtered out these extraneous signals and permitted detection of defect in the annular grout layer.

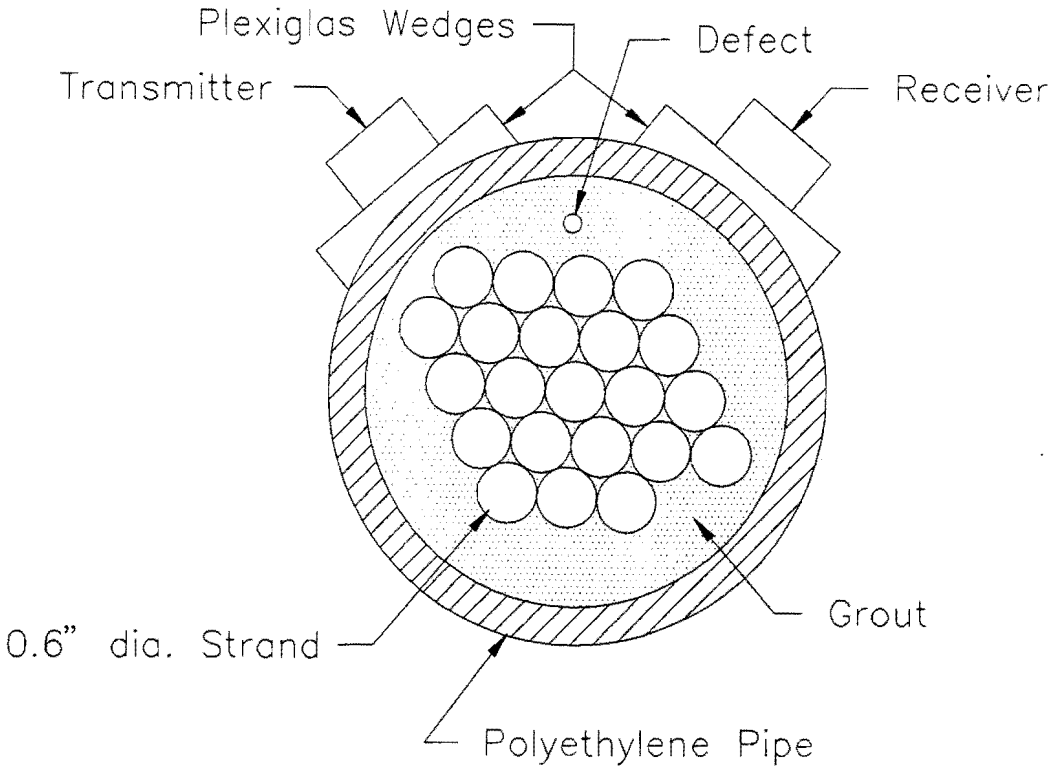

Figure 29. Probe arrangement for inspection of grout.

Results

Initially, the response of the ultrasonic system to the presence of defects was assessed using a 4.5 in. (114.3 mm) O.D. PE pipe which was filled with grout at the Neches River Bridge site as described earlier. The sample was inspected in through-transmission mode at locations where manufactured defects existed and where the grout was defect free. The defect consisted of a 0.5 in. (12.7 mm) diameter hole drilled longitudinally from the end of the sample beneath the PE pipe. Figures 30(a) and 30(b) show two independent signals obtained at different locations on the pipe for the no-defect condition. As shown in Figure 30(c), the difference between these two signals has essentially zero amplitude. Signals corresponding to locations with and without a defect present in the path of the ultrasonic pulse are shown in Figures 31(a) and

31(b), respectively. As is expected, the signal obtained with the hole located directly beneath the transmitting transducer is much stronger than a similar signal for a defect-free condition due to reflection of energy off the drilled hole toward the receiving probe. The difference between these two signals is shown in Figure 31(c), which clearly shows the effect of the hole when compared to Figure 30(c).

Upon successful application of the ultrasonic test equipment, numerous experiments were conducted on both the 4.5 in. (114 mm) O.D. and 5.0 in. (127 mm) O.D. cable-stay specimens. For each of these experiments, ultrasonic signals were obtained in through-transmission mode for a defect-free chord through the grout layer, and for a path encountering a defect between the two probes. Such signals were obtained, subtracted, and analyzed for longitudinal and radial holes of various diameters. Repeatability trials were performed at each of the probe locations to assure that representative signals were obtained. The repeatability of these experiments was found to be good, with the difference between two or more similar signals being negligible.

Typical waveform displays obtained from an experiment on the 5 in. (127 mm) diameter cable-stay specimen are shown in Figure 32. Figures 32(a) and 32(b) show signals acquired from the defect-free and defect conditions, respectively. The defect in this case was a 0.1875 in. (4.76 mm) longitudinal hole drilled between the PE pipe and the steel cables. Figure 32(c) shows the difference between these two signals. As can be seen from this figure, there is an observable difference between the defect-free and defect conditions. The amplitude of the resulting signal is significantly greater than that obtained from subtraction of the repeatability trials performed on the defect-free area.

The first arrivals in Figures 32(a) and 32(b), observed at approximately 26 μs, have nearly the same shape and amplitude, resulting in a reduced amplitude in Figure 32(c). These arrivals were caused by a direct wave travelling through the grout just beneath the surface of the PE pipe. If the defect were adjacent to the PE pipe, the signals arriving in this time frame would show distinct differences. The large arrival at approximately 34 μs in Figure 32(b) is due to the reflection of ultrasonic energy from the hole, and a significant spike shows up at this time in the subtracted signal.

Similar signals for the same cable sample with a 0.25 in (6.4 mm) longitudinal hole are shown in Figure 33. As shown in Figure 33(b), the defect signal has a smaller amplitude than

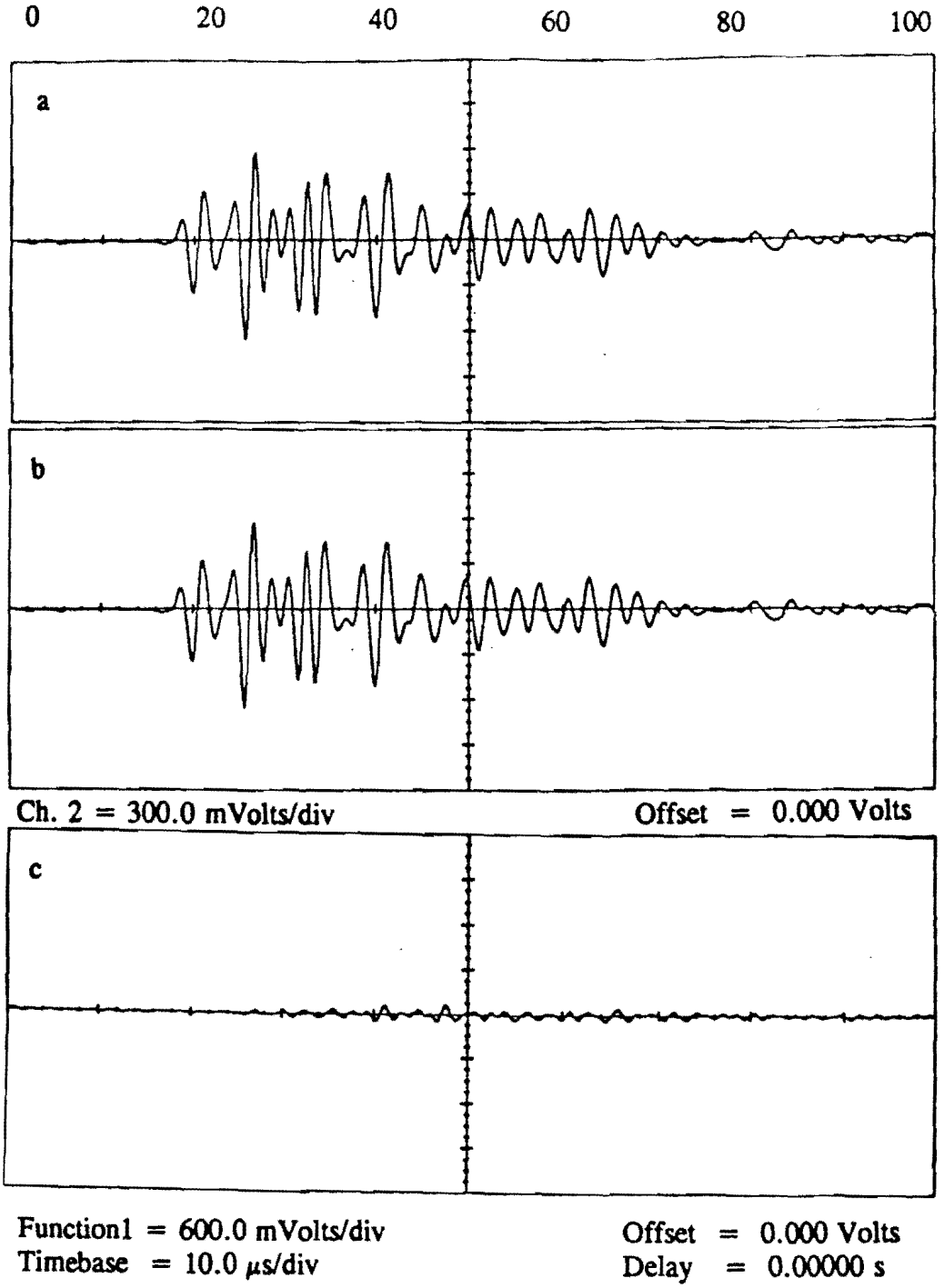

Figure 30. Ultrasonic signal display from grouted sample, (a) trial-1 with no defect, (b) trial-2 with no defect and (c) difference.

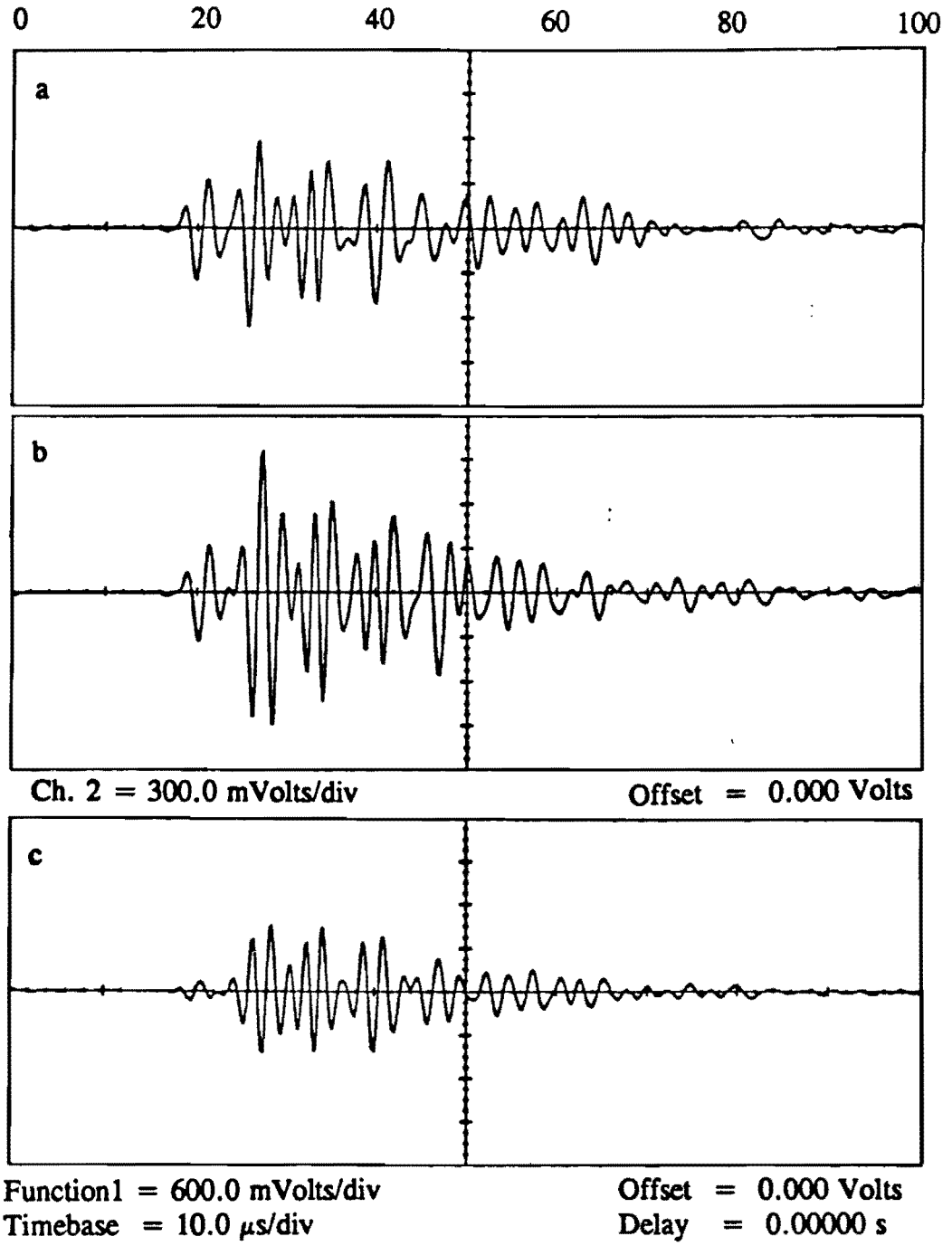

Figure 31. Ultrasonic signal display from grouted sample for 0.5 in. longitudinal hole, (a) no defect, (b) with defect, and (c) difference.

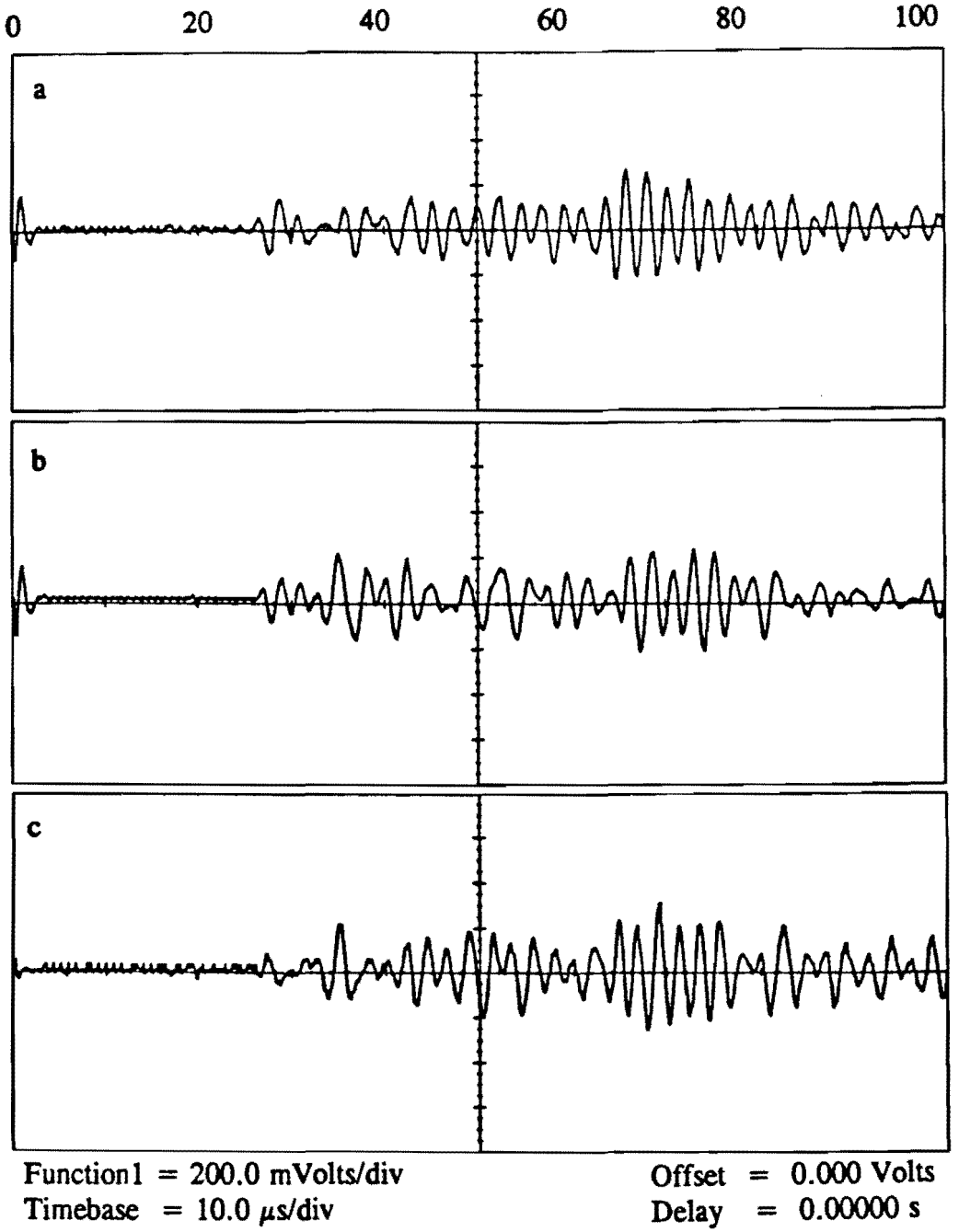

Figure 32. Ultrasonic signal from 5 in. (127 mm) cable stay with 0.1875 in. (4.7 mm) longitudinal hole, (a) no defect, (b) with defect, and (c) difference.

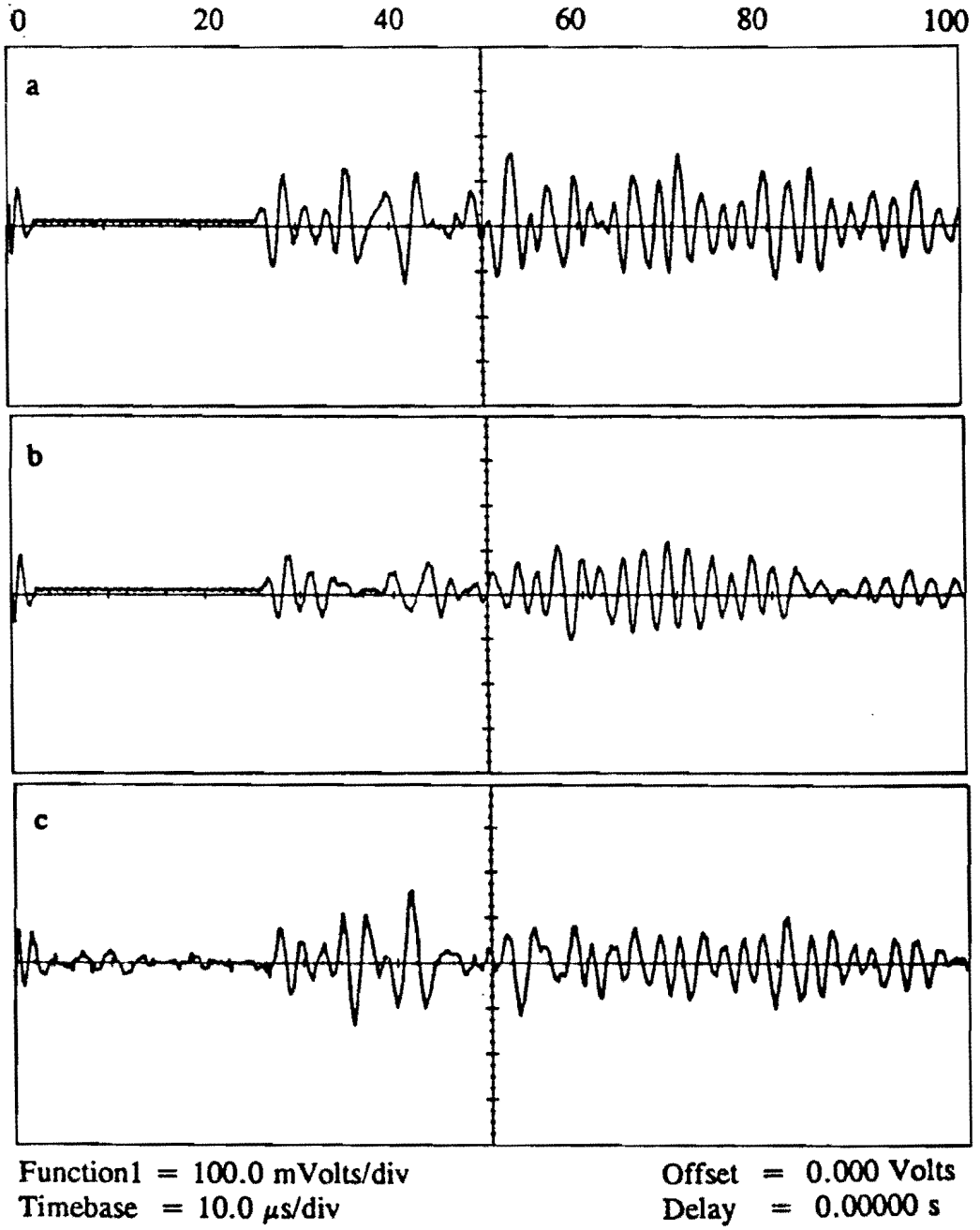

Figure 33. Ultrasonic signal from 5 in. (127 mm) cable stay with 0.25 in. (6.4 mm) longitudinal hole, (a) no defect, (b) with defect, and (c) difference.

that shown in Figure 32(b). This is attributed to greater dispersion of the ultrasonic signal caused by the larger defect.

A more marked difference can be seen in Figure 34 for a 0.25 in. (6.4 mm) radial hole drilled in the side of the 5 in. (127 mm) O.D. cable-stay sample. Once again, the low amplitudes observed in Figure 34(b) can be attributed to the hole (which extends almost to the steel cables) preventing energy from passing through the grout to the receiving probe.

In addition to the time domain, frequency content of these signals was also analyzed. In instances where a defect was present, it was noted that the higher frequency components of the signal were damped out and the central frequency was reduced significantly. It is theorized that the lower frequency components, having larger wavelengths, were able to traverse the defect, while the higher frequency components were scattered.

Summary

These experimental results clearly confirmed the potential for using ultrasonic techniques to inspect cable stays and detect anomalies in the annular region of grout between the PE pipe and cables. The digital signal subtraction technique was found to be particularly useful in performing the inspection trials since the presence of a defect can be readily identified when compared to a defect-free reference signal. Although this method is limited to detecting voids in the outer annular region of grout, and is not useful for detecting grout defects between the steel stands, it was felt that the potential advantages of a high-speed ultrasonic inspection unit that could inspect the annular region of grout outweighed this limitation. Therefore, based on the results of this feasibility study, a multi-probe inspection scheme, utilizing rolling contact transducers, was conceived and evaluated as described in the following section.

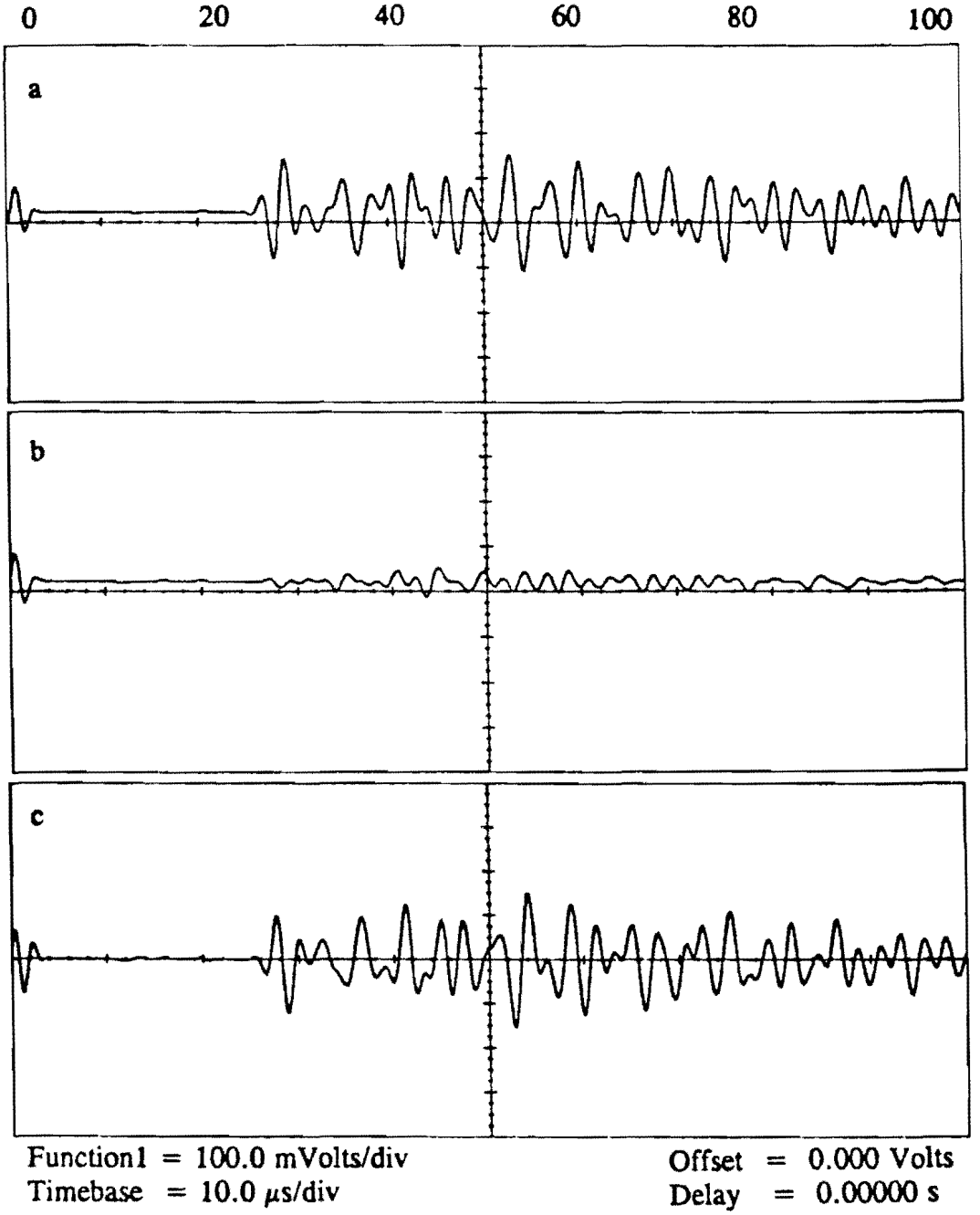

Figure 34. Ultrasonic signal from 5 in. (127 mm) cable stay with 0.25 in. (6.4 mm) radial hole, (a) no defect, (b) with defect, and (c) difference.

PROTOTYPE ULTRASONIC SYSTEM DEVELOPMENT

Laboratory investigations of actual cable-stay specimens demonstrated the feasibility of applying ultrasonic principles to the inspection of the protective grout layer. However, since static coupled probes, such as those used in the initial inspection trials, would not be suitable for practical field unit, a more sophisticated inspection system was devised. The recommended system incorporates rolling contact transducers in a multi-wheel arrangement around the circumference of the PE pipe. The feasibility of such a system was investigated by constructing a partially configured prototype unit as discussed below.

Prototype Design

It was not within the scope or budget of this study to design and construct a fully operational field inspection unit. However, as mentioned above, a partially configured system was constructed and used to evaluate the feasibility of using rolling transducers to inspect the cable stays.

The prototype unit, shown in Figure 35, employs two ultrasonic wheels spaced 72 deg apart. As shown in Figure 35, the wheels are mounted to an aluminum support frame which consists of two end rings and several cross beams. The rings have an 18 in. (457 mm) inner diameter (I.D.), a 20.5 in. (521 mm) outer diameter (O.D.), and are 0.75 in. (19 mm) thick. The cross beams to which the rolling probes are attached are 22.5 in. x 4 in. x 0.75 in. (572 mm x 102 mm x 19 mm) in dimension and are supported at their edges by the rings. Hard rubber wheels are placed on either side of the ultrasonic wheels for positioning and guidance. In the absence of additional ultrasonic wheels, two additional cross beams with hard rubber wheels were mounted to the frame for positioning, stability, and weight distribution. Metal shims or spacers were provided at each wheel locations to permit adjustment of the unit for different diameter pipes. The prototype unit is 22.5 in. (572 mm) in length and weighs approximately 100 lb (45 kg). A fully operational field unit would utilize 5 ultrasonic wheels equally spaced at 72 deg increments to provide full coverage of the cable and would have a total weight of approximately 180 lb (82 kg).

Figure 36 shows a closeup of one of the ultrasonic wheels. The soft neoprene tires conform to the curvature of the PE pipe, permitting good acoustic coupling and minimizing the amount of energy lost through beam divergence. Each wheel contains two 500 kHz transducers.

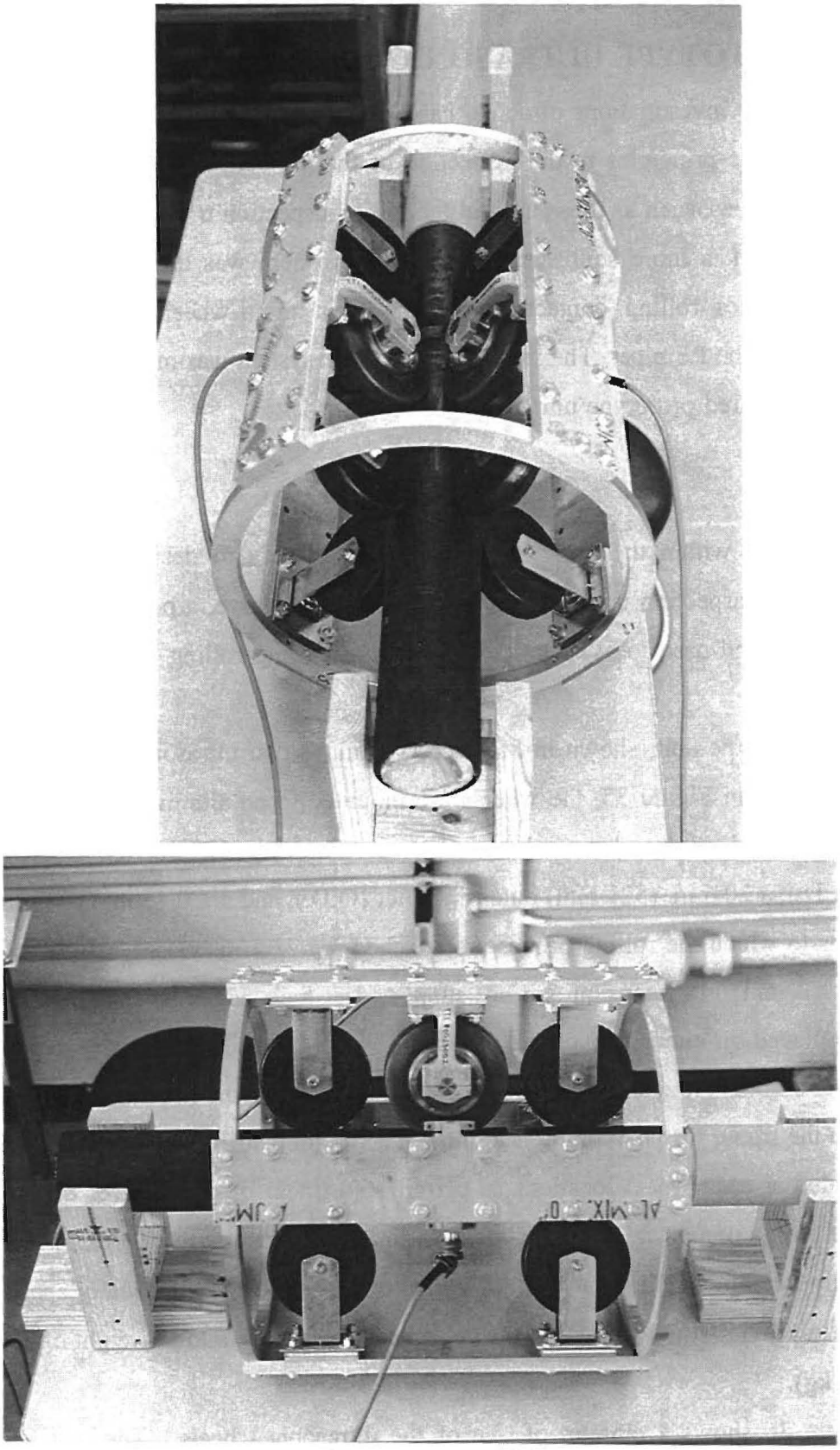

Figure 35. Prototype ultrasonic inspection unit.

Figure 36. Ultrasonic wheel.

One is a 0-deg or normal probe, and the other is a side-looking or angle-beam probe. The angle-beam probe is mounted in such a way as to provide an optimal incident angle of 18 deg at the tire/PE pipe interface (see Figure 37). This determination was made by applying Snell's Law to calculate the angle of refraction at each interface, taking into account the circular geometry of the cable stay.

The prototype unit was designed to operate in through-transmission mode with the ultrasonic wheels inspecting along a chord through the grout as the device travels longitudinally along the axis of the cable. Thus, through proper positioning and sequencing of the probes, full circumferential inspection can be achieved.

Sample Preparation

In order to evaluate the performance of the prototype inspection unit, an 8 ft (2.4 m) cable-stay specimen was constructed according to the specifications of the Neches River Bridge. The specimen consisted of nineteen 0.6 in. (15.2 mm) diameter, 7-wire prestressing strands encased in a 4.5 in. (114 mm) diameter PE pipe. The pipe was grouted from the bottom up at the same angle as the cable stays on the Neches River Bridge. The grout itself was obtained at

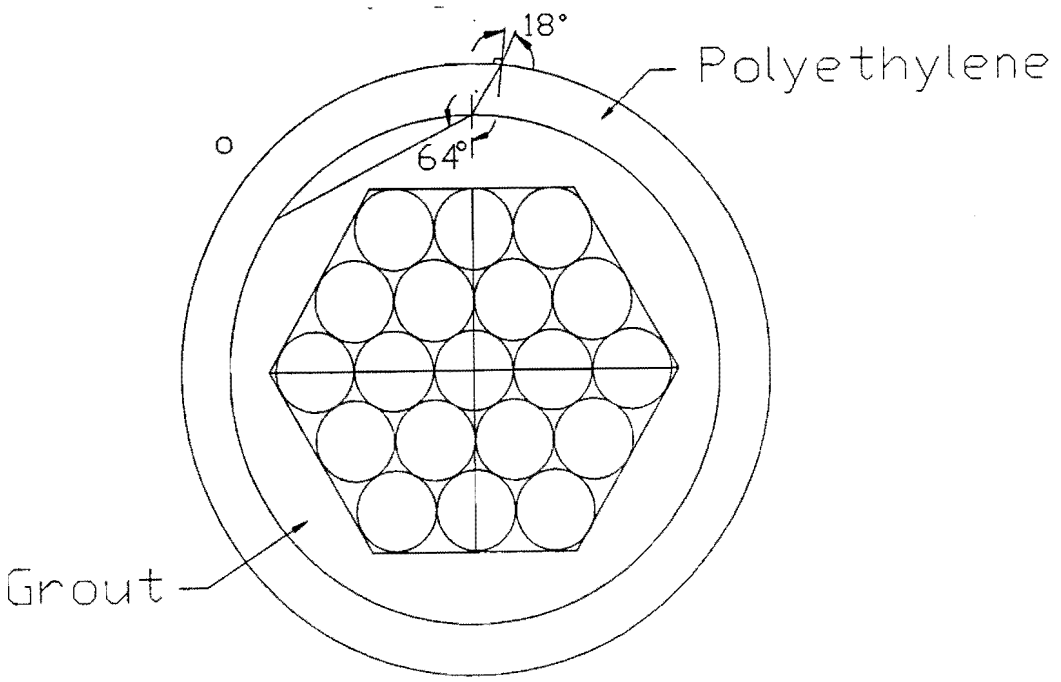

Figure 37. Ray path for angle-beam inspection.

the bridge site and contained the required admixtures to increase flowability, reduce bleed water, and minimize shrinkage. Wooden templates were used to offset the cables inside the PE pipe to simulate the variable grout thickness around the steel strands that is encountered in the field. A representative cross section of the cable-stay specimen is shown in Figure 38.

During fabrication of the stay, numerous air-filled and water-filled defects were manufactured from plastic tubing and placed at various positions along the length and circumference of the cable bundle. The defects ranged in size from 0.125 to 0.5 in. (3.18 to 12.7 mm) in diameter, and 1 to 4 in. (25.4 to 102 mm) in length. In addition, a small spacer wire was twisted around the cable bundle at a 6 in. (152 mm) pitch along a short distance of cable. Table 3 provides a mapping of the size, position, and content of the various defects placed within the stay. Figure 39 shows the cable-stay specimen after grouting.

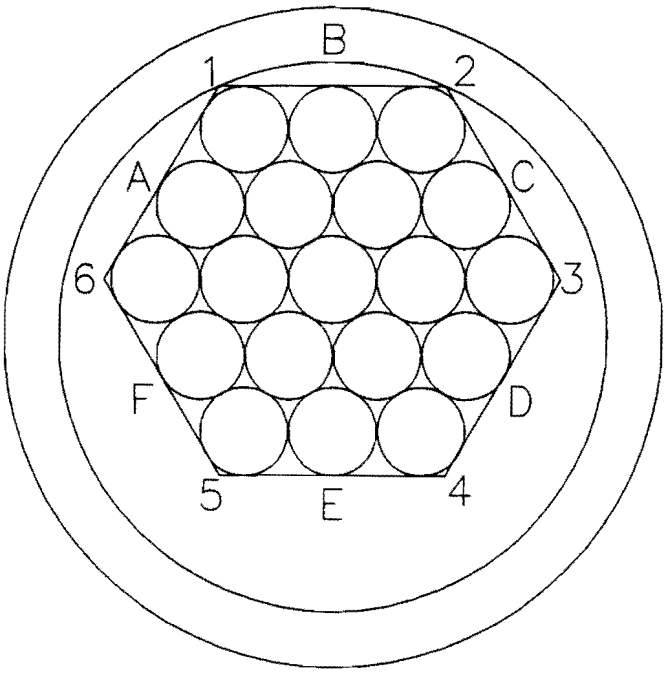

Figure 38. Cross section of cable stay with displaced strands.

Table 3. Defect mapping for cable-stay specimen.

Defect #	Diameter (in.)	Length (in.)	Content	Orientation	Long. Dist. from end (in.)	Face/Corner[1]
1	0.5	2	water	longitudinal	15-17	F
2	0.5	2	air	longitudinal	15-17	C
3	0.25	2	water	longitudinal	24-26	F
4	0.25	2	air	longitudinal	24-26	3
5	0.5	4	water	longitudinal	31-35	E
6	0.5	4	air	longitudinal	38-42	E
7	0.125	1	water	transverse	44	F
8	0.25	2	air	transverse	20.5	D
9	0.5	1	water	transverse	48	D
wire	0.125	6" pitch	--	spiral wrap	43-65	--

[1] Refer to Figure 38.

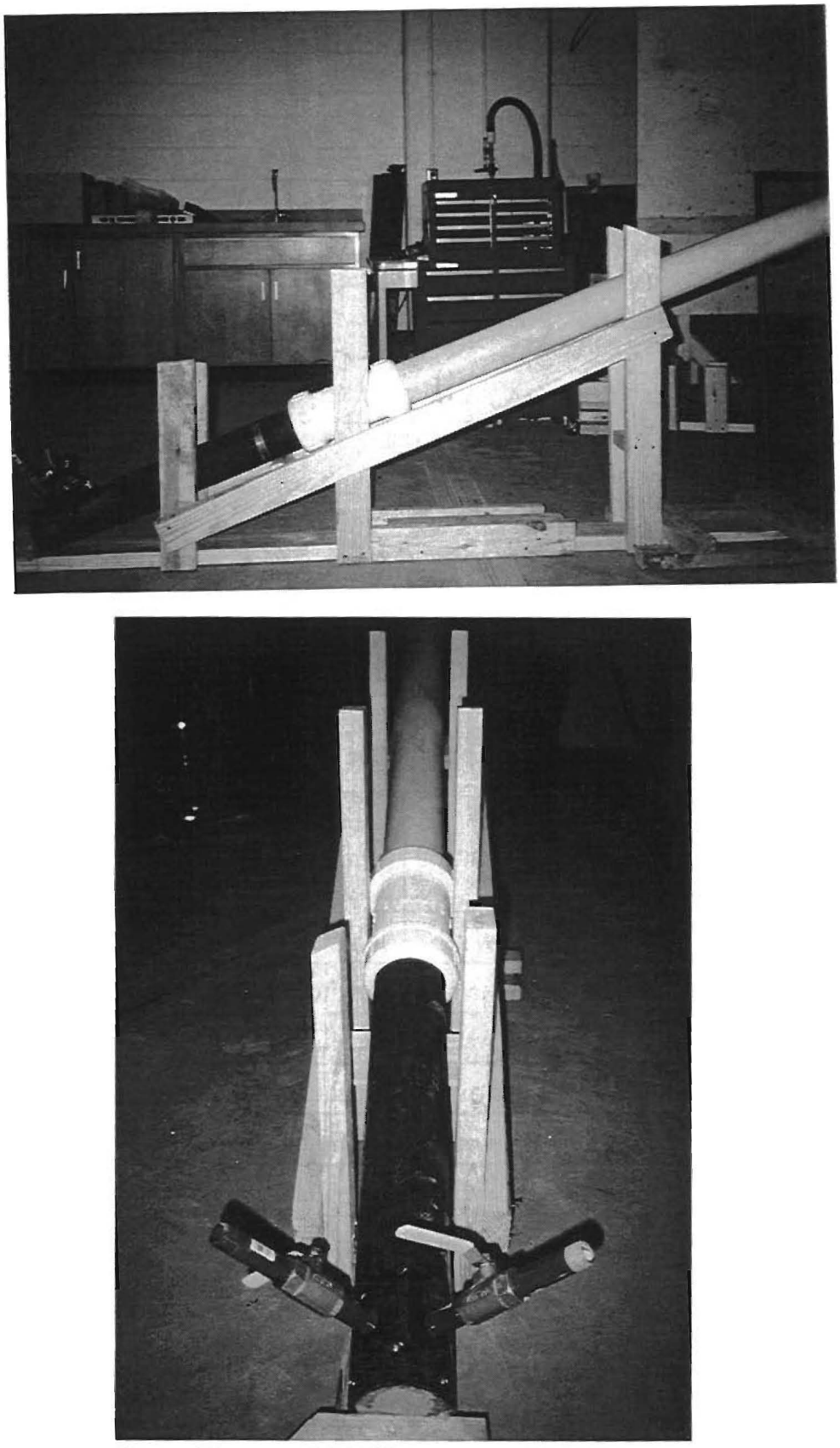

Figure 39. Inclined cable-stay sample after grouting.

Laboratory Investigation

For purposes of conducting laboratory experiments, the cable specimen was supported on blocks so that the inspection carriage was free to slide along the cable (see Figure 40). The wheels were operated in through-transmission mode using both the normal and angle-beam probes. A preliminary investigation indicated that the angle-beam transducers provided better signal transmission across the grout layer, and they were subsequently used in the remainder of the laboratory experiments.

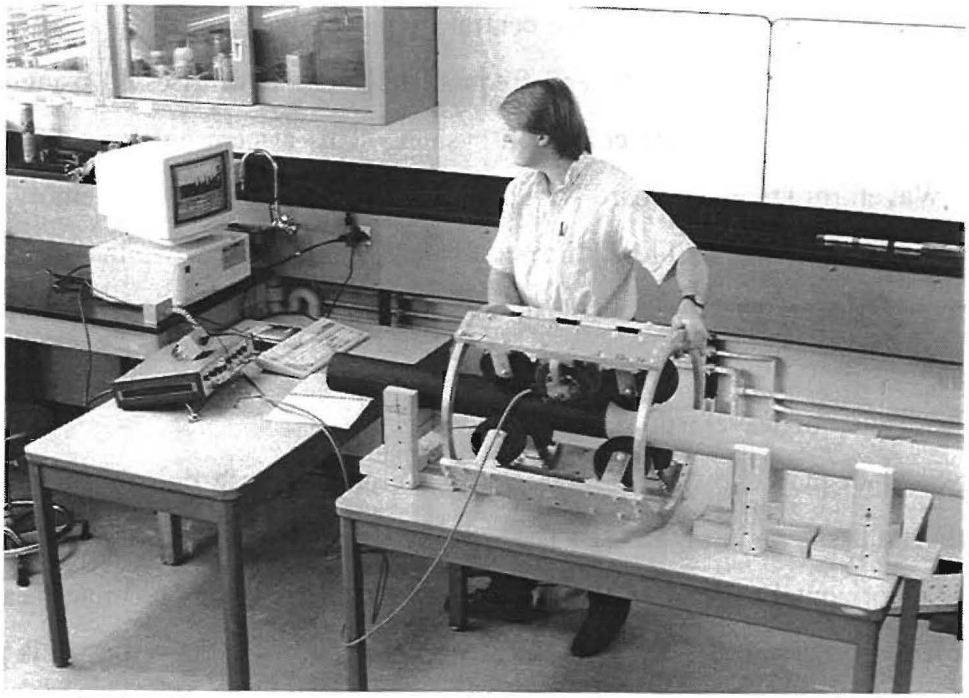

Figure 40. Laboratory setup for ultrasonic inspection carriage.

Numerous inspection trials were performed on the cable-stay sample. An appropriate inspection path was marked for each of the manufactured defects identified in Table 3. The signals received through the grout layer were stored at 1 in. (25.4 mm) increments as the unit was moved along each of these inspection paths. A water/glycerin mixture was used as a couplant.

Successive signals along each inspection path were then subtracted from each other and analyzed to assess whether or not a defect was detected. A moving reference was used in order to account for any gradual changes in cable alignment that might occur along the length of the stay. The subtracted signals were analyzed using the various signal analysis techniques described below.

Signal Analysis

Several different methods were employed to analyze and compare the subtracted signals obtained along a given defect path. In the time domain, differences in the maximum amplitude, maximum peak-to-peak amplitude, and root-mean-square (RMS) of the subtracted signals were studied in an attempt to evaluate their usefulness and accuracy in identifying the location of a defect. In addition, the frequency spectrum of the subtracted signals were studied in an attempt to determine whether or not the presence of a defect was accompanied by a corresponding change in frequency content such as a shift in the central frequency.

The maximum peak amplitude and frequency content were assessed using a computer-based digital oscilloscope and data collection system. This system employs a Sonix STR825 High Speed Waveform Digitizer Board with a 64K high speed static RAM memory buffer, a 25 MHz transient sampling rate, 200 MHz time equivalent sampling, and two independent channels with a common trigger. The data acquisition software real-time waveform displays with a continuous data collection mode, variable FFT lengths, and two channel operation for simultaneous display of waveform and frequency spectra.

A typical display showing a subtracted waveform in time domain and its associated frequency spectra is shown in Figure 41. The waveform is displayed with a vertical scale of 0.25 volts/div and a horizontal scale of 16 μsec/div. From this display, the maximum peak amplitude of the subtracted signal can be identified and recorded. The frequency spectra is plotted on a horizontal scale from 0 to 2 MHz for the portion of the waveform that falls within a specified gate. For the waveform depicted in Figure 41, the central frequency of the subtracted signal is shown to be approximately 450 kHz which is close to the 500 kHz resonant frequency of the ultrasonic transducers being used.

In independent trials, a LeCroy 9310M dual channel 300 MHz oscilloscope was used to determine the maximum peak-to-peak amplitude and the RMS of the subtracted signals along each defect path. As shown in Figure 42, the LeCroy oscilloscope can display all three waveforms of interest simultaneously. The top signal is a real-time display of the signal being received at the current location of the wheel transducers. The middle signal is a reference signal stored from the previous position of the inspection unit. The bottom signal is a real-time display of the difference between the current signal and the reference signal. Various built-in mathematical functions are available to analyze the displayed waveforms. As shown in Figure

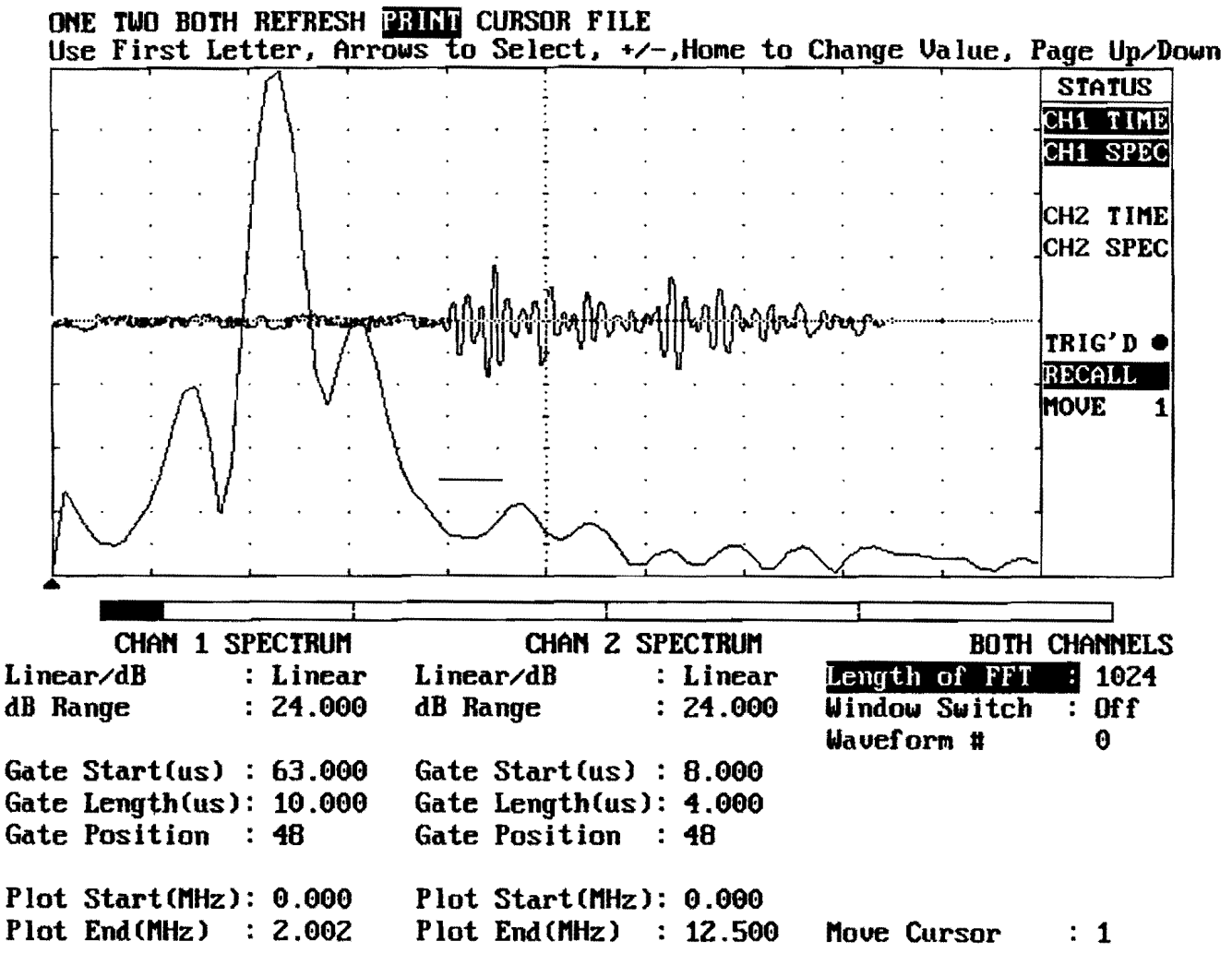

Figure 41. Typical waveform and frequency spectra from grout inspection using computer based digital oscilloscope.

42, the maximum peak-to-peak amplitude and RMS of the subtracted signal can be obtained. The maximum pk-to-pk amplitude measurement corresponds to a certain discrete portion of the signal, and provides no other information regarding any other differences that may exist. The RMS, on the other hand, is a measure of the total deviation of the subtracted signal from a zero baseline. All of the methods described above were studied to see which measure of the subtracted signal provided the most useful interpretation of the data.

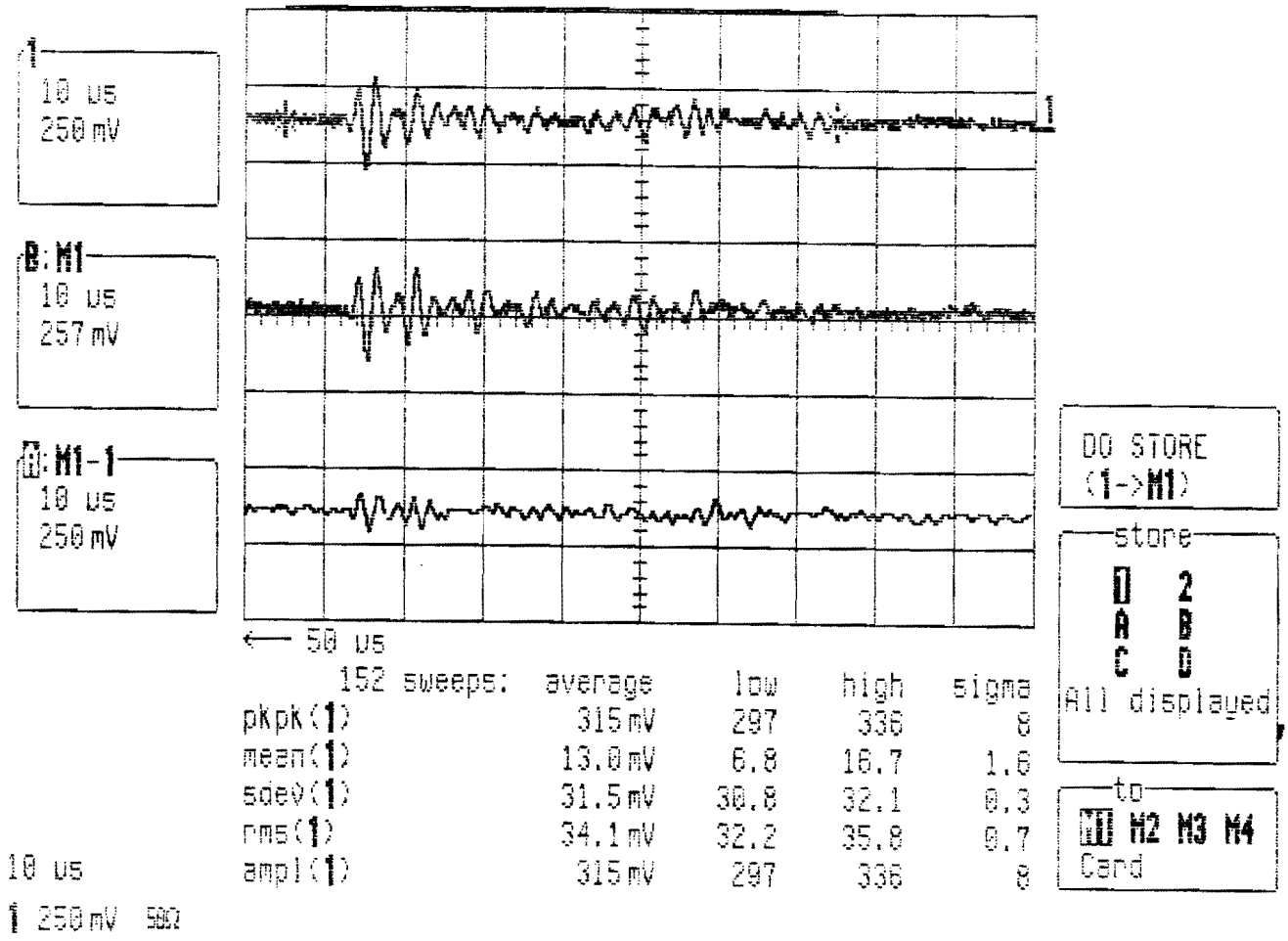

Figure 42. Successive waveforms and difference obtained from grout inspection by LeCroy oscilloscope.

Results

As mentioned above, numerous inspection trials were performed for each inspection path in which a defect was present. Figures 43(a) and 43(b) show waveforms which were saved at consecutive inspection points along a path containing defect 6 (see Table 3). Figure 43(c) shows the difference between these two signals. The relatively small peak amplitude (0.5 div) of the subtracted signal indicates that there is no defect present at the location being inspected. Figure 44 shows a similar set of signals for the next two points along the same inspection path. As shown in Figure 44(c), the difference between these signals clearly indicates that a defect is

present. The maximum peak amplitude of the subtracted signal is 3.5 times that shown in Figure 44(c).

Such an analysis was performed for each of the different signal analysis methods being investigated, namely maximum peak amplitude, maximum peak-to-peak amplitude, and root-mean-square. For visualization and comparison purposes, the results of these analyses were plotted as a function of location along the defect path for each of the manufactured defects listed in Table 3. The resulting graphs are shown in Figures 45 through 53 for defects 1 through 9, respectively.

Considering that different signal analysis techniques were used, and that for each technique an independent inspection was conducted, the consistency shown in these figures is somewhat surprising, but encouraging. Although additional indications are sometimes present, each defect appears to have been detected by one or more of the methods studied. Some of the additional indications were correlated to other nearby defects, the small spiral spacer wire which was wrapped around a short section of cable, cable ties, or some other physical explanation. However, several of these indications elluded explanation and may be attributed to internal defects or anomalies of unknown origin.

With the exception of defect 9 (Figure 53), the maximum peak amplitude method appears to show reasonably good correlation with the known defect locations. The other two methods, maximum peak-to-peak amplitude and RMS, have very close agreement between each other and also appear to show a high degree of correlation with the known defects.

Some of the defect indications, such as those for defect 2 and 4 (Figures 46 and 48), appear to be shifted from the expected location based on Table 3. This may be due to movement of the defect during the fabrication and grouting procedures, or may be attributed to human error in identifying the correct location of the defect. Whatever the reason, the consistency of all three difference measurements for these defect locations seems to imply that the defect indications are valid.

As described above, the frequency spectrum of the subtracted signals obtained along the defect paths was also investigated. Figure 54 shows the frequency spectra for consecutively subtracted signals along defect path 1. In reference to the horizontal scale shown in Figure 45, the spectra shown in Figures 54(a) through 54(d) correspond to signals obtained at locations 5, 6, 7, and 8 in. (152, 178, 203 mm) along the path, respectively. As shown in these figures, the

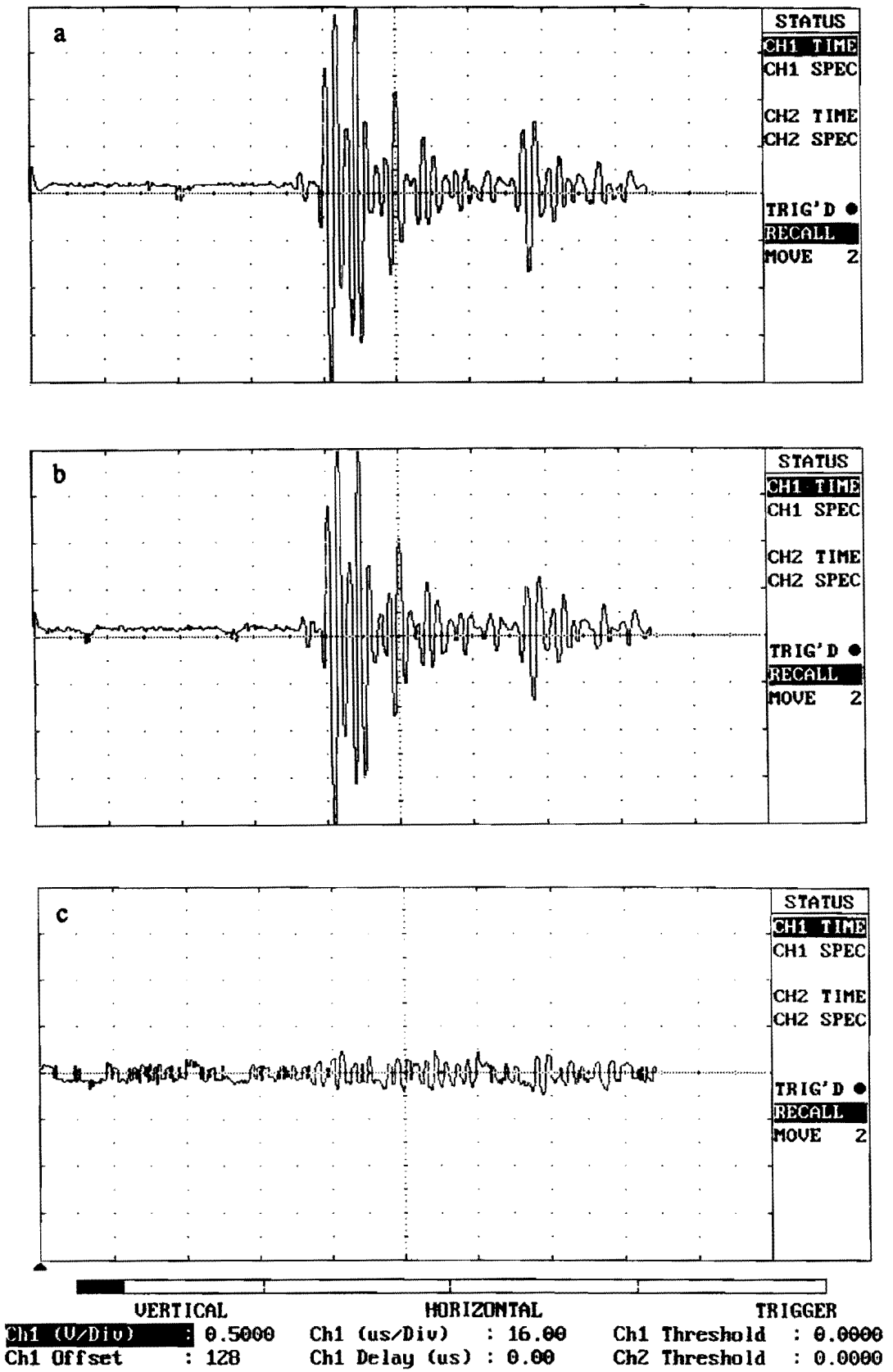

Figure 43. Ultrasonic signals obtained along defect path 6, (a) position 1, (b) position 2, and (c) difference.

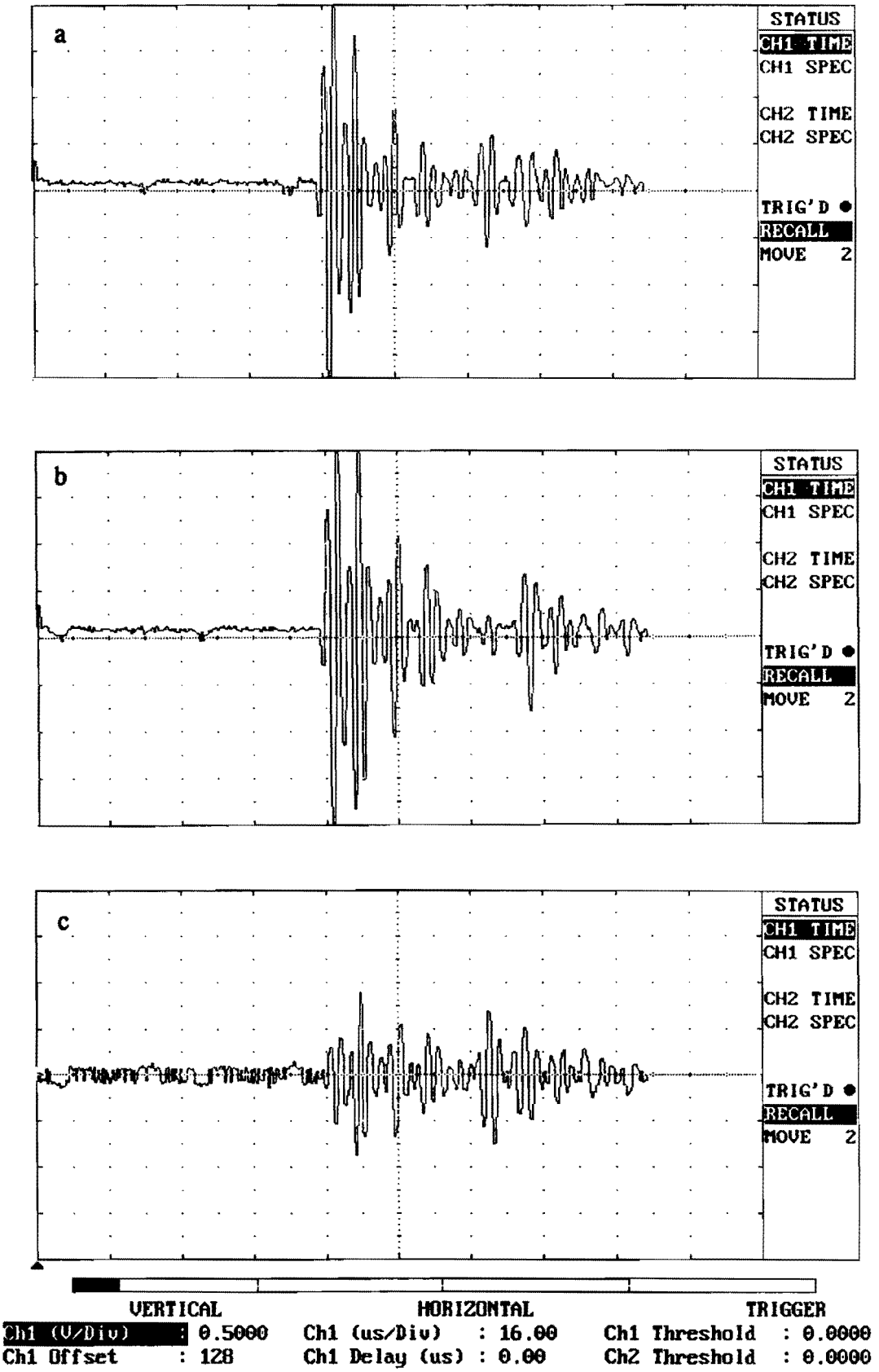

Figure 44. Ultrasonic signals obtained along defect path 6, (a) position 3, (b) position 4, and (c) difference.

spectra in Figure 54(d) shows a significant change. There is no pronounced central frequency of the received energy, and a much wider band of frequencies is present. As shown in Table 3, this location seems to correlate with the presence of a defect. However, similar inspection of other defect paths was inconclusive and further work is needed to more fully analyze the information contained within the frequency spectra.

The results the inspections were meaningful from the standpoint of locating the position of defects along the cable. However, information pertaining to the content and size of the defect is inconclusive. There is no clear trend in the results presented in Figures 45 through 53 that would indicate a larger peak amplitude or RMS for an air-filled void or a defect of larger diameter. Clearly additional research in the analysis and interpretation of this information is still needed.

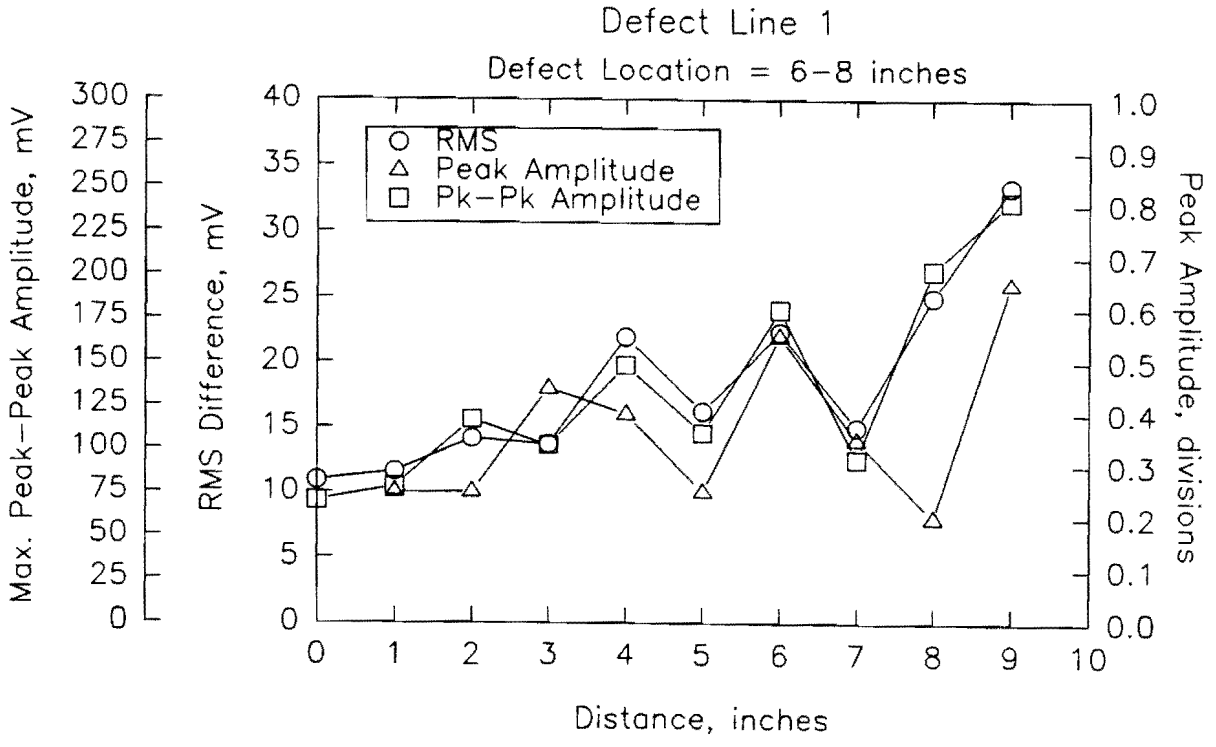

Figure 45. Differences obtained from ultrasonic inspection of defect path 1.

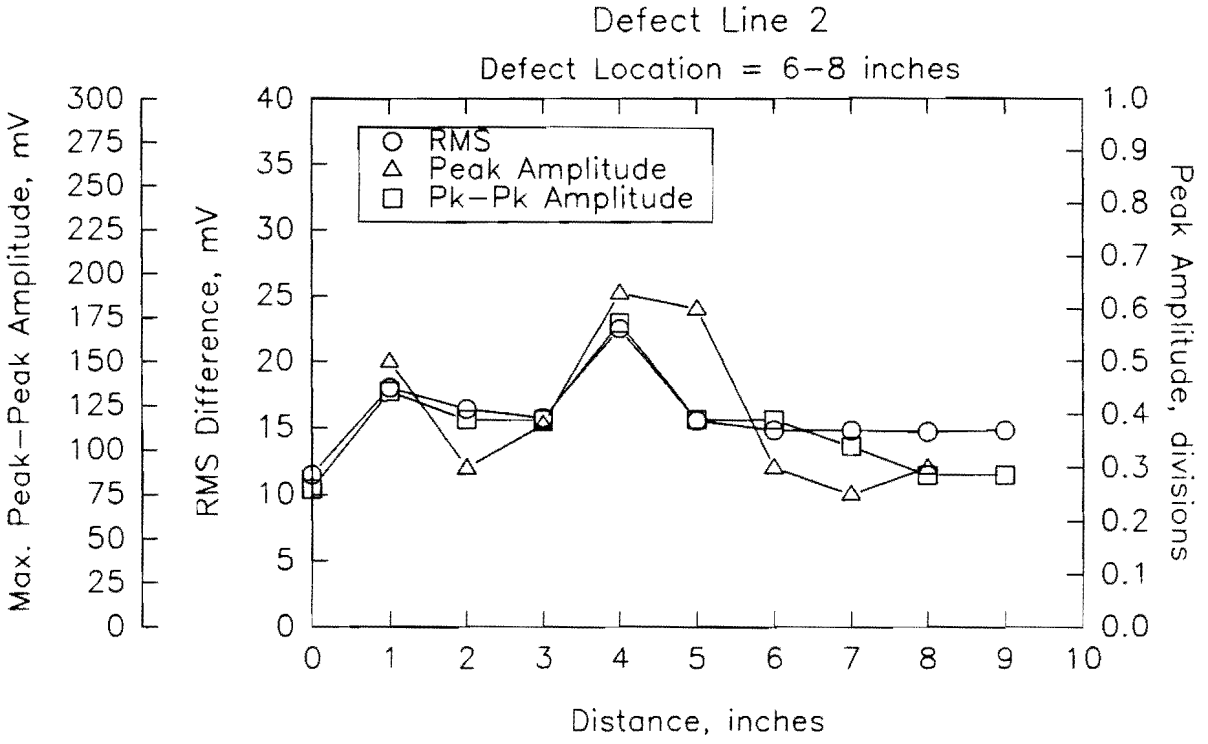

Figure 46. Differences obtained from ultrasonic inspection of defect path 2.

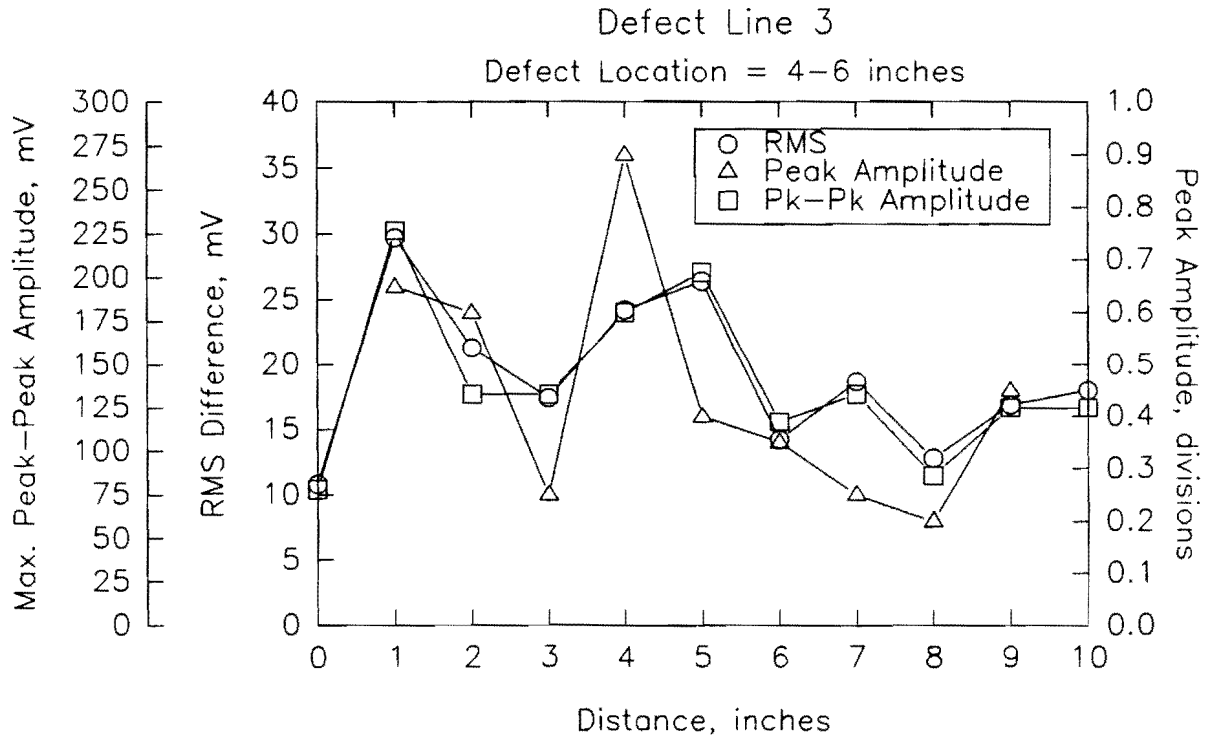

Figure 47. Differences obtained from ultrasonic inspection of defect path 3.

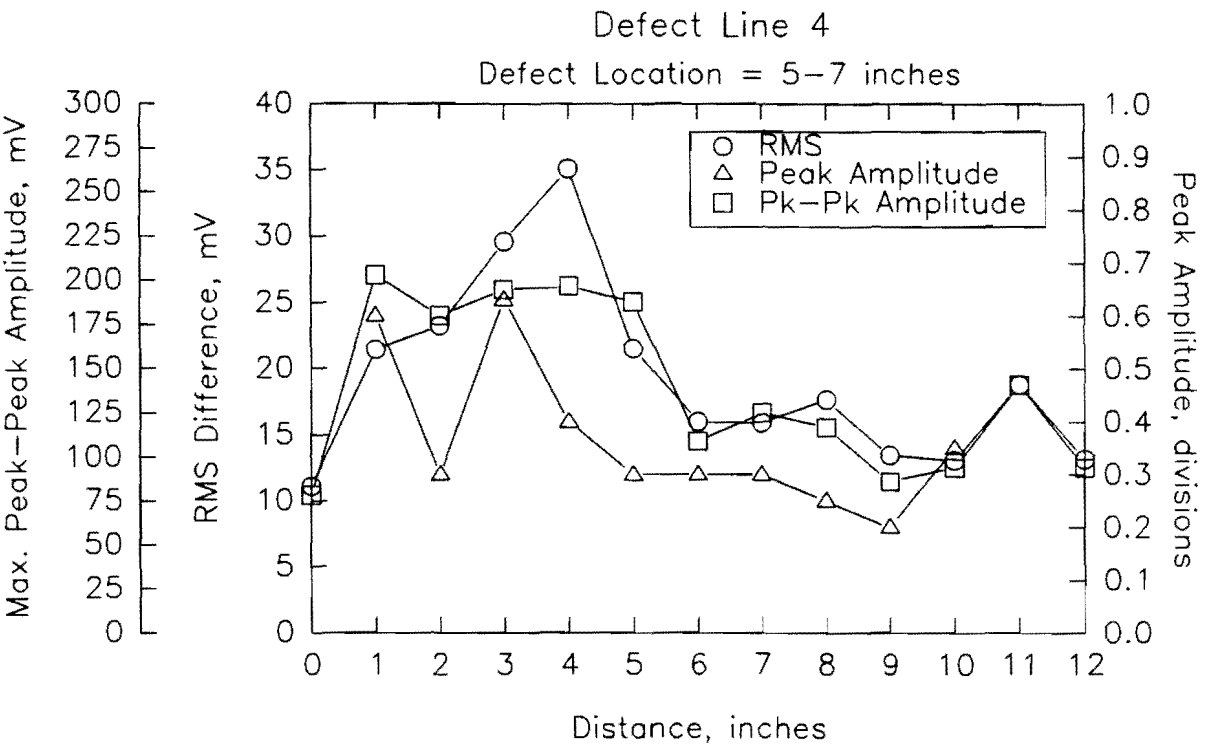

Figure 48. Differences obtained from ultrasonic inspection of defect path 4.

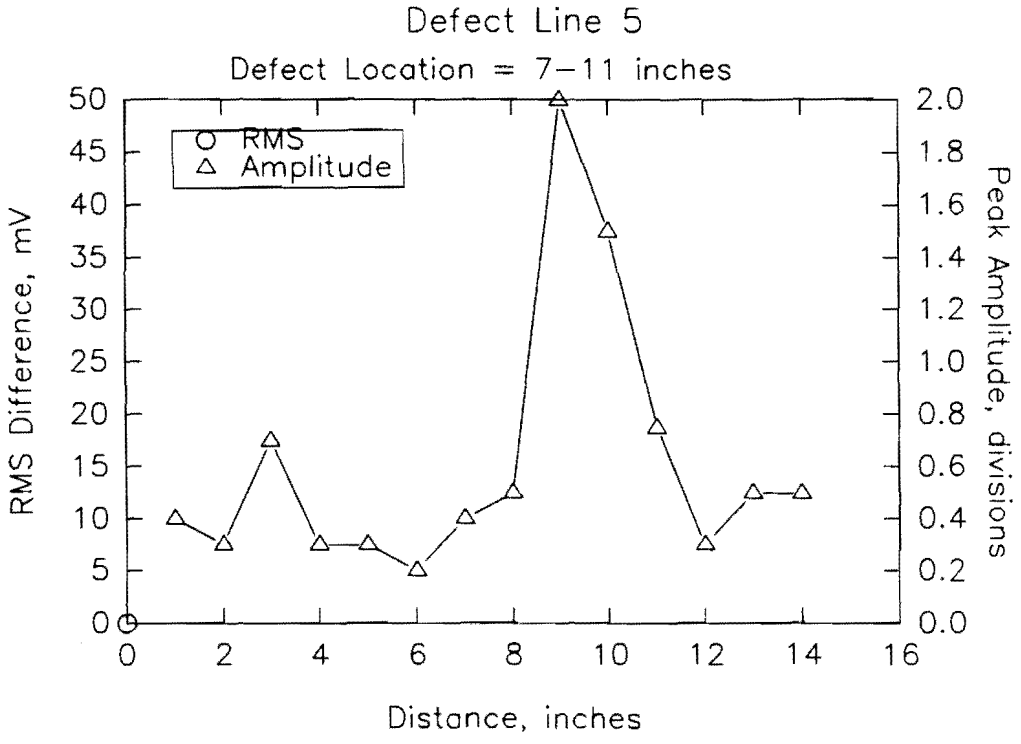

Figure 49. Differences obtained from ultrasonic inspection of defect path 5.

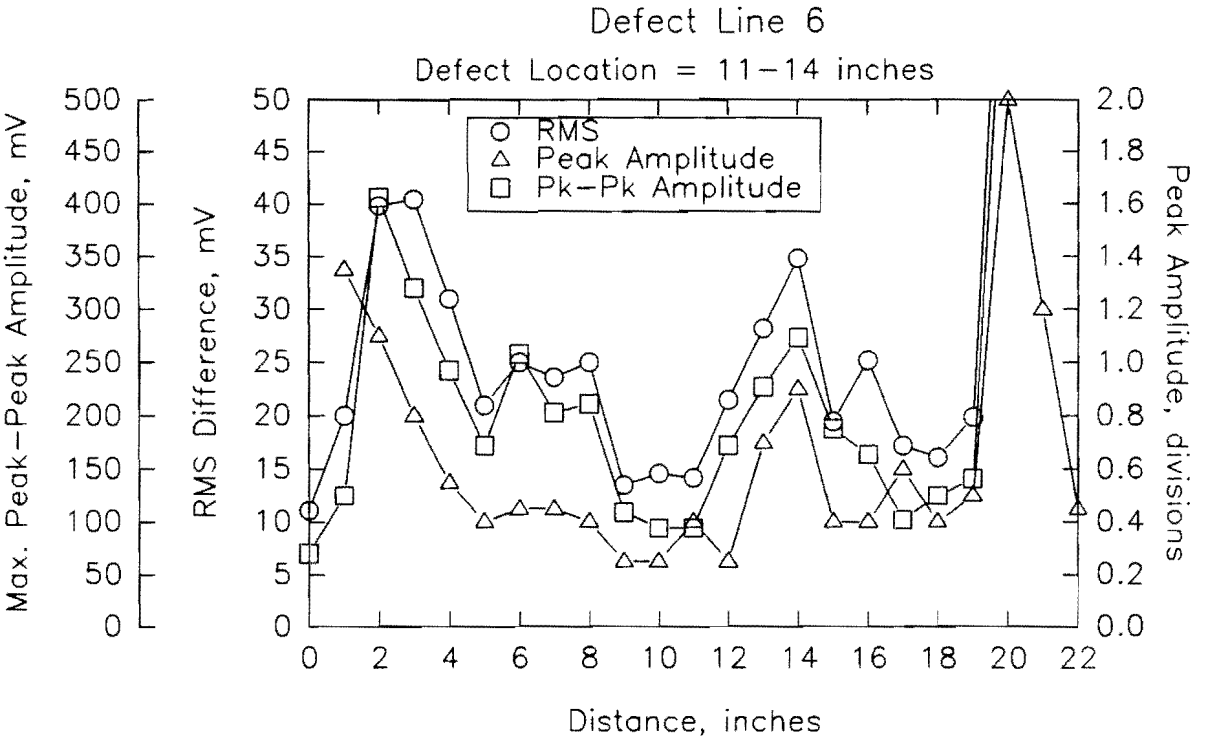

Figure 50. Differences obtained from ultrasonic inspection of defect path 6.

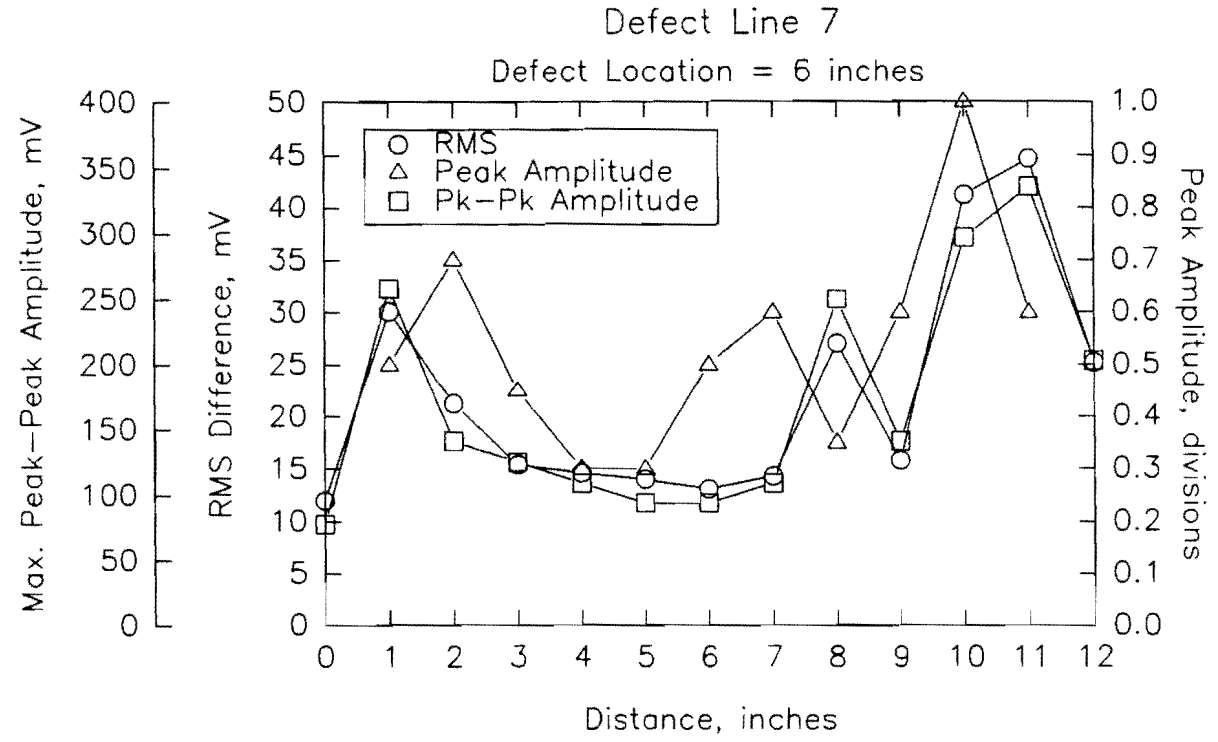

Figure 51. Differences obtained from ultrasonic inspection of defect path 7.

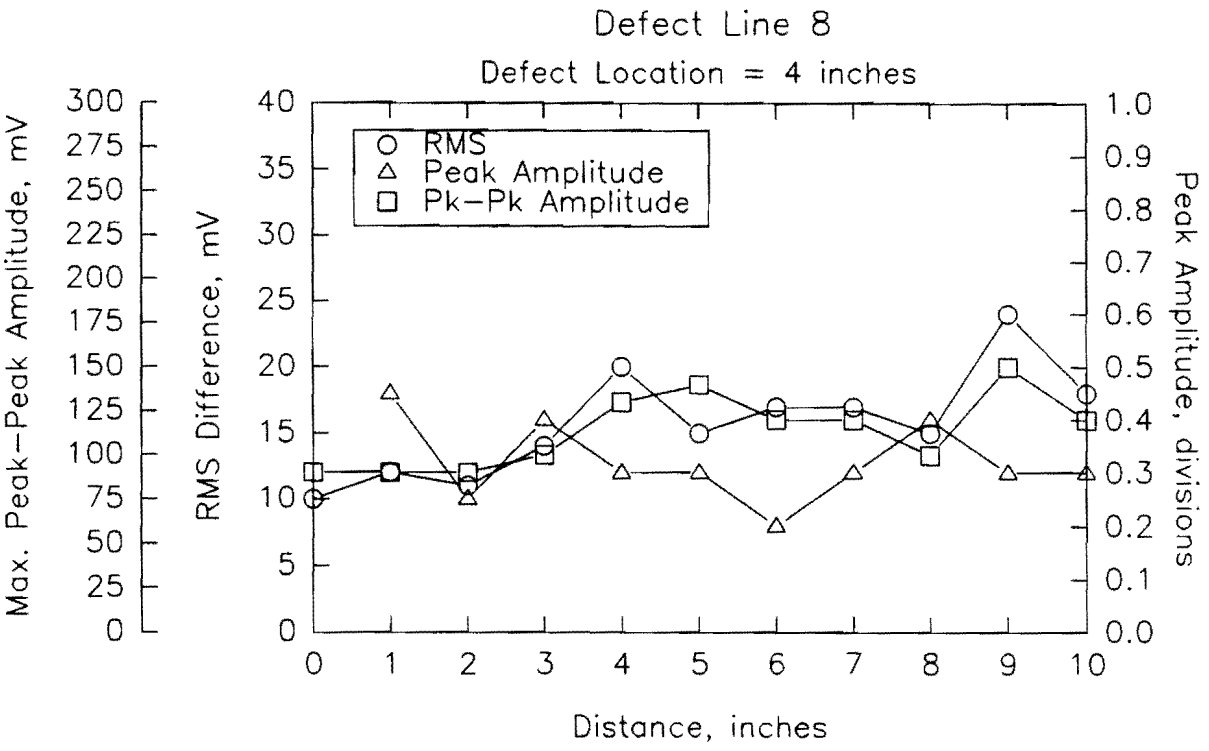

Figure 52. Differences obtained from ultrasonic inspection of defect path 8.

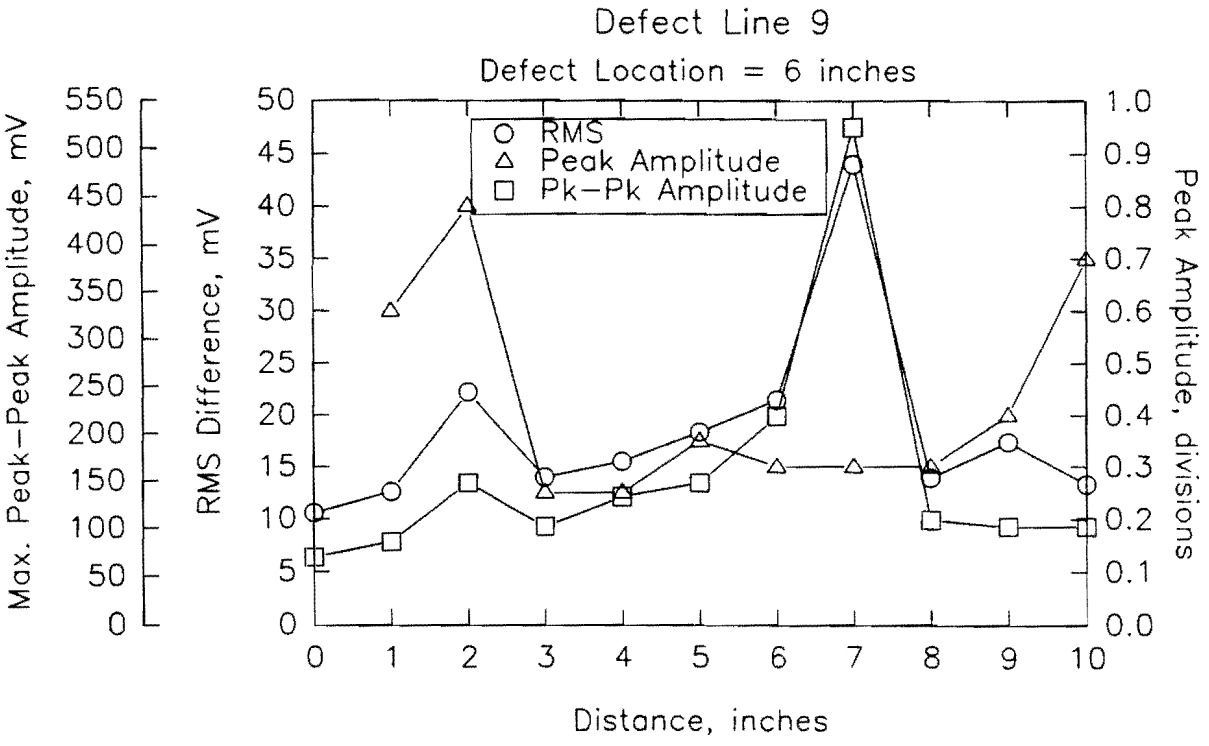

Figure 53. Differences obtained from ultrasonic inspection of defect path 9.

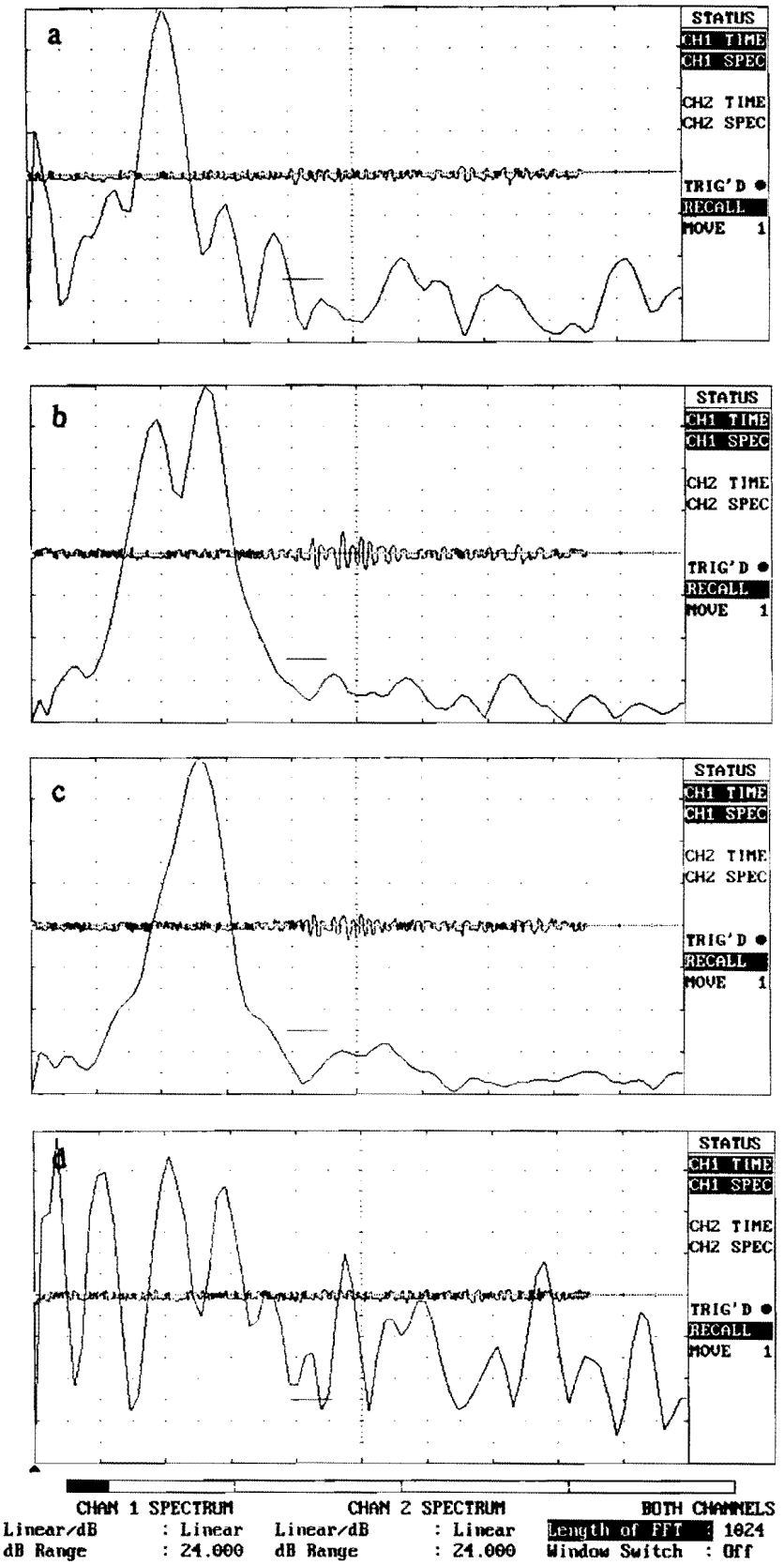

Figure 54. Frequency spectra obtained along defect path 1, (a) location 5, (b) location 6, (c) location 7, and (d) location 8 (defect).

CONCLUSIONS AND RECOMMENDATIONS

Bridge cable stays may be susceptible to corrosion of the steel strands due to bleed water accumulation in voids that may be trapped during the grouting operation. However, previous work has mostly concentrated on inspection of the cables for fatigue fracture or significant loss of section due to corrosion damage. Little study has been devoted to the detection of grout problems which might lead to this corrosion. The objective of this research was to evaluate various nondestructive inspection techniques for use in the early detection of such grout problems.

As evident from discussions and results presented herein, current NDE technologies have been found to hold significant promise for the inspection of cable stays for grout defects. The feasibility of using computed tomography for inspection of the grout layer has been demonstrated. Voids as small as 0.04 in. (1 mm) in the annular region and inside the steel cable bundle were identified in actual cable-stay samples using both X-ray and gamma-ray sources. Although some of these voids were manufactured, many of those found were a result of the grouting operation during fabrication of the specimens, an observation which lends urgency to the need for an inspection system.

CT technology offers the unique advantages of precisely locating defects within the cable, as well as characterizing their size and shape. Experiments were also performed which indicate that the content of a void can be determined for voids as small as 0.08 in. (2 mm) in diameter. This can be a significant factor when trying to determine whether or not corrective action is warranted.

The technology for developing a portable scanning device exists and can be readily adapted to the cable-stay inspection problem. Although X-ray sources have the potential for scanning the cable more rapidly, the cost of deploying a high-energy X-ray source is much greater than for an isotope. It is therefore envisioned that an isotope such as ^{192}Ir or ^{60}Co will serve as the source for such a system. Scan times as short as 1 min per linear inch of cable appear to be feasible, since the requirements for resolution are not very demanding. However, even with these relatively short scan times, the time required to use a CT system for the complete inspection of a bridge would be excessive.

A portable system, if developed, could be used on several cables to provide a quality check of the grout or to perform a more detailed inspection of known problem areas identified

by other means. Such a system also appears to be the best alternative for inspecting the lower regions of the cable stays where the geometry is complicated due to anchorage details and fire and crash protection measures.

Other radiographic technology such as the MINAC system, a portable linear accelerator unit, appears to offer promise for inspecting the anchorages and saddles which attach the cables to the structure. The capabilities of this system have been demonstrated for inspection of suspension cable sockets and cable-stay anchorages. Space limitations and large material thicknesses will likely preclude the use of other types of inspection systems in these areas.

Experimental results on actual cable-stay samples indicate that ultrasonic techniques can be effectively utilized to locate manufactured defects in the annular grout layer. A digital signal subtraction technique was found to be particularly useful in performing this type of inspection, since the presence of an anomaly can be readily identified when compared to a defect-free reference signal.

A prototype inspection unit which employs two rolling contact transducers was designed and constructed. The wheels operate in through-transmission mode using 500 kHz angle-beam transducers. Through proper positioning and sequencing of the probes, a fully operational system of this design would be capable of providing full circumferential inspection of the grout layer while travelling longitudinally along the length of the cable. A signal subtraction technique was used in conjunction with a moving reference signal to account for any gradual changes in the cable configuration along the length of the stay.

Laboratory investigations on cable stays with manufactured defects were conducted. Several methods of signal analysis were used to evaluate the subtracted signals, and a high degree of consistency was found to exist. The location of the manufactured defects were identified, but information regarding the size and content of the defects was inconclusive.

The ultrasonic approach is limited in its ability to inspect the lower regions of the cable in the zones of fire and crash protection and in detecting voids between the individual steel strands. However, the initial cost of such a system is relatively low and it is felt that the potential usefulness of the device as a quick means of inspecting the annular region of grout appear to outweigh these limitations.

Recommendations

The feasibility of using computed tomography and ultrasonics for the inspection of the protective grout layer surrounding the steel strands in cable stays has been demonstrated. It is recommended that operational field inspection units be fully developed for both of these technologies. The technology for developing a portable CT inspection device currently exists and is strictly a matter of cost. Due to the potential nationwide application of such a device and the high initial development cost, it is recommended that such a device be funded and developed at a national level.

Further development of an ultrasonic inspection unit is also recommended. Much of the groundwork for development of a fully operational field inspection device has been accomplished within this study. However, additional work is first needed to more fully analyze and interpret the content of the received signals in order to permit characterization of flaw size and content.

Development of a fully operational field unit would involve incorporation of a multiplexer to control the sequencing of the array of ultrasonic wheels, and a linear and/or rotational encoder to define the position of the transducers along the cable and trigger the data acquisition system. It would also be beneficial to design a new A/D board for the specific application of the cable inspection. For a modest cost, a board could be developed which incorporates signal subtraction and peak detection capability directly on the hardware. This would greatly increase the efficiency of the data acquisition system and significantly reduce memory storage requirements.

REFERENCES

1. Krishna, P., Arya, A.S. and Agrawal, T.P., "Effect of Cable Stiffness on Cable-Stayed Bridges," *Journal of Structural Engineering*, ASCE, Vol. 111, No. 9, Sept. 1985, pp. 2008-2020.

2. Podolny, W. and Scalzi, B. J., *Construction and Design of Cable-Stayed Bridges*, John Wiley & Sons, New York, 1986.

3. "Bridge," *Civil Engineering*, ASCE, Vol. 54, No. 7, July 1984, pp. 31-33.

4. Aboul-ella, F., "Analysis of Cable-stayed Bridges Supported by Flexible Towers," *Journal of Structural Engineering*, ASCE, Vol. 114, 1988, pp. 2741-2754.

5. State Department of Highways and Public Transportation, Item 4518--Stay Cables, Project No. F-839 (17), Houston Ship Channel Crossing, Laporte - Baytown.

6. "Recommendations for Stay Cable Design and Testing," Post-Tensioning Institute Ad Hoc Committee on Cable-Stayed Bridges, Phoenix, Arizona, January 1986.

7. Leonhardt, F. and Zellner, W., "Cable-stayed Bridges: Report on latest developments," *Proceedings of the Canadian Structural Engineering Conference*, 1970, 27 pp.

8. Watson, S. C. and Stafford, D., "Cables in Trouble," *Civil Engineering*, ASCE, Vol. 58, No. 4, April 1988, pp. 38-41.

9. Haibach, E., Hohle, H., and Weischedel, H. R., "Methods for and Findings from Bridge Cable Inspections," *8th Annual International Bridge Conference*, Pittsburgh, PA, 1991.

10. Moore, J. A., Burkett, W. R., and Frank, K. H., "Fatigue and Static Tests of 43-Strand Stay Cable Specimen for the Baytown Bridge," test report for VSL Corporation, University of Texas, Austin, TX, May 1989.

11. Burkett, W. R. and Frank, K. H., "Fatigue and Static Tests of 55-Strand Stay Cable Specimen for the Baytown Bridge," test report for VSL Corporation, University of Texas, Austin, TX, August 1989.

12. Frank, K. H., "Fatigue and Static Tests of Second 55-Strand Stay Cable Specimen for the Baytown Bridge," test report for VSL Corporation, University of Texas, Austin, TX, March 1990.

13. Breen, J., "Corrosion Protection for Post-Tension Tendons and Cable Stay Systems," presentation at Area IV research committee meeting, College Station, TX, April 1992.

14. Ghorbanpoor, A. and Shew, T., "Detection of Flaws in Bars and Cables in Concrete Bridge Structures," *Transportation Research Record 1211*, Transportation Research Board, National Research Council, Washington, D. C., 1989, pp. 84-91.

15. Teller, C.M., Suhler, S. A., and Matzkanin, G. A., "Nondestructive Inspection of Stay-Cables on the Pasco-Kennewick Bridge Using the MPC System," Final Report Submitted to Federal Highway Administration, Texas Research Institute, Austin, TX, 1990.

16. Teller, C. M., Suhler, S. A., and Matzkanin, G. A., "Recent Results with the Magnetic Perturbation Cable Inspection System in Laboratory and Field Trials on Bridge Stay-Cables," Proceedings Spring Conference, American Society for Nondestructive Testing, San Antonio, TX, 19-22 March, pp. 229-231.

17. Niehues, F., Coen, G., Kretschmer, R., and Biercher, M., "Radiographic Inspection of Prestressed Concrete up to 1600 mm Wall Thickness Using a 9 MeV Linear Accelerator," *Proceedings 11th World Conference on Nondestructive Testing*, American Society for Nondestructive Testing, Las Vegas, NV, 1985, pp. 528-534.

18. Clarke, E. T., "Cobalt-60 Radiography of Concrete," *Materials Evaluation*, Vol. 47, No. 10, 1989, pp. 1200-1203.

19. Evans, G. V., Parsons, T. V., and Wallace, M. R. G., "Nuclear Grout Monitoring of Offshore Platforms," *Proceedings Offshore Technology Conference*, Houston, TX, 1980, pp. 477-482.

20. Gilboy, W. B., and Foster, J., "Industrial Applications of Computerized Tomography with X- and Gamma-radiation," *Research Techniques in Nondestructive Testing*, R. S. Sharpe, Ed. VI, Academic Press, NY, 1982, pp. 255-287.

21. Ellinger, H., Morgan, I. L., Klinksiek, R., and Hopkins, F., "Tomographic Analysis of Structural Materials," *Proceedings of the Society of Photo-Optical Instrumentation Engineers*, 1979, pp. 179-186.

22. "Suspension Bridge Cable Socket and Radiographic Inspection Report," *Suspension Bridge Operator's Conference*, Poughkeepsie, NY, April 17-18, 1991.

23. Muenow, R. A., and Randall, F. A., Jr., "Pulse-echo Testing," *Concrete International*, Vol. 31, February 1986, pp. 129-134.

24. Knab, L. I., Blessing, G. V. and Clifton, J. R., "Laboratory Evaluation of Ultrasonics for Crack Detection in Concrete," *ACI Journal*, Vol. 80, No. 1, 1983, pp. 17-27.

25. Chung, H. W., and Law, K. S., "Diagnosing in situ Concrete by Ultrasonic Pulse Technique," *Concrete International*, Vol. 5, No. 10, 1983, pp. 42-49.

26. Cumming, N. A., Seabrook, P. T., and Malhotra, V. M., "Nondestructive Testing Techniques for Locating Voids in Grouted Tendon Ducts," *Transportation Research Record*, Transportation Research Board, Washington, D. C., presented January 1990.

27. Carino, N. J., Sansalone, M., and Hsu, N. N., "A Point Source-Point Receiver, Pulse-Echo Technique for Flaw Detection in Concrete," *ACI Journal*, Vol. 83, No. 2, 1986, pp. 199-208.

28. Burdekin, F. M., John, D. G., Payne, P. A., Smith, T. A., and Gaydecki, P. A., "Non-destructive Methods for Field Inspection of Embedded or Encased High Strength Steel Rods and Cables," Final Report, NCHRP Project 10-30(3), Transportation Research Board, National Research Council, Washington, D. C., July 1990.

29. Mlaker, P. F. and Walker, R. E., "Accoustic Emission Behavior of Concrete," *ACI Special Publication 82*, 1984.

30. Ohtsu, M., "Acoustic Emission Characteristics in Concrete Diagnostic Applications," *Journal of Acoustic Emission*, Vol. 6, No. 2, 1987.

31. Wang, M. S., "Application of Acoustic Emission to the Detection of Reinforcing Steel Corrosion in Concrete," *Corrosion*, Vol. 38, No. 1, 1982.

32. Chung, T. and Carter, C. R., "Pavement Thickness Determination and Detection of Pavement Cavities Using Radar," Report MAT-91-03, Ontario Ministry of Transportation, Ontario, Canada, April, 1991.

33. Maser, K. and Scullion, T., "Use of Radar Technology for Pavement Layer Evaluation," *Second International Symposium on Pavement Response Monitoring Systems for Roads and Airfields*, Hanover, NH, September 9-12, 1991.

34. Manning, D. G., "Detecting Defects and Deterioration in Highway Structures," National Research Council, Transportation Research Board, Washington, D. C., 1985.

35. Ansari F., "Real-Time Condition Monitoring of Concrete Structures By Embedded Optical Fibers," *Nondestructive Testing of Concrete Elements and Structures*, American Society of Civil Engineers, Structures Congress, San Antonio, TX, April 13-15, 1992.

36. Wolff, R., "Applications With Optical Fiber Sensor Systems for Monitoring Prestressed Concrete Structures," Structures Congress Abstracts, ASCE, New York, 1990, pp. 94-95.

37. Nanni, A., Yang, C. C., Pan, K., Wang, J., Michael, Jr., R. R., "Fiber Optic Sensors for Concrete Strain/Stress Measurement," *ACI Materials Journal*, Vol. 88, No. 3, May-June 1991, pp. 257-264.

38. Bray, D. E. and Stanley, R. K., *Nondestructive Evaluation*, McGraw-Hill Book Company, New York, 1989.

39. Mitchell, T. M., "Radioactive/Nuclear Methods," Chapter 10, *CRC Handbook on Nondestructive Testing of Concrete*, CRC Press, Boca Raton, FL, 1991.

40. *Handbook on Quality Assurance Guidelines for Nondestructive Testing*, Chapter VI, Neutron Radiography, U.S. Army Missile Command, Alabama, March 1986.

41. Kohutek, T. and Frank, K., "Application of Photon Tomography to the Inspection of Bridge Weldments," Paper 85-WA/NDE-2, American Society of Mechanical Engineers, New York, 1985.

42. Miller, W. H., "Design and Implementation of a Portable Computerized Axial Tomography System for Field Use," *Nuclear Instruments and Methods in Physics Research*, A270, North-Holland, Amsterdam, 1988, pp. 590-597.

43. Miller, W. H., Baldwin, J. W., and Thomas, H., "Implementation of a Portable Computerized Axial Tomography Scanner for Wooden Utility Pole Inspection," *International Conference on Wood Poles and Piles*, Fort Collins, CO, October 25-27, 1989, 10 pp.

44. Champion, M. and Dufay, J.-C., "Naissance du SCORPION: Systeme de Radioscopie Televisee Haute Energie par Rayonnement Pour L'inspection des Ouvrages en Beton," *Rev. Gen. Routes Aerodromes*, Vol. 582, No. 7, 1982.

APPENDIX A

Specifications for Panametrics Ultrasonic Analyzer model 5058

Pulse voltage : 0 to 900 V (step-wise and continuous modes)

Energy control : Through pulse voltage switch

Receiver attenuation : 0 to 80 dB in steps of 1 dB

Receiver gain : 40 or 60 dB

Bandwidth:

HP Filter : Five position rotary switch provides low frequency cutoff points at 0.03, 0.1, 0.3, 1.0 MHz. 'Out' position gives ≈ 11 kHz

LP Filter : Five position rotary switch provides high frequency cutoff points at 0.5, 1.0, 3.0, 5.0 MHz. 'Out' position gives ≈ 10 MHz

Auxiliary Preamplifier : Gain : 30 dB

Bandwidth : 600 Hz to 5 MHz

Operating modes : Pulse-echo and through transmission